

Kimmo Sääskilahti

## **Functional renormalization group study of quantum spin chains**

### **School of Science**

Thesis submitted for examination for the degree of Master of  
Science in Technology.

Espoo 16.5.2011

### **Thesis supervisor:**

Prof. Päivi Törmä

### **Thesis instructor:**

Prof. Dr. Carsten Honerkamp



**Aalto University**  
School of Science

Author: Kimmo Säskilahti		
Title: Functional renormalization group study of quantum spin chains		
Date: 16.5.2011	Language: English	Number of pages:5+87
Department of Applied Physics		
Professorship: Computational physics		Code: Tfy-105
Supervisor: Prof. Päivi Törmä		
Instructor: Prof. Dr. Carsten Honerkamp		
<p>In this thesis, the functional renormalization group (FRG) method is applied to quantum spin chains. FRG is a well-known method in the treatment of correlated fermion systems, but the method has been applied to spin systems only recently[1]. The method has been used, however, only as a qualitative tool to find phase boundaries for frustrated spin systems with multiple competing interactions. The main goal of this work is to critically assess the general accuracy of the method by studying toy models, for which quantitative comparison with exact results is possible.</p> <p>After a full derivation of the flow equations for spin systems, the numerical solution of the resulting non-linear system of differential equations is presented. It is shown that in the antiferromagnetic two-site Heisenberg model, FRG can reproduce some known properties of the singlet state but the ground state energy, for example, disagrees with the exact result by 36 %. In addition, the quasiparticle self-energy and dynamic spin-spin correlation functions are of an incorrect form. Unphysical fluctuations in the particle number are shown to be large. In the antiferromagnetic Heisenberg chain, it is shown that whereas the use of properly truncated flow equations regularizes the unphysical antiferromagnetic instability, the resulting ground state is disordered and not critical as expected.</p> <p>[1] J. Reuther and P. Wölfle, Phys. Rev. B <b>81</b>, 144410 (2010).</p>		
Keywords: Many-body physics, spin physics, renormalization group		

Tekijä: Kimmo Sääskilahti		
Työn nimi: Funktionaalirenormalisaatioryhmämenetelmän sovellus kvanttispin-ketjuille		
Päivämäärä: 16.5.2011	Kieli: Englanti	Sivumäärä: 5+87
Teknillisen fysiikan laitos		
Professori: Laskennallinen fysiikka		Koodi: Tfy-105
Valvoja: Prof. Päivi Törmä		
Ohjaaja: Prof. Dr. Carsten Honerkamp		
<p>Työssä tutkitaan funktionaalirenormalisaatioryhmämenetelmän sovelluksia kvanttispin-ketjuille. Menetelmää on yleisesti käytetty korreloituneiden elektronisysteemien tutkimuksessa jo pitkään, mutta sitä sovellettiin spin-systeemeille vasta hiljattain[1]. Tuolloin menetelmää käytettiin kuitenkin vain laadullisena työkaluna faasitransitiotiloiden arvioimiseen systeemeissä, joissa on monia kilpailevia vuorovaikutuksia. Työn tarkoituksena on arvioida kriittisesti menetelmän yleistä luotettavuutta tutkimalla yksinkertaisia malleja, joiden tarkat ratkaisut tunnetaan.</p> <p>Renormalisaatioryhmäyhtälöiden johtamisen jälkeen työssä esitetään kyseisen epälineaarisen differentiaaliyhtälösystemin numeerinen ratkaisu. Kahden spinin antiferromagneettisessa Heisenbergin mallissa menetelmä onnistuu tuottamaan tietyistä singlettitilan fysikaalisia ominaisuuksia, mutta esimerkiksi perustilan energia eroaa tarkasta tuloksesta 36 %:lla. Lisäksi kvasihiukkasten itseisenergia ja dynaamiset spin-spin-korrelaatiofunktiot ovat väärää muotoa ja epäfysikaaliset hiukkaslukumääräheilahtelut merkittäviä. Antiferromagneettisessa Heisenbergin ketjussa perustila on epäjärjestynyt, ei kriittinen kuten tarkasta ratkaisusta tunnetaan.</p> <p>[1] J. Reuther ja P. Wölfle, Phys. Rev. B <b>81</b>, 144410 (2010).</p>		
Avainsanat: Monihiukkasfysiikka, spin-systeemit, renormalisaatioryhmä		

## Acknowledgements

This work was carried out at the Institute for Theoretical Solid State Physics at RWTH Aachen University. I am deeply grateful to my advisor Prof. Dr. Carsten Honerkamp for the opportunity to work in his group between September 2010 and March 2011. His infinite hospitality, kindness, knowledge and genuine excitement about everything physics-related will inspire me for the years to come. I would also like to thank all the colleagues with whom I had the pleasure to collaborate during my stay in Aachen, especially Stefan Göttel, Dr. Dirk Schuricht and Prof. Dr. Sabine Andergassen. I am also grateful to Prof. Päivi Törmä for supervising the thesis. My former advisors D.Sc. Ari Harju, D.Sc. Ari Alastalo and D.Sc. Tomi Mattila taught me a lot of the physics I know today. I would also like to acknowledge financial support by the Career Services of Aalto University, without which this work could not have been done. In addition, financial support by the Julius Tallberg foundation, the Student Union of Helsinki University of Technology and the Society of Engineers and Architects in Lapland is acknowledged.

I would like to thank all my friends both in Finland and in Germany. Without you, I would not have sat at all the lectures and exercise sessions at 8 o'clock or had the greatest time of my life in and out of school. Finally, I would like to thank my parents for their love and support during these years.

Otaniemi, 13.5.2011

Kimmo Sääskilahti

# Contents

<b>1</b>	<b>Introduction</b>	<b>1</b>
<b>2</b>	<b>Heisenberg model in one dimension</b>	<b>5</b>
2.1	Introduction . . . . .	5
2.2	Heisenberg model as effective interaction . . . . .	9
2.3	Fermionization . . . . .	12
<b>3</b>	<b>Green's functions</b>	<b>16</b>
3.1	Introduction . . . . .	16
3.2	Symmetries of the spin Hamiltonian . . . . .	18
3.3	Grassmann variables and fermionic functional integrals . . . . .	26
3.4	Generating functionals . . . . .	32
<b>4</b>	<b>Functional renormalization group</b>	<b>37</b>
4.1	Introduction . . . . .	37
4.2	Exact flow equation for fermions . . . . .	39
4.3	Flow equations for the 1PI vertex functions . . . . .	43
4.4	Truncations . . . . .	48
4.5	Choice of the cut-off function . . . . .	50
4.6	Flow equations for the spin system . . . . .	52
<b>5</b>	<b>Results</b>	<b>59</b>
5.1	Discussion of numerics . . . . .	59
5.2	Computational complexity . . . . .	63
5.3	Two-site Heisenberg model . . . . .	64
5.3.1	Numerics . . . . .	64
5.3.2	Physical observables . . . . .	67
5.4	Quantum Heisenberg spin chain . . . . .	71
<b>6</b>	<b>Conclusions</b>	<b>77</b>
	<b>Bibliography</b>	<b>78</b>
<b>A</b>	<b>Flow equations</b>	<b>84</b>

# Chapter 1

## Introduction

Ever since Ising first studied spin interactions as a model for magnetism[1], spin models have played a major role in theoretical and experimental statistical physics. Although Ising was not able to demonstrate spontaneous magnetization, Onsager showed that true long-range magnetic order can exist in higher dimensions even at non-zero temperatures[2]. Onsager's finding showed how microscopic interactions can give rise to macroscopic collective behaviour, reviving the theoretical research on phase transitions.

Although theory of spin models was mostly dominated by their classification according to universality classes, general interest in quantum magnetism was truly awoken when Anderson proposed that quantum spin fluctuations could be the source of superconductivity in cuprate oxides[3]. Although it is nowadays accepted that the main ingredient of high- $T_c$  compounds is the strong repulsive electron interaction, the under-doped material is in the Mott insulating phase and the electron motion in copper oxide planes is well described by the two-dimensional Hubbard model, there is still no satisfying understanding of the full phase diagram of cuprate oxides (for a recent review on the subject, see e.g. Ref. [4]). Interestingly, in the limit of strong electron interaction and half-filling, the Hubbard model reduces to the antiferromagnetic Heisenberg model, and many properties of high- $T_c$  superconductivity can be understood based on the pure spin model[5]. Therefore, quantum magnetism has become an integral part of condensed matter physics.

Meanwhile, the concept of renormalization was devised as a method to handle unphysical divergencies appearing in relativistic field theories[6]. By replacing the possibly infinite bare parameters of the theory by their "physical" counterparts, one could derive accurate results e.g. for the Lamb shift in hydrogen[7]. After Wilson was able to show that instead of being a mere unpleasant mathematical trick, renormalization is the correct tool to take the continuum limit in any field theory[8], renormalization group has become one of the standard textbook methods in both statistical physics and particle physics.

Functional renormalization group (FRG) can be considered to be an extension of Wilson's idea of "mode elimination". Although Wilson's method to integrate out high-energy modes from the functional integral in order to obtain an effective low-energy theory was physically intuitive, the mode elimination is in practice

more convenient to do by solving differential flow equations for so-called generating functionals[9, 10]. The physical information included in approximate flow equations also depends on the way the mode elimination is done and therefore, new approximation schemes can be found. In addition to statistical physics[11], FRG has also proven useful in condensed matter physics as a method to approach the long-standing problem of strongly correlated electrons[12, 13]. The common idea in all studies is to first modify the free-electron theory such that dominant low-energy modes lying close to the Fermi surface are suppressed. In the fully interacting model, this leads to a suppression of electron-hole excitations, or quantum fluctuations. Fluctuations are then slowly turned on by the solution of differential flow equations, which turns out to be equivalent to an approximate summation of the diagrammatic series to infinite order.

Recently, fermionic functional renormalization group was for the first time applied to frustrated quantum spin systems[14]. The motivation for the use of FRG was that if the method proved to be reliable, it could overcome e.g. the finite-size scaling limitations of various other methods. In addition, RG methods are tailor-made for problems where there are many competing interactions, since the method is completely unbiased and the relative magnitude of competing instabilities can be assessed quantitatively. The idea was to present the spin operators as spin operators of localized fictitious fermions. The related mapping is exact, if each site is occupied by exactly one fermion, but to use the well-known methods of many-body theory such as diagrammatic perturbation theory, one has to relax the strict constraint of half-filling and allow unphysical fluctuations in the particle number. Once one has moved to the grand canonical ensemble in this way, one can apply all known methods to calculate the thermodynamic observables of the fermion system, which should, if the unphysical states do not play a significant role, coincide with those of the quantum spin system.

However, the fermionic Hamiltonian is pathological in the sense that since there is no dimensionless parameter in the model, one cannot use perturbation theory. This can be artificially fixed by introducing a cutoff  $\Lambda$  in the free theory, which, in addition to regularizing infrared divergencies, allows one to derive a perturbative series in  $J/\Lambda$ , where  $J$  is the spin-spin interaction. To approach the physical limit  $\Lambda \rightarrow 0$ , one then uses functional renormalization group to sum diagrams up to an infinite order by the solution of differential flow equations. In Ref. [14], it was shown how FRG was able to reproduce correct phase boundaries for the  $J_1$ - $J_2$  model in two dimensions. Thereafter, the method was applied to a triangular lattice [15] and also extended to three dimensions[16]. To summarize the findings, it was demonstrated that FRG can deliver useful information on the physics of frustrated spin systems.

However, earlier work has focused solely on determining phase boundaries for models that contained multiple competing interactions. It is therefore not clear if FRG is also a reliable quantitative tool: can one reproduce e.g. the correct ground state energies and spin susceptibilities? The first goal of this work is to apply the method to simple toy models for which exact solutions are known. This allows one to benchmark the accuracy of the method, which is crucial if one wants to apply the method e.g. to spin transport in future. Also, the performance of FRG in

one spatial dimension is unknown. Can FRG reproduce the exotic quasi-long-range order of antiferromagnetic quantum Heisenberg model, or does the method predict unphysical order or disorder? In addition, there remains some work in putting the "spin-FRG" on a firmer theoretical basis. For example, the symmetries of the model, which play a very crucial role in an efficient numerical solution, were not fully discussed in earlier work. We would also like to be sure that the numerical solution of the flow equations is free of all numerical artifacts, which was not demonstrated earlier. All these questions and inadequacies will be addressed in this work.

The thesis is organized as follows. In Chapter 2, we discuss the most important properties of the quantum Heisenberg model in one dimension. After a brief introduction to theoretical progress and review of essential methods such as Bethe Ansatz, we see how the antiferromagnetic Heisenberg interaction is the effective interaction for strongly interacting localized electrons. Finally we introduce fermionization transformation that allows us to use functional renormalization group methods on the spin system. We also discuss the first approximation of allowing unphysical particle and hole excitations. Chapter 3 is devoted to the general theory of interacting fermions. After introducing Green's functions and their parametrization using the symmetries of the spin model, we end the chapter by deriving the functional integral formula, which leads us to the definition of generating functionals. The most important of these functionals for our purposes is the generating functional of one-particle irreducible vertex functions, also known as the effective action.

In Chapter 4, we derive the functional renormalization group flow equations by introducing a new scale parameter in the model and then differentiating the effective action with respect to this parameter. Since the flow equations bear a close resemblance to diagrammatic perturbation theory, we stress the diagrammatic representation throughout in order to understand the physical meaning of each term. In order to derive the flow equations of interest to us, we then parametrize the vertex functions by using the symmetries presented in Chapter 3. This allows us to solve the flow equations numerically, which is the goal of Chapter 5. After discussing the details of the numerical solution and showing that the results are free of any numerical artifacts, we present the results for the two-site Heisenberg model, for which exact solutions are easy to derive. After benchmarking the accuracy of FRG, we see how the method performs in the problem of an antiferromagnetic quantum spin chain. Most importantly, we see whether FRG is able to reproduce critical behaviour or if the method delivers physically false correlations such as true long-range order. Finally, we summarize our findings and state conclusions in Chapter 6.

For clarity, we restrict our studies to antiferromagnetic spin interactions. Ferromagnetic interactions could be easily studied by modifying the initial condition in the numerical solution of the flow equations, but we choose the antiferromagnetic initial condition for the following reasons: 1) antiferromagnetic interactions are more interesting due to their role in the theory of high-temperature superconductivity, 2) half-integer antiferromagnetic quantum spin chains exhibit exotic physics such as quasi-long range order, and as a related fact 3) the one-dimensional spin-FRG can be pushed to the limit in the antiferromagnetic system, since the corresponding



ground state is known to be of much more complicated form than the ferromagnetic ground state. Of course, studies on simple toy models such as the two-site model could also be done using a ferromagnetic interaction, but apart from some changes of signs, the results are identical. In addition, we only study the rotationally symmetric case, i.e. pure Heisenberg model. Functional renormalization group calculations have been extended[17, 18] to anisotropic models as well, but for our purposes, this is an unnecessary complication.

# Chapter 2

## Heisenberg model in one dimension

*The goal of this chapter is to introduce our system of interest, the antiferromagnetic Heisenberg model in one spatial dimension. Section 2.1 is devoted to an overview of the theoretical progress in the exact solution of the model. In Section 2.2, we show how the antiferromagnetic interaction arises from the kinetic hybridization between localized electrons. We end the chapter in Section 2.3 by presenting the fermionization transformation and discussing the transition to the grand canonical ensemble.*

### 2.1 Introduction

Spin models were born when Ernest Ising looked for spontaneous magnetization in the simple model

$$H = J \sum_{i=1}^N S_i^z S_{i+1}^z, \quad (2.1)$$

which is nowadays known as the Ising model[1]. We always assume periodic boundary conditions such that  $S_{N+1} = S_1$ . A few years later Heisenberg studied a more general model, in which each of the spins was allowed to point into any direction[19]. The Heisenberg spin chain Hamiltonian can be written as

$$H = J \sum_{i=1}^N \mathbf{S}_i \cdot \mathbf{S}_{i+1}, \quad (2.2)$$

where, for spin  $S$ , the spin operators  $\mathbf{S}_i = (S_i^1, S_i^2, \dots, S_i^n)$  constitute a  $(2S + 1)$ -dimensional representation of the  $SU(2)$  algebra. Our model of interest will be the typical case of  $S = 1/2$  and  $n = 3$ . Whereas the classical and quantum versions of the Ising model coincide, since the phase spaces are identical, for Heisenberg model the quantum nature of spins is of great importance. This is most pronounced in the fact that the antiferromagnetic Neel state  $|\uparrow, \downarrow, \dots, \uparrow, \downarrow\rangle$  is not an eigenstate of the Hamiltonian. This also means that the exact solution of the antiferromagnetic model

is much more complicated than the ferromagnetic case. In 1931, Bethe introduced a very powerful method for the calculation of eigenstates, nowadays known as Bethe Ansatz[20]. Due to the importance of Bethe Ansatz in one-dimensional quantum physics, we present the main ideas of the method[21, 22, 23].

In order to gain more physical insight in the model, let us write the Hamiltonian (2.2) in terms of ladder operators  $S^+$  and  $S^-$ :

$$\begin{cases} S_i^+ = S_i^x + iS_i^y, \\ S_i^- = S_i^x - iS_i^y. \end{cases} \quad (2.3)$$

Then it is easy to show that

$$S_i^x S_{i+1}^x + S_i^y S_{i+1}^y = \frac{1}{2} [S_i^+ S_{i+1}^- + S_i^- S_{i+1}^+] \quad (2.4)$$

and the Heisenberg Hamiltonian becomes

$$H = J \sum_{i=1}^N \left[ S_i^z S_{i+1}^z + \frac{1}{2} (S_i^+ S_{i+1}^- + S_i^- S_{i+1}^+) \right]. \quad (2.5)$$

The second term describes the spin-flip of oppositely aligned spins at neighboring sites. If we assume our reference state to be the ferromagnetic Ising state  $|F\rangle = |\uparrow\uparrow \dots \uparrow\rangle$ , this term can be imagined to represent the propagation of a perturbation (down-spin) in the system. The first term is the nearest-neighbor interaction.

Since the Hamiltonian commutes with the total spin- $z$  operator  $S^z$ , one can diagonalize the Hamiltonian separately in each subspace  $S^z = -N/2, \dots, N/2$ . We assume  $N$  to be even throughout. If  $r$  spins are flipped with respect to the reference state  $|F\rangle$ , meaning that  $S^z = N/2 - r$ , the Hilbert space is  $\binom{N}{r}$ -dimensional. Any Ising basis state belonging to this subspace can be written in the form  $|n_1, \dots, n_r\rangle$  where the indices  $n_1 < n_2 < \dots < n_r$  are the positions of down-spins. To find the eigenstates, one must choose the coefficients  $a(n_1, \dots, n_r)$  in the general state

$$|\psi_r\rangle = \sum_{1 \leq n_1 < \dots < n_r \leq N} a(n_1, \dots, n_r) |n_1, \dots, n_r\rangle \quad (2.6)$$

such that the state is an eigenstate of the Hamiltonian (2.5).

For  $r = 1$ , the discrete Schrödinger equation for  $a(n)$  becomes

$$\frac{J}{2} [a(n-1) - 2a(n) + a(n+1)] = \tilde{E}a(n). \quad (2.7)$$

Here  $\tilde{E} = E - E_F$ ,  $E_F = -NJ/4$  being the energy of the ferromagnetic state. The discrete equation is of the same form as the discrete "hopping Hamiltonian" familiar from the tight-binding method. The solutions are planewave states  $a(n) = e^{ikn}/\sqrt{N}$ , where  $k = 2\pi j/N$ ,  $j = 0, 1, \dots, N-1$ . The energy dispersion is the free particle dispersion  $\tilde{E}(k) = J[\cos k - 1]$ . This low-energy excitation of the ferromagnetic chain is called magnon.

For  $r = 2$ , the situation is already more complicated. If  $n_2 > n_1 + 1$ , i.e. the down-spins are not located next to each other, the Schrödinger equation simply corresponds to two independent magnon excitations. If  $n_2 = n_1 + 1$ , however, the form of the equation is different since the hopping of a down-spin to a site already occupied by a down-spin is forbidden and also the interaction term is different. This corresponds to an interaction between magnons. Miraculously, one can still find a solution that corresponds to two planewaves. The coefficients  $A_{12}$  and  $A_{21}$  appearing in the general planewave state

$$a(n_1, n_2) = A_{12}e^{ik_1n_1+ik_2n_2} + A_{21}e^{ik_1n_2+ik_2n_1}$$

can be chosen such that the extra terms appearing in the equation for  $a(n_1, n_1 + 1)$  vanish. Due to the one-dimensionality and short-ranged interaction, there is always the correct number of such equations to fix the values of all coefficients. Typically the coefficients are complex, meaning that the planewaves are shifted in phase. This corresponds to scattering between magnons.

In order to solve for the ground state energy of the antiferromagnetic chain, one simply has to solve Bethe's equations for  $r = N/2$ , since the ground state is known to be a singlet due to Marshall's theorem[24]. Of course, the equations are quite complicated, and the analytical solution is far from trivial. Hulthén[25] calculated the exact ground state energy per spin of the antiferromagnetic Heisenberg chain in the thermodynamic limit to be  $E/N = -J \ln 2$ . Solving Bethe's equations for  $r = N/2 \pm 1$ , des Cloizeaux and Pearson[26] were able to show the low-energy excitation spectrum to be of the form  $\omega_q = \pi J/2 |\sin q|$ . Surprisingly, the exact dispersion disagreed with Anderson's[27] spin wave theoretical result  $\omega_q = J |\sin q|$  only by the coefficient, although elementary excitations in the antiferromagnetic chain are not spin waves in the sense that they cannot be considered to be small fluctuations around a symmetry-broken ground state. Later, it was understood[28] that the elementary excitation in the spin chain is a spin-1/2 quasiparticle nowadays called spinon, and des Cloizeaux and Pearson's excitation corresponds to a  $S = 1$  magnon state built from two spinons. The excitation spectrum was confirmed experimentally[29] in 1974.

The theoretical interest in quantum spin chains was renewed when the methods of quantum field theory made it possible to calculate e.g. spin-spin correlation functions, which is out of reach for Bethe Ansatz. Using various field-theoretical methods[30, 31, 32], it was shown that the spin-spin correlations of the  $S = 1/2$  chain decay as

$$\langle S^z(x) S^z(0) \rangle = C_1 \frac{1}{x^2} + C_2 (-1)^x \frac{\sqrt{\ln(x)}}{x}, \quad (2.8)$$

where  $C_1$  and  $C_2$  are some constants. The ground state is neither long-range ordered nor disordered, since the correlations decay algebraically. At non-zero temperature, however, the system becomes disordered in accordance with Mermin-Wagner theorem[33]. To derive the correlation functions, a typical procedure is to use "fermionization" of the model, either using the transformation discussed in the next section or Jordan-Wigner transformation[34, 35]. In the Jordan-Wigner transformation, a spin-down state corresponds to an, say, empty site and a spin-up state

to a state occupied by a spinless fermion. In order to respect commutation relations, one must also include an extra term known as "Jordan-Wigner string" in the transformation. If we consider for a moment a slightly more general anisotropic spin Hamiltonian

$$H = J \sum_{i=1}^N (S_i^x S_{i+1}^x + S_i^y S_{i+1}^y + \Delta S_i^z S_{i+1}^z) \quad (2.9)$$

with anisotropy factor  $\Delta$ , Jordan-Wigner transformation delivers the Hamiltonian[22]

$$H = -\frac{J}{2} \sum_i (c_i^\dagger c_{i+1} + c_{i+1}^\dagger c_i) + J\Delta \sum_i \left(n_{i+1} - \frac{1}{2}\right) \left(n_i - \frac{1}{2}\right), \quad (2.10)$$

where  $c_i$  and  $c_i^\dagger$  are the fermionic annihilation and creation operator for a spinless fermion at site  $i$ . Since the interaction between fermions is proportional to  $\Delta$ , XY-model corresponding to  $\Delta = 0$  is trivial to solve in this transformation. For the interacting model, the bosonization solution of this Luttinger-Tomonaga type Hamiltonian is a typical textbook problem, and the low-energy Hamiltonian for the canonical fields  $\Phi$  and  $\phi$  turns out to be the sine-Gordon Hamiltonian[22]

$$H = \frac{1}{2\pi} \int dx \left[ uK(\pi\Pi(x))^2 + \frac{u}{K}(\nabla\phi(x))^2 \right] - \frac{2g_3}{(2\pi\alpha)^2} \int dx \cos(4\phi(x)). \quad (2.11)$$

Various coefficients appearing in the Hamiltonian can be related to those of the spin model exactly by using Bethe Ansatz[36, 37]. The cosine term arises from the Umklapp scattering between Jordan-Wigner fermions. For  $|\Delta| < 1$ , this term is an irrelevant perturbation and the low-energy properties correspond to the XY-model. At the isotropic point  $\Delta = 1$ , the Umklapp term is marginal and leads to the logarithmic corrections appearing in Eq. (2.8).

The importance of topology in the physics of quantum spin chains was noticed by Haldane[38, 39], who showed that whereas the effective field theory of large- $S$  integer quantum spin chains is the non-linear sigma model, half-integer spin chains possess an extra term, which is topological in nature. This fundamental difference lead Haldane to further conjecture that the excitation spectrum of any integer spin chain is massive and all half-integer chains share the gaplessness of the  $S = 1/2$  chain.

In addition to Bethe Ansatz and field-theoretical methods, there are naturally also other approaches available. Because of the existence of exact solutions, one-dimensional systems offer an excellent possibility to test the accuracy of numerical methods. Exact diagonalization of the Hamiltonian has the same advantages and disadvantages as in higher dimensions. The method delivers exact eigenstates and wavefunctions and allows the calculation of real-time correlation functions at zero or non-zero temperature, but the practicality of the method is severely restricted by finite-size limitations, since the dimension of the Hilbert space grows typically exponentially as a function of system size. In order to circumvent this problem, White[40] introduced the density matrix renormalization group, which has become one of the most popular methods in the treatment of one-dimensional problems[41].

The usefulness of the method relies on the fact that only low-energy properties are included in the renormalization procedure and one can therefore proceed to very long systems without running into computational limits. This allows one to calculate e.g. long-range asymptotics of correlation functions, which is out of reach for bare exact diagonalization.

## 2.2 Heisenberg model as effective interaction

To understand the origin of the antiferromagnetic Heisenberg model, let us study the simplest realistic model of localized, strongly interacting electrons: the two-site Hubbard model with the Hamiltonian

$$H = -t \sum_{\sigma} (c_{1\sigma}^{\dagger} c_{2\sigma} + c_{2\sigma}^{\dagger} c_{1\sigma}) + U(\hat{n}_{1\uparrow} \hat{n}_{1\downarrow} + \hat{n}_{2\uparrow} \hat{n}_{2\downarrow}), \quad (2.12)$$

where  $t > 0$  is the hopping matrix element between atoms and  $U \gg t$  is the local Coulomb interaction. Here e.g. the state  $c_{1\uparrow}^{\dagger} |0\rangle \equiv |\uparrow, 0\rangle$  corresponds to an electron in the Wannier orbital that is localized on atom 1. The number of electrons with spin  $\sigma$  at site  $i$  is given by the number operator  $\hat{n}_{i\sigma} = c_{i\sigma}^{\dagger} c_{i\sigma}$ . Focusing on the two-particle sector, the Hilbert space consists of the Fock states

$$\underbrace{|\uparrow, \uparrow\rangle_-, |\downarrow, \downarrow\rangle_-}_{S=1, S_z^{\text{tot}}=1}, \underbrace{|\uparrow, \downarrow\rangle_-, |\downarrow, \uparrow\rangle_-, |\uparrow\downarrow, 0\rangle_-, |0, \uparrow\downarrow\rangle_-}_{S=0, S_z^{\text{tot}}=0}, \quad (2.13)$$

where the minus signs in the subscript denote antisymmetrization. The ferromagnetic states  $|\sigma, \sigma\rangle_-$  are eigenstates of the Hamiltonian with energy  $E = 0$ . In the  $S_z = 0$  sector and basis  $\{|\uparrow, \downarrow\rangle_-, |\downarrow, \uparrow\rangle_-, |\uparrow\downarrow, 0\rangle_-, |0, \uparrow\downarrow\rangle_-\}$ , the Hamiltonian matrix becomes

$$H = \left( \begin{array}{cc|cc} & & -t & -t \\ & & t & t \\ \hline -t & t & U & \\ -t & t & & U \end{array} \right). \quad (2.14)$$

The matrix could be straightforwardly diagonalized to get the full solution of the problem, but our goal is to derive an effective Hamiltonian for the space of singly-occupied sites  $|\uparrow, \downarrow\rangle_-, |\downarrow, \uparrow\rangle_-$  in the limit  $U \gg t$ . In Brillouin-Wigner perturbation theory (see e.g. Ref. [42]), given a general eigenvalue equation of the form

$$\begin{pmatrix} H_{11} & H_{12} \\ H_{21} & H_{22} \end{pmatrix} \begin{pmatrix} \psi_1 \\ \psi_2 \end{pmatrix} = E \begin{pmatrix} \psi_1 \\ \psi_2 \end{pmatrix}, \quad (2.15)$$

one solves, say, the lower equation for  $\psi_2$ :

$$\psi_2 = (E - H_{22})^{-1} H_{21} \psi_1. \quad (2.16)$$

Substituting this to the upper equation, one gets an effective eigenvalue problem for  $\psi_1$ :

$$H^{\text{eff}} \psi_1 = E \psi_1, \quad (2.17)$$

where the effective Hamiltonian is

$$H^{eff} = H_{11} + H_{12}(E - H_{22})^{-1}H_{21}. \quad (2.18)$$

The second term corresponds to an effective coupling between states  $|1\rangle$  and  $|2\rangle$ . Physically, a particle at state  $|1\rangle$  can hop to state  $|2\rangle$  (corresponding to  $H_{21}$ ), "propagate" in state  $|2\rangle$  (Green's function  $(E - H_{22})^{-1}$ ) and return to state  $|1\rangle$  ( $H_{12}$ ). Applied to the Hamiltonian matrix (2.14), one gets the exact effective Hamiltonian for the  $\{|\uparrow, \downarrow\rangle_-, |\downarrow, \uparrow\rangle_-\}$  sector:

$$H^{eff} = \begin{pmatrix} -t & -t \\ t & t \end{pmatrix} \begin{pmatrix} \frac{1}{E-U} & \\ & \frac{1}{E-U} \end{pmatrix} \begin{pmatrix} -t & t \\ -t & t \end{pmatrix} \quad (2.19)$$

$$= \frac{2t^2}{E-U} \begin{pmatrix} 1 & -1 \\ -1 & 1 \end{pmatrix}. \quad (2.20)$$

Focusing on the low-lying energies  $E \ll U$ , one gets the energy-independent effective Hamiltonian

$$H^{eff} \approx \frac{J}{2} \begin{pmatrix} -1 & 1 \\ 1 & -1 \end{pmatrix}, \quad (2.21)$$

with  $J = 4t^2/U$ . If there was no hybridization  $t$ , the effective Hamiltonian for the singly-occupied sites would simply be  $H^{eff} = 0$ . In the diagonal elements, the hopping leads to a reduction in energy due to virtual process in which, for example, an electron of spin up hops from the first site (matrix element  $-t$ ) to the second site already occupied by an electron with spin down (factor of  $1/U$ ) and then returns to the first site ( $-t$ ).

The off-diagonal terms represent so-called indirect exchange, in which, instead of the spin-up electron, the spin-down electron hops to the site 1 in order to avoid the virtual double occupancy described above. This corresponds to matrix element  $+t$  and the sign of the process is reversed. Effectively, this process is a spin-flip. The eigenstates of the Hamiltonian (2.21) are the singlet state

$$|s\rangle = \frac{1}{\sqrt{2}} (|\uparrow, \downarrow\rangle_- - |\downarrow, \uparrow\rangle_-)$$

with energy  $E_s = -J$  and one of the triplet states,

$$|t_0\rangle = \frac{1}{\sqrt{2}} (|\uparrow, \downarrow\rangle_- + |\downarrow, \uparrow\rangle_-)$$

with energy  $E_t = 0$ .

In this way, we have shown that the eigenstates correspond to the eigenstates of the Heisenberg Hamiltonian

$$H = J\mathbf{S}_1 \cdot \mathbf{S}_2 - \frac{J}{4}. \quad (2.22)$$

This is easiest to show by writing the spin interaction in the form

$$\mathbf{S}_1 \cdot \mathbf{S}_2 = \frac{1}{2} (\mathbf{S}^2 - \mathbf{S}_1^2 - \mathbf{S}_2^2). \quad (2.23)$$

The eigenstates of total spin  $\mathbf{S}^2 = (\mathbf{S}_1 + \mathbf{S}_2)^2$  are the singlet state  $|s\rangle$  ( $S = 0$ ) and triplet states  $|t_0\rangle$ ,  $|t_+\rangle$  and  $|t_-\rangle$  ( $S = 1$ ), corresponding to eigenvalues 0 and 2, respectively. Therefore, using  $\mathbf{S}_i^2 = 3/4$  for spin-1/2, the eigenenergies of the Heisenberg Hamiltonian  $H = J\mathbf{S}_1 \cdot \mathbf{S}_2 - J/4$  are  $E_s = -J$  and  $E_t = 0$ , which coincide with the eigenstates of the effective Hamiltonian (2.21). The additional term  $-J/4$  can be dropped. To conclude, we have shown that the effective model of the two-site Hubbard model in the limit of strong interaction is the antiferromagnetic Heisenberg model. Physically, the Hubbard Hamiltonian favours antiparallel configuration of the spins, because this allows kinetic exchange process that lower the energy. For parallel spins, no hopping would be allowed due to Pauli exclusion principle. This demonstrates how it is the interplay between strong Coulomb interaction and the Pauli statistics that drives quantum magnetic phenomena.

The above calculation can be generalized in a straightforward manner[43]. In the subspace of singly-occupied states, the effective Hamiltonian of the general lattice Hubbard model

$$H = -t \sum_{\langle i,j \rangle, \sigma} (c_{i\sigma}^\dagger c_{j\sigma} + c_{j\sigma}^\dagger c_{i\sigma}) + U \sum_i \hat{n}_{i\downarrow} \hat{n}_{i\uparrow} \quad (2.24)$$

is the quantum Heisenberg model

$$H = J \sum_{\langle i,j \rangle} \left( \mathbf{S}_i \cdot \mathbf{S}_j - \frac{1}{4} \right) + \mathcal{O}(J^2) \quad (2.25)$$

with  $J = 4t^2/U$ . Away from half-filling, the calculation is a bit more intricate and leads to the  $t$ - $J$ -model[44]

$$H = -P \left[ -t \sum_{\langle i,j \rangle, \sigma} c_{i\sigma}^\dagger c_{j\sigma} + J \sum_{\langle i,j \rangle} \left( \mathbf{S}_i \cdot \mathbf{S}_j - \frac{1}{4} \hat{n}_i \hat{n}_j \right) \right] P, \quad (2.26)$$

where  $P$  is the projection operator to the subspace of non-occupied or singly-occupied sites, i.e. the projector removes any states with doubly-occupied sites. Due to the projector, the  $t$ - $J$ -model is notoriously difficult to study analytically, but can be handled numerically. Note that in the subspace of singly-occupied sites, the  $t$ - $J$ -Hamiltonian reduces to the Heisenberg model, as expected.

In a more realistic model than the Hubbard model, the situation is more complicated. If the exchange integral  $V_x = \langle \phi_1 \phi_2 | V | \phi_2 \phi_1 \rangle$  between orbitals  $\phi_1$  and  $\phi_2$  is large, the electrons favor spin alignment in order to minimize the Coulomb energy. This is the Hund's rule familiar from molecular physics. However, if the virtual hopping process described above is dominant, meaning that  $t^2/U$  is large, antiferromagnetism prevails[45].

For completeness, let us mention that antiferromagnetic interaction can also arise from so-called superexchange[46]. The basic idea is that electrons localized at next-to-nearest neighbor atoms can form a hybridized state by hopping to a diamagnetic atom lying between the atoms. The special feature of superexchange is that unlike in the case of direct exchange, the superexchange practically always leads



to an effectively antiferromagnetic interaction. The superexchange is the source of antiferromagnetism e.g. in cuprate oxides, where holes localized at copper cations hybridize through the oxygen anion.

## 2.3 Fermionization

Let us now begin the description of our method to solve the quantum spin problem. In order to study general quantum spin systems, we choose to fermionize the spin system by a more general transformation than the Jordan-Wigner transformation, since the latter is only practical in one spatial dimension. The Hamiltonian is assumed to be of the general form

$$H = \sum_{\substack{i,j=1 \\ i \neq j}}^N J_{ij} \mathbf{S}_i \cdot \mathbf{S}_j. \quad (2.27)$$

The spin operators satisfy the angular momentum commutation relations

$$[S_i^\alpha, S_j^\beta] = i\epsilon^{\alpha\beta\gamma} S_i^\gamma \delta_{ij}. \quad (2.28)$$

Here  $\epsilon^{\alpha\beta\gamma}$  is the totally antisymmetric tensor. Let us now write the spin operators as spin operators of a fermionic particle,

$$S_i^k = \frac{1}{2} c_{i\alpha}^\dagger \sigma_{\alpha\beta}^k c_{i\beta}, \quad (2.29)$$

where  $\sigma^k$  are the Pauli matrices satisfying the commutation relations

$$[\sigma^i, \sigma^j] = 2i\epsilon^{ijk} \sigma^k \quad (2.30)$$

and the operators  $c, c^\dagger$  satisfy the anticommutation relations

$$\{c_{i\alpha}, c_{j\beta}^\dagger\} = \delta_{ij} \delta_{\alpha\beta}. \quad (2.31)$$

Here and in the following we always sum over repeated spin indices. It is straightforward to show that the angular momentum commutation relations are preserved in the transformation. With this substitution, one gets the Hamiltonian

$$H = \sum_{\substack{i,j=1 \\ i \neq j}}^N \frac{J_{ij}}{4} \sigma_{\alpha\beta}^k \sigma_{\gamma\delta}^k c_{i\alpha}^\dagger c_{i\beta} c_{j\gamma}^\dagger c_{j\delta}. \quad (2.32)$$

In addition to Greek spin indices, we also sum over the Pauli index  $k$  without specifying it explicitly. Since there are no local spin interactions, the Hamiltonian can be normal-ordered to the form

$$H = \frac{1}{2} \sum_{i,j=1}^N \frac{J_{ij}}{4} \sigma_{\alpha\beta}^k \sigma_{\gamma\delta}^k c_{i\alpha}^\dagger c_{j\gamma}^\dagger c_{j\delta} c_{i\beta}, \quad (2.33)$$

where we define  $J_{ii} = 0$ .

One could argue that the fermionization transformation (2.29) is no true transformation, if the spins were electron spins in the first place. However, in the derivation of the Heisenberg Hamiltonian (2.25), we restricted the Hilbert space to the space of singly-occupied sites, and the Heisenberg form is only valid in this subspace. Therefore, Hamiltonians (2.27) and (2.33) are not equivalent in general: assuming that the system contains  $N$  sites, the original Heisenberg Hamiltonian operates in a Hilbert space of dimension  $2^N$ , whereas the Fock space of the fermionized Hamiltonian contains also empty and doubly occupied sites, making the Hilbert space  $4^N$ -dimensional. States with empty or doubly-occupied sites are termed unphysical. Given a state  $|unphys\rangle_i$  with an unphysical occupation number  $n_i = 0$  or  $n_i = 2$  at the site  $i$ , the state has the important property that

$$S_i^k |unphys\rangle_i = 0 \quad (2.34)$$

for any spin operator  $S_i^k$ ,  $k = x, y, z$ . Note that if we had chosen the  $c$ -operators to satisfy bosonic commutation relations, the unphysical Hilbert space would be much larger.

It is important to note that since the Hamiltonian (2.33) commutes with all occupation number operators  $\hat{n}_i$  (see Sect. 3.2), the eigenstates can be classified according to their occupation numbers. Therefore, all eigenstates are either purely physical,  $n_i = 1 \forall i$ , or unphysical,  $n_i \neq 1$  for some  $i$ . The physicality of the ground state is a reasonable assumption for the spin system, since vacancy or double-occupation at any site corresponds to a spin system in which the site has been removed. This follows directly from Eq. (2.34). Therefore, assuming the ground state to be close to the ordered state, one could expect the unphysical states to be separated from the ground state by a gap  $\sim J$ .

In order to use methods of many-body theory, we would like to relax the strict constraint  $n_i = 1$  and allow fluctuations in the particle number. Basically, we would like to work in the grand canonical ensemble with a chemical potential  $\mu$ . How do the unphysical states affect the thermodynamic properties of the system in that case? Let us assume  $|n\rangle$  to be an unphysical state such that  $\hat{n}_i |n\rangle = 0$  for some site  $i$ . Then, the state  $|\tilde{n}\rangle = c_{i\uparrow}^\dagger c_{i\downarrow}^\dagger |n\rangle$  satisfies  $\hat{n}_i |\tilde{n}\rangle = 2|\tilde{n}\rangle$ . From Eq. (2.34), it follows that the matrix elements  $\langle n|H|n\rangle$  and  $\langle \tilde{n}|H|\tilde{n}\rangle$  agree. Then in the grand canonical partition function, the contribution from these two states is

$$Z = \text{Tr} e^{-\beta(\tilde{H}-\mu N)} \quad (2.35)$$

$$\supset \langle n|e^{-\beta(\tilde{H}-\mu N)}|n\rangle + \langle \tilde{n}|e^{-\beta(\tilde{H}-\mu N)}|\tilde{n}\rangle \quad (2.36)$$

$$= e^{\beta\mu(N-1)} (1 + e^{2\beta\mu}) \langle n|e^{-\beta H}|n\rangle. \quad (2.37)$$

By choosing the chemical potential to be  $\mu = i\pi/2\beta$ , the term in parentheses is zero, and therefore the contribution from unphysical states cancels in the partition function. This cancellation was first noticed by Popov and Fedotov[47]. Therefore, at any finite temperature, all thermodynamic variables for the grand canonical fermion system agree exactly with the corresponding variables for the spin system.

What happens at  $T = 0$ ? Since the thermodynamic potential is then completely determined by the ground state, thermodynamic variables are unaffected by the presence of any unphysical states, as long as the ground state is physical. Therefore one can choose simply  $\mu = 0$ , meaning that the grand canonical and canonical potentials agree with the internal energy and therefore e.g. the ground state energy of the fermion system should automatically agree with the energy of the spin system.

In practice, however, one is also interested in calculating correlation functions (see next chapter) between operators  $A$  and  $B$ ,

$$\mathcal{G}_{AB}(\tau) = \langle T_\tau A(\tau) B \rangle, \quad (2.38)$$

where  $A(\tau) = e^{H\tau} A e^{-H\tau}$ . The instant correlation function corresponds to  $\tau = 0$ , and is for  $T = 0$  simply the ground-state expectation value

$$\mathcal{G}_{AB}(0^+) = \langle G | AB | G \rangle. \quad (2.39)$$

If the ground state  $|G\rangle$  is physical, the instant correlation function is unaffected by the presence of unphysical states.

For  $\tau \neq 0$ , the correlation function contains time evolution and the unphysical states could play a role. To see if this is true, let us consider the dynamic correlation function

$$\mathcal{G}_{AB}(\omega) = \int_0^\infty d\tau e^{i\omega\tau} \mathcal{G}_{AB}(\tau) \quad (2.40)$$

in the Lehmann representation:

$$\mathcal{G}_{AB}(\omega) = \sum_n \frac{\langle n | A | G \rangle \langle G | B | n \rangle}{i\omega - (E_n - E_G)} + c.c., \quad (2.41)$$

where  $\{|n\rangle\}$  is an eigenbasis of the Hamiltonian. It seems that due to the summation over all states, the influence of unphysical states is only suppressed by the gap between the ground state and the unphysical states. However, if the operators  $A$  and  $B$  commute with local occupation number operators  $\hat{n}_i$ , the matrix elements between the ground state and any unphysical state must vanish. This can be seen by noting that for any site  $i$

$$0 = \langle n | [\hat{n}_i, A] | G \rangle = (n_i - 1) \langle n | A | G \rangle, \quad (2.42)$$

where  $n_i$  is the occupation at site  $i$  in the state  $|n\rangle$ . Therefore, if any  $n_i \neq 1$ ,  $\langle n | A | G \rangle = 0$ . Therefore, correlations of any local single-particle operators such as spin operators are unaffected by the unphysical states. Similarly, density-density correlations should only contain contributions from the physical states. Later, we will calculate both instant and dynamic correlation functions to see if the agreement with exact results is better for either of them.

As a first step in attacking the Hamiltonian (2.33), we make our first approximation: we implement the constraint  $n_i = 1$  only on average, i.e.  $\langle \hat{n}_i \rangle = 1$ . Due to particle-hole symmetry, this can be achieved by choosing  $\mu = 0$ . Working in the grand canonical ensemble allows us to calculate Green's functions and to gain

information about the basic excitations in the system using the well-known methods of many-body theory. We focus only on zero temperature, since in this case the unphysical states should play automatically no role, as shown above. There has been some work to extend the functional renormalization group method presented in the forth-coming chapters to a finite temperature[17], but the success of this extension is currently unknown.

Let us note already that Hamiltonian (2.33) is very special, since there is no kinetic term. Therefore, the free system which will be used as a reference state in future calculations is completely dispersionless. The interaction term is of a typical Coulomb interaction form, with the exception that instead of a spin-conserving  $\delta_{\alpha\beta}$ , the interaction vertex contains an  $SU(2)$  generator  $\sigma_{\alpha\beta}^k/2$ . This is analogous to gauge theories: in quantum chromodynamics, for example, the interaction vertex between fermions and gauge bosons contains an  $SU(3)$  generator, whose representation can be chosen to be the corresponding Gell-Mann matrix.

The goal of the next chapter is to introduce many-body theory and pave the way for the functional renormalization group solution of the Hamiltonian (2.33).

# Chapter 3

## Green's functions

*Chapter 3 is devoted to the fermionic many-body theory. In Section 3.1, we briefly review the importance of Green's functions and introduce the imaginary-time formalism used in all calculations. The symmetries of the spin Hamiltonian and how they constrain the Green's functions is the subject of Section 3.2. In Section 3.3, we introduce Grassmann variables and derive the functional integral formulas for the partition function and Matsubara Green's functions. Finally Section 3.4 introduces the generating functionals, for which the functional renormalization group flow equations will be calculated in Chapter 4.*

### 3.1 Introduction

The ultimate goal of quantum many-body theory is to calculate so-called Green's functions of the theory, since they can be used to determine all thermodynamic observables and response functions of the system [48, 49, 50, 51]. Physically, the most interesting Green's function of two operators  $A$  and  $B$  is the retarded Green's function

$$G_{AB}^R(t, t') = -i\theta(t - t')\langle[A(t), B(t')]_{-\xi}\rangle. \quad (3.1)$$

Here  $\xi = +$  if  $A$  and  $B$  are bosonic operators and  $\xi = -$  for fermionic operators. The (anti-)commutator is defined

$$[A, B]_{-\xi} = AB - \xi BA. \quad (3.2)$$

We assume that the operators are time-independent in the Schrödinger picture, so the time evolution in expressions such as  $A(t)$  is always given by the Heisenberg picture<sup>1</sup>:

$$A(t) = e^{iKt} A e^{-iKt}, \quad (3.3)$$

where  $K = H - \mu N$ . Here  $H$  is the Hamiltonian operator,  $\mu$  the chemical potential and  $N$  the total particle number. We work in the grand canonical ensemble.

---

<sup>1</sup>We choose our units such that  $\hbar = k_B = 1$ , where  $\hbar$  is the Planck's constant and  $k_B$  is the Boltzmann constant.

The expectation value (3.1) is defined

$$\langle A(t) \rangle = \text{Tr}(\rho A(t)), \quad (3.4)$$

where  $\rho$  is the density operator of the system in the Heisenberg picture. Although non-equilibrium Green's functions can be straightforwardly handled by defining the so-called Keldysh contour, we will restrict our analysis on equilibrium systems, meaning that all thermodynamic observables and response functions can be extracted by working solely in the imaginary time axis, as discussed below. In thermodynamic equilibrium,

$$\rho = \frac{1}{\mathcal{Z}} e^{-\beta K}, \quad (3.5)$$

where  $\beta = 1/T$  is the inverse temperature and  $\mathcal{Z}(T, V, \mu) = \text{Tr}(e^{-\beta K})$  is the grand canonical partition function. The grand canonical potential of system, from which all thermodynamic observables can be calculated, is then

$$\Omega(T, V, \mu) = -T \ln \mathcal{Z}(T, V, \mu). \quad (3.6)$$

The retarded Green's function (3.1) is important, since it determines the response of the system to external perturbations. Assuming a small perturbing Hamiltonian  $H' = F(t)B$ , where  $F(t)$  is an ordinary function that is non-zero only for  $t > t_0$ , the response of an observable  $A$  in the linear order in  $F$  is

$$\langle \delta A \rangle(t) = \int_{t_0}^{\infty} dt' G_{AB}^R(t, t') F(t'). \quad (3.7)$$

This is the famous Kubo formula[52]. Importantly, the Green's function in the expression above is defined with respect to the *unperturbed* Hamiltonian, meaning that the linear non-equilibrium response of the system is fully determined by the equilibrium properties.

The probing of linear response is not just of experimental relevance, but also of direct theoretical interest: the probe can be a fictitious operator that measures the instabilities of the system. Since instabilities lead to phase transitions, the microscopic response of the system gives information about macroscopic collective behaviour. For example, the ferromagnetic transition translates to a divergence in the spin-spin correlation function, whereas the superconducting BCS transition is an instability in the particle-particle (or hole-hole) correlation function, corresponding to generation of Cooper pairs.

In many-body physics, one is typically most interested in how particle and hole excitations propagate in the system. Therefore the main case of interest is  $A = c_{i_1}$  and  $B = c_{i_2}^\dagger$ , where  $i_1$  and  $i_2$  contain all relevant single-particle quantum numbers, typically e.g. momentum and spin. At  $T = 0$ , one can then calculate the effect of many-body interactions perturbatively[49] by deriving perturbative expressions for the time-ordered Green's function

$$\mathcal{G}_{i_1 i_2}(t_1, t_2) = -i \left\langle G \left| T_t c_{i_1}(t_1) c_{i_2}^\dagger(t_2) \right| G \right\rangle, \quad (3.8)$$

where  $T_t$  is the chronological time-ordering operator:

$$T_t A(t_1) B(t_2) = \begin{cases} A(t_1) B(t_2), & t_1 > t_2 \\ \xi B(t_2) A(t_1), & t_1 < t_2 \end{cases} \quad (3.9)$$

and  $|G\rangle$  is the ground state of the interacting system. At  $T > 0$ , real-time Green's functions become awkward objects to expand in the interaction parameter, since the interaction operator appears in two places: both in the Heisenberg time-evolution  $\exp(iKt)$  and in the density operator  $\rho = \exp(-\beta K)/\mathcal{Z}$ . Therefore, one defines imaginary time as  $\tau = it$ , where  $\tau$  is a real number. In this way, the density operator  $\rho = e^{-\beta K}/\mathcal{Z}$  can be simply understood as time evolution in imaginary time. The time-ordered imaginary-time  $m$ -particle Green's function is defined

$$\mathcal{G}^{(m)}(1', \dots, m' | 1, \dots, m) \equiv (-1)^m \langle T_\tau c_{1'} \dots c_{m'} c_m^\dagger \dots c_1^\dagger \rangle, \quad (3.10)$$

where each composite index  $j = (\tau_j, i_j)$  consists of a time-index  $\tau_i$  and a single-particle quantum number  $i_j$ . As stated in Sect. 2.3, we will work at  $T = 0$ , and therefore the introduction of imaginary time is not necessary, in principle. Although one could perhaps derive the functional renormalization group equations even for real-time Green's functions, we contend with using the better-known imaginary-time formalism. The price to pay is that we get all correlation functions  $\chi(z)$  on the imaginary axis ( $z = i\omega$ ) and analytic continuation  $i\omega \rightarrow \omega + i0^+$  is necessary to calculate e.g. the spectral function. This is a well-known problem shared by e.g. the Quantum Monte Carlo method.

Since we will later work in frequency space, let us define our convention for the Fourier transformed Green's function:

$$\tilde{\mathcal{G}}^{(m)}(\tilde{1}', \dots, \tilde{m}' | \tilde{1}, \dots, \tilde{m}) = \int d\tau_{1'} \dots d\tau_{m'} d\tau_1 \dots d\tau_m e^{i(\sum \omega_i \tau_i - \sum \omega_{i'} \tau_{i'})} \mathcal{G}^{(m)}(1', \dots, m' | 1, \dots, m), \quad (3.11)$$

where  $\tilde{j} = (\omega_j, i_j)$ . Later we will drop the tildes in the variables, since the composite index may equally well contain either the time index or frequency index. We also denote the Fourier transformed functions with the same letter as the original function, since there should be no danger of confusion.

The goal of the next section is to see how the symmetries of the spin Hamiltonian (2.33) restrict the form of the Green's functions. Symmetries play a very important role in the numerical solution, since they determine the structure of the Green's function in frequency, spin and position arguments. The computational effort of determining the full general Green's function directly with no parametrizations would be insurmountable.

## 3.2 Symmetries of the spin Hamiltonian

### Spin rotational invariance

Let us begin by global spin rotations. In the following, we will only concentrate on spin-1/2 fermions, for which the finite-dimensional representations of spin rotations

are two-dimensional. The annihilation and creation operators for a fermion of spin  $\alpha$  are notated by  $c_\alpha$  and  $c_\alpha^\dagger$ , where all quantum numbers except for spin are suppressed. Let us define the spin rotation operator  $\hat{R}$  such that

$$\begin{cases} \hat{R}c_\alpha\hat{R}^\dagger &= R_{\alpha\beta}c_\beta, \\ \hat{R}c_\alpha^\dagger\hat{R}^\dagger &= c_\beta^\dagger R_{\alpha\beta}^*, \end{cases} \quad (3.12)$$

where  $R_{\alpha\beta}$  is the representation of the spin rotation and sums over all repeated indices are implicitly assumed. To respect the anti-commutation relations,  $R$  has to be a unitary matrix, i.e.  $R \in U(2)$ . In addition, since we are only interested in continuous rotations without reflections, we restrict our analysis on the special unitary group  $SU(2)$ . It then follows that the matrix can be expressed in the form

$$R = \exp\left(-i\epsilon^k \frac{\sigma^k}{2}\right), \quad (3.13)$$

where  $\sigma^k$ ,  $k = 1, 2, 3$  are the Pauli matrices, i.e. the generators of  $SU(2)$ . Since  $SU(2)$  is a Lie group and all finite transformations can be inferred from the infinitesimal ones, we can assume that  $\epsilon^k$  are infinitesimal to make calculations simpler.

Let us now see how different operators transform in this operation. The spin operator

$$S^k = \frac{1}{2}c_\alpha^\dagger \sigma_{\alpha\beta}^k c_\beta \quad (3.14)$$

becomes

$$\hat{R}S^k\hat{R}^\dagger = \frac{1}{2}c_\gamma^\dagger R_{\gamma\alpha}^* \sigma_{\alpha\beta}^k R_{\beta\delta} c_\delta \quad (3.15)$$

$$= c_\gamma^\dagger \left( \frac{1}{2}\sigma^k + i\epsilon^j \underbrace{[\sigma^j/2, \sigma^k/2]}_{i\epsilon^{jkm}\sigma^m/2} + \mathcal{O}(\epsilon^2) \right)_{\gamma\delta} c_\delta \quad (3.16)$$

$$= S^k + \epsilon^{kjm}\epsilon^j S^m + \mathcal{O}(\epsilon^2), \quad (3.17)$$

where  $\epsilon^{ijk}$  is the fully anti-symmetric Levi-Civita symbol. This means that the spin operators transform in the adjoint (vector) representation of  $SU(2)$ , i.e. basically in the rotation group  $SO(3)$ , as expected. It is also clear that dot products of the form  $\mathbf{S}_i \cdot \mathbf{S}_j$ , where  $i$  and  $j$  are site indices, are invariant in global spin rotations. One can also easily show that density interactions, being of the form

$$\hat{V} \sim \delta_{\alpha_1\alpha_4} \delta_{\alpha_2\alpha_3} c_{\alpha_1}^\dagger c_{\alpha_2}^\dagger c_{\alpha_3} c_{\alpha_4}, \quad (3.18)$$

are invariant.

Since the operator  $\hat{R}$  is unitary, states  $\{\hat{R}^\dagger|m\rangle\}$  form a complete set if  $\{|m\rangle\}$  is a complete set. Therefore, the spin structure of the two-particle Matsubara Green's



function has to obey (suppressing time indices)

$$\mathcal{G}_{\alpha\beta} = -\langle T_\tau c_\alpha c_\beta^\dagger \rangle \quad (3.19)$$

$$= -\sum_m \langle \hat{R}^\dagger m | \rho_H T_\tau c_\alpha c_\beta^\dagger | \hat{R}^\dagger m \rangle \quad (3.20)$$

$$= -\sum_m \langle m | \hat{R} \rho_H \hat{R}^\dagger T_\tau \hat{R} c_\alpha \hat{R}^\dagger \hat{R} c_\beta^\dagger \hat{R} | m \rangle \quad (3.21)$$

$$= -\sum_m \langle m | \rho_H T_\tau R_{\alpha\gamma} c_\gamma c_\delta^\dagger R_{\beta\delta}^* | m \rangle \quad (3.22)$$

$$= R_{\alpha\gamma} \mathcal{G}_{\gamma\delta} R_{\beta\delta}^*. \quad (3.23)$$

Here we have assumed spin rotational invariance,  $H = \hat{R} H \hat{R}^\dagger$ . The logic used here will be used basically in all symmetry-related derivations below, with the exception that e.g. for time-reversal symmetry one has to be careful about the correct time-ordering in the manipulations.

We have thus showed that the spin structure of the Green's function has to obey

$$\mathcal{G} = R \mathcal{G} R^\dagger \quad (3.24)$$

for an arbitrary  $R \in SU(2)$ . Here  $\mathcal{G}$  is a matrix with elements  $\mathcal{G}_{\alpha\beta}$ . Since  $\mathcal{G}$  is Hermitian in the spin space if  $\mathcal{G}$  is symmetric in other quantum numbers (this is usually the case e.g. in position and momentum bases), it can be expanded as

$$\mathcal{G} = a \mathbf{I} + b^k \sigma^k. \quad (3.25)$$

Equation (3.24) then directly implies that  $b^k = 0$ ,  $k = 1, 2, 3^2$ , meaning that

$$\mathcal{G}_{\alpha\beta} \sim \delta_{\alpha\beta}, \quad (3.26)$$

i.e. the Green's function is diagonal in spin space. For a spin-rotationally invariant system this is, of course, quite a trivial result, but the full machinery of rigorous manipulations of this type becomes necessary e.g. for many-particle Green's functions. For the two-particle Green's function, spin-rotational invariance implies

$$\mathcal{G}_{\alpha_1\alpha_2;\alpha_3\alpha_4} = R_{\alpha_1\beta_1} R_{\alpha_2\beta_2} \mathcal{G}_{\beta_1\beta_2;\beta_3\beta_4} R_{\alpha_4\beta_4}^* R_{\alpha_3\beta_3}^*. \quad (3.27)$$

Since the only invariants are the Kronecker deltas  $\delta_{\alpha_1\alpha_3} \delta_{\alpha_2\alpha_4}$ ,  $\delta_{\alpha_1\alpha_4} \delta_{\alpha_2\alpha_3}$  and linear combinations of them, the spin structure is

$$\mathcal{G}_{\alpha_1\alpha_2;\alpha_3\alpha_4} = A \delta_{\alpha_1\alpha_3} \delta_{\alpha_2\alpha_4} + B \delta_{\alpha_1\alpha_4} \delta_{\alpha_2\alpha_3}. \quad (3.28)$$

---

<sup>2</sup>In a finite magnetic field  $h$ , only rotations around z-axis are allowed and this argument only holds for  $k = 1, 2$ .

## Local particle number conservation

In addition to the usual global  $U(1)$  symmetry of quantum mechanics, corresponding to the conservation of the total particle number, the Heisenberg Hamiltonian has a *local*  $U(1)$  symmetry. Due to locality of the Hamiltonian  $H$ , the Hamiltonian commutes with all local particle number operators  $\hat{n}_i$ :  $[H, \hat{n}_i] = 0$ . Therefore, the Hamiltonian remains unchanged in the phase transformation

$$\begin{cases} c_{i\alpha} & \rightarrow e^{i\varphi_i \hat{n}_i} c_{i\alpha} e^{-i\varphi_i \hat{n}_i} = e^{-i\varphi_i} c_{i\alpha}, \\ c_{i\alpha}^\dagger & \rightarrow e^{i\varphi_i \hat{n}_i} c_{i\alpha}^\dagger e^{-i\varphi_i \hat{n}_i} = e^{i\varphi_i} c_{i\alpha}^\dagger. \end{cases} \quad (3.29)$$

The local phase transformation symmetry means that the two-point function is local:

$$\mathcal{G}_{ij} = -\langle T_\tau c_i c_j^\dagger \rangle \quad (3.30)$$

$$\stackrel{\text{Eq. (3.29)}}{=} -\langle T_\tau e^{-i\varphi_i} c_i e^{i\varphi_j} c_j^\dagger \rangle \quad (3.31)$$

$$= e^{i(\varphi_j - \varphi_i)} \mathcal{G}_{ij}, \quad (3.32)$$

which can only hold for arbitrary  $\varphi_i, \varphi_j$  if  $\mathcal{G}_{ij} \propto \delta_{ij}$ . Combined with spin-rotational invariance, we therefore know that the one-particle Green's function is of the form

$$\mathcal{G}(i_1, \alpha_1, \omega_1; i_2, \alpha_2, \omega_2) = \mathcal{G}(\omega_1; \omega_2) \delta_{i_1 i_2} \delta_{\alpha_1 \alpha_2}, \quad (3.33)$$

where we also assumed translational invariance so that  $\mathcal{G}(\omega_1; \omega_2)$  does not depend on the site index.

For the two-particle function  $-\langle T_\tau c_{i_1} c_{i_2} c_{i_4}^\dagger c_{i_3}^\dagger \rangle$ , the symmetry implies that the function can only be non-vanishing if either  $i_1 = i_3$  and  $i_2 = i_4$  or  $i_1 = i_4$  and  $i_2 = i_3$ . Assuming also spin-rotational invariance, the two-point function must be of the form ( $\xi = (\omega, i, \alpha)$ )

$$\begin{aligned} \mathcal{G}(\xi_1, \xi_2; \xi_3, \xi_4) &= A_{i_1 i_2}(\omega_1, \omega_2; \omega_3, \omega_4) \delta_{\alpha_1 \alpha_3} \delta_{\alpha_2 \alpha_4} \delta_{i_1 i_3} \delta_{i_2 i_4} \\ &\quad + B_{i_1 i_2}(\omega_1, \omega_2; \omega_3, \omega_4) \delta_{\alpha_1 \alpha_4} \delta_{\alpha_2 \alpha_3} \delta_{i_1 i_3} \delta_{i_2 i_4} \\ &\quad + C_{i_1 i_2}(\omega_1, \omega_2; \omega_3, \omega_4) \delta_{\alpha_1 \alpha_3} \delta_{\alpha_2 \alpha_4} \delta_{i_1 i_4} \delta_{i_2 i_3} \\ &\quad + D_{i_1 i_2}(\omega_1, \omega_2; \omega_3, \omega_4) \delta_{\alpha_1 \alpha_4} \delta_{\alpha_2 \alpha_3} \delta_{i_1 i_4} \delta_{i_2 i_3}. \end{aligned} \quad (3.34)$$

Using the anti-symmetry of the Green's function in the exchange ( $1 \leftrightarrow 2$ ), one gets

$$D_{i_2 i_1}(\omega_2, \omega_1; \omega_3, \omega_4) = -A_{i_1 i_2}(\omega_1, \omega_2; \omega_3, \omega_4) \quad (3.35)$$

and

$$C_{i_2 i_1}(\omega_2, \omega_1; \omega_3, \omega_4) = -B_{i_1 i_2}(\omega_1, \omega_2; \omega_3, \omega_4). \quad (3.36)$$

Therefore,

$$\begin{aligned} \mathcal{G}(\xi_1, \xi_2; \xi_3, \xi_4) &= [A_{i_1 i_2}(\omega_1, \omega_2; \omega_3, \omega_4) \delta_{\alpha_1 \alpha_3} \delta_{\alpha_2 \alpha_4} \\ &\quad + B_{i_1 i_2}(\omega_1, \omega_2; \omega_3, \omega_4) \delta_{\alpha_1 \alpha_4} \delta_{\alpha_2 \alpha_3}] \delta_{i_1 i_3} \delta_{i_2 i_4} \\ &\quad - \text{exchange } (1 \leftrightarrow 2). \end{aligned} \quad (3.37)$$

For spin interactions, it is convenient to reparametrize the spin structure by using the  $SU(N)$  identity

$$T_{\alpha\beta}^k T_{\gamma\delta}^k = T_F \left( \delta_{\alpha\delta} \delta_{\beta\gamma} - \frac{1}{N} \delta_{\alpha\beta} \delta_{\gamma\delta} \right) \quad (3.38)$$

for  $N = 2$ ,  $T^k = \sigma^k/2$  and  $T_F \equiv \text{Tr}(T^k T^k) = 1/2$  (no sum over  $k$ ). Defining

$$\mathcal{G}_{si_1 i_2}(\omega_1, \omega_2; \omega_3, \omega_4) = \frac{1}{2} B_{i_1 i_2}(\omega_1, \omega_2; \omega_3, \omega_4) \quad (3.39)$$

and

$$\mathcal{G}_{di_1 i_2}(\omega_1, \omega_2; \omega_3, \omega_4) = A_{i_1 i_2}(\omega_1, \omega_2; \omega_3, \omega_4) + \frac{1}{2} B_{i_1 i_2}(\omega_1, \omega_2; \omega_3, \omega_4), \quad (3.40)$$

the Green's function becomes

$$\begin{aligned} \mathcal{G}(\xi_1, \xi_2; \xi_3, \xi_4) = & [\mathcal{G}_{si_1 i_2}(\omega_1, \omega_2; \omega_3, \omega_4) \sigma_{\alpha_1 \alpha_3}^k \sigma_{\alpha_2 \alpha_4}^k \\ & + \mathcal{G}_{di_1 i_2}(\omega_1, \omega_2; \omega_3, \omega_4) \delta_{\alpha_1 \alpha_3} \delta_{\alpha_2 \alpha_4}] \delta_{i_1 i_3} \delta_{i_2 i_4} \\ & - \text{exchange } (1 \leftrightarrow 2). \end{aligned} \quad (3.41)$$

The property

$$\mathcal{G}(\xi_1, \xi_2; \xi_3, \xi_4) = \mathcal{G}(\xi_2, \xi_1; \xi_4, \xi_3) \quad (3.42)$$

then implies

$$\mathcal{G}_{s/d, i_1 i_2}(\omega_1, \omega_2; \omega_3, \omega_4) = \mathcal{G}_{s/d, i_2 i_1}(\omega_2, \omega_1; \omega_4, \omega_3). \quad (3.43)$$

## Time-reversal invariance

Let us now move on to discrete symmetries and start with time-reversal invariance. We will not give a full review on the time-reversal operator but contend with stating the most important properties[45, 53]. Intuitively, we want the time-reversal operator  $T$  to satisfy

$$T \hat{x} T^{-1} = \hat{x}, \quad T \hat{p} T^{-1} = -\hat{p}, \quad T \hat{S} T^{-1} = -\hat{S}, \quad (3.44)$$

where  $\hat{x}$ ,  $\hat{p}$  and  $\hat{S}$  are the position, momentum and spin operators, respectively. From the requirement of translational invariance,

$$T(\hat{x} + a)T^{-1} = \hat{x} + a, \quad (3.45)$$

it follows by using  $\hat{x} + a = \exp(i\hat{p}a)\hat{x}\exp(-i\hat{p}a)$  that  $T$  has to be an antilinear operator:  $T\lambda = \lambda^*T$  for  $\lambda \in \mathbb{C}$ . Moreover, it is straightforward to show that the intuitive definition

$$T|x, \alpha\rangle = |x, -\alpha\rangle, \quad (\text{wrong!}) \quad (3.46)$$

which is equivalent to  $T|p, \alpha\rangle = |-p, -\alpha\rangle$ , does not satisfy  $T\hat{S}T^{-1} = -\hat{S}$  for the  $x$  and  $y$ -components of spin. Here  $\alpha = \pm 1/2$  is the  $z$ -component of spin. A working definition is

$$T|x, \alpha\rangle = e^{i\pi\alpha}|x, -\alpha\rangle. \quad (3.47)$$

Then it is easy to show that all the requirements of Eq. (3.44) are satisfied and that  $T$  is antiunitary, i.e. for all  $|\psi\rangle$  and  $|\chi\rangle$  it satisfies

$$\langle\psi|T\chi\rangle = \langle T^{-1}\psi|\chi\rangle^*, \quad (3.48)$$

where, in contrast to linear unitary operators, the complex conjugation is necessary due to the antilinearity of  $T$ .

For the creation and annihilation operators, definition (3.47) leads to

$$\begin{cases} Ta_{i\alpha}^\dagger T^\dagger &= e^{i\pi\alpha} a_{i\bar{\alpha}}^\dagger, \\ Ta_{i\alpha} T^\dagger &= e^{-i\pi\alpha} a_{i\bar{\alpha}}. \end{cases} \quad (3.49)$$

Here  $i$  is the lattice site index and  $\bar{\alpha} = -\alpha$ . It is then straightforward to show that the spin operators indeed satisfy  $\mathbf{S} \rightarrow -\mathbf{S}$  and therefore, the Heisenberg Hamiltonian is time-reversal invariant.

To see what implications the time-reversal invariance has for the Green's functions, let us first see how Heisenberg operators transform. In imaginary time, Heisenberg operators transform as

$$TA(\tau)T^\dagger = Te^{Ht}T^\dagger TAT^\dagger Te^{-Ht}T^\dagger = \tilde{A}(\tau)_{\tilde{H}}, \quad (3.50)$$

where  $\tilde{A} = TAT^\dagger$ ,  $\tilde{H} = THT^\dagger$  and the lower index in the final expression means that time-evolution is given by the Hamiltonian  $\tilde{H}$ . Thermal expectation values satisfy

$$\langle A(\tau) \rangle \equiv \sum_m \langle m | \rho_H A(\tau) | m \rangle \quad (3.51)$$

$$= \sum_m \langle T^\dagger m | \rho_H A(\tau) | T^\dagger m \rangle \quad (3.52)$$

$$= \sum_m \langle m | T \rho_H T^\dagger T A(\tau) T^\dagger | m \rangle^* \quad (3.53)$$

$$= \sum_m \langle m | \rho_{\tilde{H}} \tilde{A}(\tau)_{\tilde{H}} | m \rangle^* \quad (3.54)$$

$$\equiv \langle \tilde{A}(\tau)_{\tilde{H}} \rangle_{\tilde{H}}^*. \quad (3.55)$$

Time-reversal invariance (TRI) implies that  $\tilde{H} = H$  and therefore

$$\langle A(\tau) \rangle = \langle \tilde{A}(\tau) \rangle^*, \quad (3.56)$$

which will be used repeatedly in the following.

For the one-particle Matsubara Green's function  $\mathcal{G}(\tau_1 i_1 \alpha_1; \tau_2, i_2, \alpha_2)$ , one gets (assume  $\tau_1 > \tau_2$  without loss of generality)

$$\mathcal{G}(\tau_1 i_1 \alpha_1; \tau_2 i_2 \alpha_2) = - \left\langle c_{i_1 \alpha_1}(\tau_1) c_{i_2 \alpha_2}^\dagger(\tau_2) \right\rangle \quad (3.57)$$

$$\stackrel{\text{TRI}}{=} - \left\langle e^{-i\alpha_1} c_{i_1 \bar{\alpha}_1}(\tau_1) e^{i\alpha_2} c_{i_2 \bar{\alpha}_2}^\dagger(\tau_2) \right\rangle^* \quad (3.58)$$

$$= e^{i(\alpha_1 - \alpha_2)} \mathcal{G}(\tau_1, i_1, \bar{\alpha}_1; \tau_2, i_2, \bar{\alpha}_2)^* \quad (3.59)$$

Fourier transformation and the substitution of Eq. (3.33) then gives

$$\mathcal{G}(\omega_1; \omega_2) = \mathcal{G}(-\omega_1; -\omega_2)^*. \quad (3.60)$$

One can also carry out the complex conjugation in Eq. (3.58) to deduce that

$$\mathcal{G}(\omega_1; \omega_2) = \mathcal{G}(\omega_2; \omega_1), \quad (3.61)$$

which is trivial in equilibrium (see later). For the two-particle Green's function, one gets (assume  $\tau_1 > \tau_2 > \tau_4 > \tau_3$ )

$$\begin{aligned} & \mathcal{G}((\tau_1, i_1, \alpha_1), (\tau_2, i_2, \alpha_2); (\tau_3, i_3, \alpha_3), (\tau_4, i_4, \alpha_4)) \\ &= \left\langle c_{i_1 \alpha_1}(\tau_1) c_{i_2 \alpha_2}(\tau_2) c_{i_4 \alpha_4}^\dagger(\tau_4) c_{i_3 \alpha_3}^\dagger(\tau_3) \right\rangle \end{aligned} \quad (3.62)$$

$$\stackrel{\text{TRI}}{=} e^{i(\alpha_1 + \alpha_2 - \alpha_3 - \alpha_4)} \left\langle c_{i_1 \bar{\alpha}_1}(\tau_1) c_{i_2 \bar{\alpha}_2}(\tau_2) c_{i_4 \bar{\alpha}_4}^\dagger(\tau_4) c_{i_3 \bar{\alpha}_3}^\dagger(\tau_3) \right\rangle^* \quad (3.63)$$

$$= e^{i(\alpha_1 + \alpha_2 - \alpha_3 - \alpha_4)} \left\langle c_{i_3 \bar{\alpha}_3}(-\tau_3) c_{i_4 \bar{\alpha}_4}(-\tau_4) c_{i_2 \bar{\alpha}_2}^\dagger(-\tau_2) c_{i_1 \bar{\alpha}_1}^\dagger(-\tau_1) \right\rangle \quad (3.64)$$

$$\begin{aligned} &= e^{i(\alpha_1 + \alpha_2 - \alpha_3 - \alpha_4)} \\ &\times \mathcal{G}((-\tau_3, i_3, \bar{\alpha}_3), (-\tau_4, i_4, \bar{\alpha}_4); (-\tau_1, i_1, \bar{\alpha}_1), (-\tau_2, i_2, \bar{\alpha}_2)). \end{aligned} \quad (3.65)$$

Fourier transformation and the substitution of Eq. (3.41) gives

$$\mathcal{G}_{s/d, i_1 i_2}(\omega_1, \omega_2; \omega_3, \omega_4) = \mathcal{G}_{s/d, i_1 i_2}(\omega_3, \omega_4; \omega_1, \omega_2). \quad (3.66)$$

## Particle-hole symmetry

Since the spin Hamiltonian is naturally at half-filling in the ground state, one may expect the Hamiltonian to be particle-hole symmetric. Let us define a unitary operator  $\hat{M}$  such that

$$\begin{cases} \hat{M} c_{i\alpha} \hat{M}^\dagger &= c_{i\bar{\alpha}}^\dagger, \\ \hat{M} c_{i\alpha}^\dagger \hat{M}^\dagger &= c_{i\bar{\alpha}}. \end{cases} \quad (3.67)$$

The spin-flip in the definition is customary but unimportant for our purposes. The spin operators transform as

$$\begin{cases} \hat{M} S^x \hat{M}^\dagger &= -S^x, \\ \hat{M} S^y \hat{M}^\dagger &= -S^y, \\ \hat{M} S^z \hat{M}^\dagger &= S^z, \end{cases} \quad (3.68)$$

meaning that the particle-hole transformation is equal to a rotation of  $\pi$  around the  $z$ -axis in the spin space. Therefore, Heisenberg Hamiltonian is particle-hole symmetric. Note that a non-zero chemical potential in the fermionic Hamiltonian would spoil the invariance.

Particle-hole symmetry (PHS) implies for the one-particle Green's function that ( $\tau_1 > \tau_2$ )

$$\mathcal{G}(\tau_1, i_1, \alpha_1; \tau_2, i_2, \alpha_2) = - \left\langle c_{i_1 \alpha_1}(\tau_1) c_{i_2 \alpha_2}^\dagger(\tau_2) \right\rangle \quad (3.69)$$

$$\stackrel{\text{PHS}}{=} - \left\langle c_{i_1 \alpha_1}^\dagger(\tau_1) c_{i_2 \alpha_2}(\tau_2) \right\rangle \quad (3.70)$$

$$= + \left\langle T_\tau c_{i_2 \alpha_2}(\tau_2) c_{i_1 \alpha_1}^\dagger(\tau_1) \right\rangle \quad (3.71)$$

$$= -\mathcal{G}(\tau_2, i_2, \alpha_2; \tau_1, i_1, \alpha_1). \quad (3.72)$$

Fourier transformation and the substitution of Eq. (3.33) delivers

$$\mathcal{G}(\omega_1; \omega_2) = -\mathcal{G}(-\omega_2; -\omega_1). \quad (3.73)$$

For the two-particle function, one gets ( $\tau_1 > \tau_2 > \tau_4 > \tau_3$ )

$$\begin{aligned} & \mathcal{G}((\tau_1, i_1, \alpha_1), (\tau_2, i_2, \alpha_2); (\tau_3, i_3, \alpha_3), (\tau_4, i_4, \alpha_4)) \\ &= \left\langle c_{i_1 \alpha_1}(\tau_1) c_{i_2 \alpha_2}(\tau_2) c_{i_4 \alpha_4}^\dagger(\tau_4) c_{i_3 \alpha_3}^\dagger(\tau_3) \right\rangle \end{aligned} \quad (3.74)$$

$$\stackrel{\text{PHS}}{=} \left\langle c_{i_1 \bar{\alpha}_1}^\dagger(\tau_1) c_{i_2 \bar{\alpha}_2}^\dagger(\tau_2) c_{i_4 \bar{\alpha}_4}(\tau_4) c_{i_3 \bar{\alpha}_3}(\tau_3) \right\rangle \quad (3.75)$$

$$= \left\langle T_\tau c_{i_3 \bar{\alpha}_3}(\tau_3) c_{i_4 \bar{\alpha}_4}(\tau_4) c_{i_2 \bar{\alpha}_2}^\dagger(\tau_2) c_{i_1 \bar{\alpha}_1}^\dagger(\tau_1) \right\rangle \quad (3.76)$$

$$= \mathcal{G}((\tau_3, i_3, \bar{\alpha}_3), (\tau_4, i_4, \bar{\alpha}_4); (\tau_1, i_1, \bar{\alpha}_1), (\tau_2, i_2, \bar{\alpha}_2)). \quad (3.77)$$

Fourier transformation and the substitution of Eq. (3.41) gives

$$\mathcal{G}_{s/d, i_1 i_2}(\omega_1, \omega_2; \omega_3, \omega_4) = \mathcal{G}_{s/d, i_1 i_2}(-\omega_3, -\omega_4; -\omega_1, -\omega_2). \quad (3.78)$$

## Frequency structure

Let us finally simplify the frequency structure. Translational invariance in imaginary time implies that one of the frequency variables can be eliminated by the conservation of frequency:

$$\mathcal{G}(\omega_1; \omega_2) = \mathcal{G}(\omega_1) \beta \delta_{\omega_1 \omega_2} \quad (3.79)$$

and

$$\mathcal{G}(\omega_1, \omega_2; \omega_3, \omega_4) = \mathcal{G}(\omega_1, \omega_2; \omega_3) \beta \delta_{\omega_1 + \omega_2, \omega_3 + \omega_4}. \quad (3.80)$$

At  $T = 0$ , the Kronecker delta  $\beta \delta_{\omega_1 \omega_2}$  is replaced by  $2\pi \delta(\omega_1 - \omega_2)$ . Using Eqs. (3.60) and (3.73), one can deduce that

$$\mathcal{G}(\omega) \stackrel{\text{PHS}}{=} -\mathcal{G}(-\omega) \stackrel{\text{TRI}}{=} -\mathcal{G}(\omega)^*, \quad (3.81)$$

meaning that the one-particle Green's function is an odd and purely imaginary function.

For the two-particle function, parametrization in terms of frequencies  $\omega_1, \omega_2$  and  $\omega_3$  is not practical, since the application of time-reversal and particle-hole symmetries

would be cumbersome. We parametrize the frequency dependence by the three bosonic Mandelstam variables

$$\begin{cases} s = \omega_1 + \omega_2 \\ t = \omega_1 - \omega_3 \\ u = \omega_1 - \omega_4 \end{cases} \Leftrightarrow \begin{cases} \omega_1 = (s + t + u)/2 \\ \omega_2 = (s - t - u)/2 \\ \omega_3 = (s - t + u)/2 \\ \omega_4 = (s + t - u)/2 \end{cases} \quad (3.82)$$

and denote the functions obtained by this change of variables by the same letter  $\mathcal{G}$ , since there should be no risk of confusion. The symmetry (site indices suppressed)

$$\mathcal{G}_{s/d}(\omega_1, \omega_2; \omega_3, \omega_4) = \mathcal{G}_{s/d}(\omega_2, \omega_1; \omega_4, \omega_3)$$

then translates to

$$\mathcal{G}_{s/d}(s, t, u) = \mathcal{G}_{s/d}(s, -t, -u), \quad (3.83)$$

time-reversal symmetry

$$\mathcal{G}_{s/d}(\omega_1, \omega_2; \omega_3, \omega_4) = \mathcal{G}_{s/d}(\omega_3, \omega_4; \omega_1, \omega_2)$$

implies that

$$\mathcal{G}_{s/d}(s, t, u) = \mathcal{G}_{s/d}(s, -t, u), \quad (3.84)$$

and the particle-hole symmetry

$$\mathcal{G}_{s/d}(\omega_1, \omega_2; \omega_3, \omega_4) = \mathcal{G}_{s/d}(-\omega_3, -\omega_4; -\omega_1, -\omega_2)$$

finally gives

$$\mathcal{G}_{s/d}(s, t, u) = \mathcal{G}_{s/d}(-s, t, -u). \quad (3.85)$$

Combining Eqs. (3.83), (3.84) and (3.85), we can deduce that the Green's functions are symmetric in each variable  $s$ ,  $t$  and  $u$  separately.

In addition, we assume translational invariance. This means that the two-particle Green's function  $\mathcal{G}_{s/d,ij}$  only depends on the relative distance of sites  $i$  and  $j$ . Given a chain of  $N$  sites, one has to consider  $N/2 + 1$  distances in the numerical solution.

### 3.3 Grassmann variables and fermionic functional integrals

The goal of this chapter is to derive the functional integral formula for the quantum-mechanical partition function, which can then be extended to a formula for the thermal Green's functions and allows the introduction of generating functionals. In order to understand the derivation, we must first review the basic properties of Grassmann variables. The mathematical foundations of Grassmann variables are reviewed e.g. in Ref. [54], so we will only state the most important properties. Given a  $D$ -dimensional vector space  $\mathcal{V}$  over  $\mathbb{C}$ , the Grassmann algebra is defined as the alternating algebra:

$$\bigwedge \mathcal{V} = \bigoplus_{n=0}^D \bigwedge^n \mathcal{V}. \quad (3.86)$$

The multiplication operator of the algebra is the wedge product. If  $\mathcal{V}$  is given a basis  $\{a_1, \dots, a_D\}$ , wedge products of the form

$$\{a_{i_1} \wedge a_{i_2} \wedge \dots \wedge a_{i_n}\}_{1 \leq i_1 < i_2 < \dots < i_n \leq D} \quad (3.87)$$

form a basis for  $\bigwedge^n \mathcal{V}$ . In the following, we drop the wedge and write simply  $a_1 \wedge a_2 = a_1 a_2$ . The most important property of the wedge products is the antisymmetry  $a_1 a_2 = -a_2 a_1$ . Note that not all elements of the Grassmann algebra anticommute, since e.g.  $(a_1 a_2) a_3 = a_3 (a_1 a_2)$ .

Given a basis  $a_1, \dots, a_D$  to  $\mathcal{V}$ , we define the Berezin integral  $\int da_1 \dots da_D$  to be the unique linear mapping that satisfies

$$\int da_1 \dots da_D a_D \dots a_1 = 1 \quad (3.88)$$

and equals zero on other elements. It is straightforward to show that given another basis  $\{b_1, \dots, b_D\}$  to  $\mathcal{V}$  such that  $b_i = \sum_j M_{ij} a_j$ , the two integrals are related by

$$\int da_1 \dots da_D = \det M \int db_1 \dots db_D, \quad (3.89)$$

so the "Jacobian" of the transformation is the inverse of what one would expect for ordinary integrals. Given a skew-symmetric matrix  $Q$ , one can then show that

$$\int da_1 \dots da_D e^{-\frac{1}{2} a^T Q a} = \sqrt{\det Q}. \quad (3.90)$$

The Gaussian integral with covariance matrix  $S$ , which is assumed to be a skew-symmetric  $D \times D$ -matrix, is defined by the relation

$$\int d\mu_S(a) e^{\sum_i b_i a_i} = e^{-\frac{1}{2} \sum_{ij} b_i S_{ij} b_j}. \quad (3.91)$$

When  $D$  is even and  $S$  is invertible, which will be the case in quantum field theory, it can be shown that

$$\int d\mu_S(a) (\cdot) = \frac{\int da_1 \dots da_D e^{-\frac{1}{2} \sum_{ij} a_i S_{ij}^{-1} a_j} (\cdot)}{\int da_1 \dots da_D e^{-\frac{1}{2} \sum_{ij} a_i S_{ij}^{-1} a_j}}. \quad (3.92)$$

To extend the definition (3.91) to a Gaussian integral over monomials, one must define differentiation. We define the set of ordered  $n$ -multi-indices to be  $\mathcal{M}_n = \{(i_1, \dots, i_n)\}_{1 \leq i_1 < \dots < i_n \leq D}$  and write  $a_I = a_{i_1} \dots a_{i_n}$  for  $I \in \mathcal{M}_n$ . The left derivative of a monomial  $a_I$  with respect to an element  $a_l$  is defined as the linear map that satisfies

$$\frac{\partial}{\partial a_l} a_I = \begin{cases} 0 & \text{if } l \notin I, \\ (-1)^{|J|} a_J a_K & \text{if } a_I = a_J a_l a_K. \end{cases} \quad (3.93)$$

It is straightforward to show that the derivative satisfies e.g. the product rule and that the derivative operators anticommute with each other.



By differentiating (3.91) with respect to  $b$ 's, one can derive the Wick theorem for fermionic fields. For example, assuming that  $D$  is even,

$$\int d\mu_S(a) a_{i_1} a_{i_2} = \frac{\partial}{\partial b_{i_1}} \frac{\partial}{\partial b_{i_2}} \int d\mu_S(a) e^{\sum_i b_i a_i} \Big|_{b=0} \quad (3.94)$$

$$= \frac{\partial}{\partial b_{i_1}} \frac{\partial}{\partial b_{i_2}} e^{-\frac{1}{2} \sum_{ij} b_i S_{ij} b_j} \Big|_{b=0} \quad (3.95)$$

$$= \frac{\partial}{\partial b_{i_1}} \left[ -\frac{1}{2} S_{i_2 j} b_j + \frac{1}{2} b_i S_{ii_2} \right] e^{-\frac{1}{2} \sum_{ij} b_i S_{ij} b_j} \Big|_{b=0} \quad (3.96)$$

$$= S_{i_1 i_2}, \quad (3.97)$$

where we also used the skew-symmetry of  $S$ . Similarly, one gets

$$\int d\mu_S(a) a_{i_1} a_{i_2} a_{i_3} a_{i_4} = S_{i_1 i_2} S_{i_3 i_4} - S_{i_1 i_3} S_{i_2 i_4} + S_{i_1 i_4} S_{i_2 i_3}. \quad (3.98)$$

Returning to quantum mechanics, we extend our Fock space to be a vector space over the Grassmann numbers, i.e. any quantum state  $|n\rangle$  can be multiplied by an element of the Grassmann algebra. In this way, annihilation operators can be shown to possess eigenstates known as fermionic coherent states. The coherent states satisfy

$$c_i |\psi\rangle = \psi_i |\psi\rangle \quad (3.99)$$

and conjugation gives

$$\langle \psi | c_i^\dagger = \langle \psi | \bar{\psi}_i, \quad (3.100)$$

which defines the conjugate variable  $\bar{\psi}_i$  of  $\psi_i$ .

The coherent states can be shown to form an overcomplete basis such that the resolution of identity reads

$$\int d(\bar{\psi}, \psi) e^{-\bar{\psi} \psi} |\psi\rangle \langle \psi| = 1, \quad (3.101)$$

where the integration measure is  $d(\bar{\psi}, \psi) := d\bar{\psi}_1 d\psi_1 d\bar{\psi}_2 d\psi_2 \dots$ . The basis is overcomplete, since the overlap of two coherent states is

$$\langle \eta | \theta \rangle = e^{\bar{\eta} \theta}. \quad (3.102)$$

Here and later we use the vector notation  $\bar{\eta} \theta = \sum_i \bar{\eta}_i \theta_i$ .

Given the completeness relation for coherent states, one can derive the path integral formula for the quantum-mechanical grand-canonical partition function

$$\mathcal{Z} = \text{Tr} \left( e^{-\beta \hat{K}} \right) \equiv \sum_n \langle n | e^{-\beta \hat{K}} | n \rangle, \quad (3.103)$$

where  $\hat{K} = \hat{H} - \mu \hat{N}$  and the states  $\{|n\rangle\}$  form a complete, orthonormal set in the Fock space. A full pedagogical derivation of the functional integral formula is

found, for example, in Refs. [50] and [35], so we present a shortened account. The Hamiltonian is assumed to be of the second-quantized form

$$\hat{H}[a^\dagger, a] = \sum_{ij} t_{ij} a_i^\dagger a_j + \frac{1}{r!} \sum_{\substack{i_1, \dots, i_r \\ j_1, \dots, j_r}} V_{i_1 \dots i_r j_1 \dots j_r} c_{i_1}^\dagger \dots c_{i_r}^\dagger c_{j_r} \dots c_{j_1}, \quad (3.104)$$

where we assume general  $r$ -particle interactions for generality. The matrix element of the Hamiltonian between two coherent states  $|\psi^{(1)}\rangle$  and  $|\psi^{(2)}\rangle$  is

$$\begin{aligned} \langle \psi^{(2)} | \hat{H} | \psi^{(1)} \rangle &= \left( \sum_{ij} t_{ij} \bar{\psi}_i^2 \psi_j^1 \right. \\ &\quad \left. + \frac{1}{r!} \sum_{\substack{i_1, \dots, i_r \\ j_1, \dots, j_r}} V_{i_1 \dots i_r j_1 \dots j_r} \bar{\psi}_{i_1}^2 \dots \bar{\psi}_{i_r}^2 \psi_{j_r}^1 \dots \psi_{j_1}^1 \right) \langle \psi^2 | \psi^1 \rangle \end{aligned} \quad (3.105)$$

$$\equiv H[\bar{\psi}^2, \psi^1] \langle \psi^2 | \psi^1 \rangle, \quad (3.106)$$

where  $H[\bar{\psi}, \psi]$  means that when sandwiched between coherent states, the operator  $H[c^\dagger, c]$  is turned into a Grassmann-valued number by simply replacing  $c^\dagger$  and  $c$  by  $\bar{\psi}$  and  $\psi$ , respectively. This only holds if the Hamiltonian is normal-ordered. To proceed, let us note that the trace can be written

$$\mathcal{Z} = \sum_n \langle n | e^{-\beta \hat{K}} | n \rangle \quad (3.107)$$

$$= \sum_n \int d(\bar{\psi}, \psi) e^{-\bar{\psi} \psi} \langle n | \psi \rangle \langle \psi | e^{-\beta \hat{K}} | n \rangle \quad (3.108)$$

$$= \int d(\bar{\psi}, \psi) e^{-\bar{\psi} \psi} \sum_n \langle -\psi | e^{-\beta \hat{K}} | n \rangle \langle n | \psi \rangle \quad (3.109)$$

$$= \int d(\bar{\psi}, \psi) e^{-\bar{\psi} \psi} \langle -\psi | e^{-\beta \hat{K}} | \psi \rangle, \quad (3.110)$$

where, in the second step, we inserted a resolution of identity and, in the third step, noted that for coherent states  $|\psi\rangle$ ,

$$\langle n | \psi \rangle \langle \psi | n \rangle = \langle -\psi | n \rangle \langle n | \psi \rangle. \quad (3.111)$$

In the final line we removed the identity operator  $\sum_n |n\rangle \langle n| = 1$ .

The basic idea in calculating all quantum-mechanical path integrals is to divide the "complex time"  $\beta$  appearing as the prefactor of the Hamiltonian  $K$  into  $N$  infinitesimal steps. The motivation behind the time slicing is the observation

$$\langle \psi^2 | e^{-\epsilon \hat{K}[a^\dagger, a]} | \psi^1 \rangle = e^{-\epsilon K[\bar{\psi}^{(2)}, \psi^{(1)}]} \langle \psi^2 | \psi^1 \rangle + \mathcal{O}(\epsilon^2), \quad (3.112)$$

i.e. for infinitesimal time evolution, we can replace the exponentiated operators by their corresponding eigenvalues. This procedure is not exact for finite  $\epsilon$ , since the

higher-order terms in the operator expansion are not normal-ordered, but they are eliminated in the limit  $\epsilon \rightarrow 0$ . To make use of this, we write ( $\epsilon = \beta/N$ )

$$\langle \psi^N | e^{-\beta \hat{K}} | \psi^0 \rangle = \langle \psi^N | \underbrace{e^{-\epsilon \hat{K}} \times e^{-\epsilon \hat{K}} \times \dots \times e^{-\epsilon \hat{K}}}_{N \text{ times}} | \psi^0 \rangle \quad (3.113)$$

$$= \langle \psi^N | e^{-\epsilon \hat{K}} \times 1^{(N-1)} \times e^{-\epsilon \hat{K}} \times 1^{(N-2)} \dots 1^{(1)} \times e^{-\epsilon \hat{K}} | \psi^0 \rangle, \quad (3.114)$$

where

$$1^{(n)} = \int d(\bar{\psi}^n, \psi^n) e^{-\bar{\psi}^n \psi^n} |\psi^n\rangle \langle \psi^n|. \quad (3.115)$$

Using the recipe (3.112) for infinitesimal time evolution, we get (suppressing terms of the order  $\mathcal{O}(\epsilon^2)$ )

$$\langle \psi^N | e^{-\beta \hat{K}} | \psi^0 \rangle = \int \prod_{n=1}^{N-1} d(\bar{\psi}^n, \psi^n) e^{-\sum_{n=0}^{N-1} (\epsilon K[\bar{\psi}^{n+1}, \psi^n] - \bar{\psi}^{n+1} \psi^n) - \sum_{n=1}^{N-1} \bar{\psi}^n \psi^n}. \quad (3.116)$$

By writing  $\psi_0 = \psi$  and requiring explicitly  $\psi^N = -\psi^0$ , the partition function (3.110) becomes

$$\mathcal{Z} = \int_{\substack{\psi^0 = -\psi^N \\ \bar{\psi}^0 = -\bar{\psi}^N}} \prod_{n=1}^N d(\bar{\psi}^n, \psi^n) \exp \left[ -\epsilon \sum_{n=0}^{N-1} \left( K[\bar{\psi}^{n+1}, \psi^n] - \frac{\bar{\psi}^{n+1} - \bar{\psi}^n}{\epsilon} \cdot \psi^n \right) \right] \quad (3.117)$$

$$\xrightarrow{N \rightarrow \infty} \int_{\substack{\bar{\psi}(0) = -\bar{\psi}(\beta) \\ \psi(0) = -\psi(\beta)}} \mathcal{D}(\bar{\psi}, \psi) e^{-S[\bar{\psi}, \psi]}, \quad (3.118)$$

where the action  $S[\bar{\psi}, \psi]$  is defined

$$S[\bar{\psi}, \psi] = \int_0^\beta d\tau [\bar{\psi}(\tau) \partial_\tau \psi(\tau) + K[\bar{\psi}(\tau), \psi(\tau)]] \quad (3.119)$$

$$= \int_0^\beta d\tau [\bar{\psi}(\tau) (\partial_\tau - \mu) \psi(\tau) + H[\bar{\psi}(\tau), \psi(\tau)]] . \quad (3.120)$$

In taking the continuum limit  $N \rightarrow \infty$ , we have (i) replaced the discrete index  $n$  by the continuous index  $\tau$ , (ii) noted that

$$- \frac{\bar{\psi}^{n+1} - \bar{\psi}^n}{\epsilon} \cdot \psi^i \rightarrow (-\partial_\tau \bar{\psi}(\tau)) \psi(\tau) \quad (3.121)$$

and integrated partially, and (iii) replaced  $K[\bar{\psi}^{n+1}, \psi^n]$  by  $K[\bar{\psi}(\tau), \psi(\tau)]$ . The last step can be heuristically validated by noticing that  $K[\bar{\psi}^{n+1}, \psi^n] = K[\bar{\psi}^n, \psi^n] + \mathcal{O}(\bar{\psi}^{n+1} - \bar{\psi}^n)$  and by discarding the correction term. This argument requires, however, that the dominant contribution to the field integral comes from "smooth" paths, for which  $\bar{\psi}^{n+1} - \bar{\psi}^n$  is small. This assumption is especially difficult to study for Grassmann-valued, fermionic fields, for which the smallness is not even well-defined.

For our purposes, it will be enough to assume that pathological complications of this type do not arise in taking the continuum limit.

The physical significance of the functional integral formula (3.118) is easy to state: one integrates over all possible values of the fields  $\{\psi_i(\tau)\}$  and  $\{\bar{\psi}_i(\tau)\}$  and weighs the integral by the exponentiated action functional  $S[\bar{\psi}, \psi]$ . In addition, the paths of fields must be antiperiodic in imaginary time. Since time-slicing and the following time-dependence of the fields was necessitated by the fact that operators appearing in the Hamiltonian did not commute, the variations of the fields as a function of  $\tau$  can be interpreted as quantum fluctuations. Due to the  $\tau$ -derivative in the action, the functional integral favours fields that are approximately constant in imaginary time, i.e. "classical" configurations. For quantum fields constant in imaginary time, the action reduces to the statistical mechanical action  $S \rightarrow \beta K[\bar{\psi}, \psi]$ .

The generalization of the above calculation for time-ordered Green's functions (3.10) is straightforward, and one gets

$$\mathcal{G}^{(m)}(1', \dots, m' | 1, \dots, m) = (-1)^m \frac{1}{\mathcal{Z}} \int \mathcal{D}(\bar{\psi}, \psi) \psi_{1'} \dots \psi_{m'} \bar{\psi}_m \dots \bar{\psi}_1 e^{-S[\bar{\psi}, \psi]}, \quad (3.122)$$

where again a composite index  $j = (\tau_j, i_j)$  includes the time  $\tau_j$  and single-particle quantum number  $i_j$ .

Since we assume the Hamiltonian to be time-independent, we switch to the Matsubara frequency representation. The discrete Fourier transformation is defined

$$\begin{cases} \psi(\omega_n) = \frac{1}{\sqrt{\beta}} \int_0^\beta d\tau \psi(\tau) e^{i\omega_n \tau}, \\ \bar{\psi}(\omega_n) = \frac{1}{\sqrt{\beta}} \int_0^\beta d\tau \bar{\psi}(\tau) e^{-i\omega_n \tau}, \end{cases} \quad (3.123)$$

so the inverse transformations are

$$\begin{cases} \psi(\tau) = \frac{1}{\sqrt{\beta}} \sum_{\omega_n} \psi(\omega_n) e^{-i\omega_n \tau}, \\ \bar{\psi}(\tau) = \frac{1}{\sqrt{\beta}} \sum_{\omega_n} \bar{\psi}(\omega_n) e^{i\omega_n \tau}. \end{cases} \quad (3.124)$$

Due to anti-periodicity, the allowed Matsubara frequencies are

$$\omega_n = \frac{(2n+1)\pi}{\beta}, \quad n \in \mathbb{Z}. \quad (3.125)$$

Substituting in Eq. (3.120), the action for Hamiltonian (3.104) becomes

$$\begin{aligned} S[\bar{\psi}, \psi] &= \sum_{ij, \omega_n} \bar{\psi}_i(\omega_n) [(-i\omega_n - \mu)\delta_{ij} + t_{ij}] \psi_j(\omega_n) \\ &+ \frac{1}{r! \beta^{r-1}} \sum_{\substack{i_1, \dots, i_r \\ j_1, \dots, j_r}} \sum_{\substack{\omega_1, \dots, \omega_r \\ \omega_{1'}, \dots, \omega_{r'}}} V_{i_1 \dots i_r j_1 \dots j_r} \bar{\psi}_{i_1}(\omega_{1'}) \dots \bar{\psi}_{i_r}(\omega_{r'}) \psi_{j_r}(\omega_r) \dots \psi_{j_1}(\omega_1) \\ &\times \delta_{\sum_r \omega_{i_r}, \sum_r \omega_{j_r}}, \end{aligned} \quad (3.126)$$

where the Kronecker delta ensures energy conservation.

The action of the fermionized spin Hamiltonian (2.33) is

$$S[\bar{\psi}, \psi] = \int_0^\beta d\tau \left[ \sum_{i\alpha} \bar{\psi}_{i\alpha}(\tau) \partial_\tau \psi_{i\alpha}(\tau) + \frac{1}{2} \sum_{ij} \sum_k \sum_{\alpha\beta\gamma\delta} \frac{J_{ij}}{4} \sigma_{\alpha\beta}^k \sigma_{\gamma\delta}^k \bar{\psi}_{i\alpha}(\tau) \bar{\psi}_{j\gamma}(\tau) \psi_{j\delta}(\tau) \psi_{i\beta}(\tau) \right]. \quad (3.127)$$

The free one-particle Green's function is the negative inverse of the one-particle part of the action, meaning that in frequency space the free propagator is

$$\mathcal{G}_0(\omega_1, i_1, \alpha_1 | \omega_2, i_2, \alpha_2) = \frac{1}{i\omega_1} \beta \delta_{\omega_1 \omega_2} \delta_{i_1 i_2} \delta_{\alpha_1 \alpha_2}. \quad (3.128)$$

### 3.4 Generating functionals

In the following, we define the generating functionals for connected, amputated and one-particle irreducible Green's functions. The functionals are called generating, since the Green's functions can be straightforwardly obtained by differentiating these functionals. The idea is familiar already from classical statistical mechanics: by introducing to a magnetic system a magnetic field  $h$  along the z-axis, such that the Hamiltonian  $H$  is modified to

$$H \rightarrow H - \int d\mathbf{x} h(\mathbf{x}) m^z(\mathbf{x}), \quad (3.129)$$

where  $m^z(\mathbf{x})$  is the magnetization field, the connected correlation function

$$G(\mathbf{x}, \mathbf{x}') = \langle m^z(\mathbf{x}) m^z(\mathbf{x}') \rangle - \langle m^z(\mathbf{x}) \rangle \langle m^z(\mathbf{x}') \rangle \quad (3.130)$$

is given by the second derivative of free energy  $F[h] = -T \ln(\mathcal{Z})$  in the limit of a vanishing field:

$$(\langle m^z(\mathbf{x}) m^z(\mathbf{x}') \rangle - \langle m^z(\mathbf{x}) \rangle \langle m^z(\mathbf{x}') \rangle) = -T \frac{\delta^2 F[h]}{\delta h(\mathbf{x}) \delta h(\mathbf{x}')} \Big|_{h(\mathbf{x})=0}. \quad (3.131)$$

Since the second derivative of the free energy also delivers susceptibility (divided by temperature), we see again how the linear response of a system to external perturbations is defined by the correlation functions. Even though this example is illustrative, one should remember that for fermionic fields in condensed matter systems, there is no real-life analogue of the source fields and they should be considered just mathematical tools.

In the following, we assume our system to be charge invariant such that only the Green's functions that contain an equal number of creation and annihilation operators are non-vanishing. When deriving the flow equations in the next chapter, we streamline the notation such that creation and annihilation operators are treated on equal footing and the assumption of charge invariance can be dropped.

The first and simplest generating function is the partition function  $Z[\bar{\eta}, \eta]$  obtained by coupling the fermionic field linearly to external sources  $\bar{\eta}$  and  $\eta$ :

$$Z[\bar{\eta}, \eta] = \int \mathcal{D}(\bar{\psi}, \psi) e^{-S[\bar{\psi}, \psi] + (\bar{\psi}, \eta) + (\bar{\eta}, \psi)}, \quad (3.132)$$

which we have normalized such that  $Z[0, 0] = 1$ . Then it is easy to show that any  $m$ -particle Green's function (3.10) can be calculated as

$$\mathcal{G}^{(m)}(1', \dots, m' | 1, \dots, m) = \frac{\delta^m}{\delta \bar{\eta}_{1'} \dots \delta \bar{\eta}_{m'}} \frac{\delta^m}{\delta \eta_m \dots \delta \eta_1} Z[\bar{\eta}, \eta] |_{\bar{\eta}=\eta=0}. \quad (3.133)$$

The full Green's function is not, however, the correlation function with which we want to work, since it contains also disconnected diagrams that do not represent particle-particle interactions. From the linked cluster theorem[49, 45], we know that the free energy, which is essentially the logarithm of the partition function, contains only contributions from connected diagrams. Therefore, we define the generator of connected Green's functions to be

$$\mathcal{W}[\bar{\eta}, \eta] = -\log Z[\bar{\eta}, \eta]. \quad (3.134)$$

The minus sign in the definition is for future convenience. One can show that all correlation functions generated by the derivatives of  $-\mathcal{W}[\bar{\eta}, \eta]$  with respect to  $\bar{\eta}$  and  $\eta$  are connected:

$$\mathcal{G}_c^{(m)}(1', \dots, m' | 1, \dots, m) \equiv (-1)^m \langle T_\tau a_{1'} \dots a_{m'} a_m^\dagger \dots a_1^\dagger \rangle_{conn} \quad (3.135)$$

$$= \frac{\delta^m}{\delta \bar{\eta}_{1'} \dots \delta \bar{\eta}_{m'}} \frac{\delta^m}{\delta \eta_m \dots \delta \eta_1} (-\mathcal{W}[\bar{\eta}, \eta]) |_{\bar{\eta}=\eta=0}. \quad (3.136)$$

We skip the algebraic proof of connectedness.

Before defining the effective action  $\Gamma$ , which is the first Legendre transform of  $\mathcal{W}$ , let us briefly define the generator of amputated Green's functions, for which one can also derive a flow equation. Assuming that the action  $S$  can be written as a sum of a quadratic part  $S_0$  and an interacting part  $S_{int}$ ,  $S = S_0 + S_{int}$ , the generator of connected amputated Green's functions is defined

$$\mathcal{W}^{ac}[\bar{\chi}, \chi] = \log \int \mathcal{D}(\bar{\psi}, \psi) e^{-S_0[\bar{\psi}, \psi] - S_{int}[\bar{\psi} + \bar{\chi}, \psi + \chi]}, \quad (3.137)$$

i.e. the interaction lives in a "background field" given by  $\bar{\chi}$  and  $\chi$ . We have again normalized the measure such that  $\mathcal{W}^{ac}[0, 0] = 1$ . Let us state without proof that the derivatives

$$\frac{\delta^m}{\delta \bar{\chi}_{1'} \dots \delta \bar{\chi}_{m'}} \frac{\delta^m}{\delta \chi_m \dots \delta \chi_1} \mathcal{W}^{ac}[\bar{\chi}, \chi] |_{\bar{\chi}=\chi=0}$$

give simply the connected Green's functions  $\mathcal{G}_c$  from which the external *free* propagators have been removed, i.e. "amputated".

The generator of one-particle irreducible Green's functions is called the effective action. It is defined as the Legendre transform

$$\Gamma[\bar{\phi}, \phi] = \mathcal{W}[\bar{\eta}, \eta] - (\bar{\phi}, \eta) - (\bar{\eta}, \phi), \quad (3.138)$$

where  $\phi$  and  $\bar{\phi}$  are defined

$$\phi_i = \frac{\delta\mathcal{W}[\bar{\eta}, \eta]}{\delta\bar{\eta}_i} \equiv -\langle\psi_i\rangle_{\bar{\eta}, \eta} \quad (3.139)$$

and

$$\bar{\phi}_i = -\frac{\delta\mathcal{W}[\bar{\eta}, \eta]}{\delta\eta_i} \equiv -\langle\bar{\psi}\rangle_{\bar{\eta}, \eta}. \quad (3.140)$$

Thus  $\phi$  and  $\bar{\phi}$  represent the average field in presence of sources  $\eta$  and  $\bar{\eta}$ . On the right-hand side of Eq. (3.138), one should write all  $\eta$ 's and  $\bar{\eta}$ 's as functions of  $\bar{\phi}$  and  $\phi$ , i.e. we assume that the relations above can be inverted. We then get

$$\begin{aligned} \frac{\delta\Gamma[\bar{\phi}, \phi]}{\delta\phi_i} &= \frac{\delta\mathcal{W}}{\delta\phi_i} - \left(\frac{\delta\bar{\phi}}{\delta\phi_i}, \eta\right) + \left(\bar{\phi}, \frac{\delta\eta}{\delta\phi_i}\right) - \left(\frac{\delta\bar{\eta}}{\delta\phi_i}, \phi\right) + \left(\bar{\eta}, \frac{\delta\phi}{\delta\phi_i}\right) \\ &= \left(\frac{\delta\mathcal{W}}{\delta\eta}, \frac{\delta\eta}{\delta\phi_i}\right) + \left(\frac{\delta\mathcal{W}}{\delta\bar{\eta}}, \frac{\delta\bar{\eta}}{\delta\phi_i}\right) + \left(\bar{\phi}, \frac{\delta\eta}{\delta\phi_i}\right) - \left(\frac{\delta\bar{\eta}}{\delta\phi_i}, \phi\right) + \bar{\eta}_i = \bar{\eta}_i, \end{aligned} \quad (3.141)$$

where, in the first line, we used the definition of  $\Gamma$ , in the second line the chain rule and the fact that  $\delta\bar{\phi}/\delta\phi = 0$ , and, finally, the relations (3.139) and (3.140) and the symmetry properties of the bilinear form. Similarly, one gets

$$\frac{\delta\Gamma[\bar{\phi}, \phi]}{\delta\bar{\phi}_i} = -\eta_i. \quad (3.142)$$

To show how the effective action generates proper vertex functions, we need to relate the functional derivatives of  $\Gamma[\bar{\phi}, \phi]$  to the derivatives of  $\mathcal{W}[\bar{\eta}, \eta]$ . To do this, we first expand  $\phi$  and  $\bar{\phi}$  in powers of  $\eta$  and  $\bar{\eta}$ , invert the relation iteratively to obtain series for  $\eta$  and  $\bar{\eta}$  in terms of  $\phi, \bar{\phi}$  and then compare the coefficients of this expansion to direct expansion. To simplify matters, we again assume charge invariance such that in the absence of sources, only the correlation functions that contain an even number of creation and annihilation operators are non-vanishing. We expand  $\bar{\phi}$  around  $(\eta, \bar{\eta}) = (0, 0)$ :

$$\bar{\phi}_{a'} = -\frac{\delta\mathcal{W}}{\delta\eta_{a'}} \quad (3.143)$$

$$= -\bar{\eta}_{b'} \frac{\delta^2\mathcal{W}}{\delta\bar{\eta}_{b'}\delta\eta_{a'}}|_{\eta=\bar{\eta}=0} - \frac{1}{2}\eta_{b'}\bar{\eta}_{d'}\bar{\eta}_{c'} \frac{\delta^4\mathcal{W}}{\delta\bar{\eta}_{c'}\delta\bar{\eta}_{d'}\delta\eta_{b'}\delta\eta_{a'}}|_{\eta=\bar{\eta}=0} + \dots \quad (3.144)$$

Let us define the inverse propagator  $S$  by demanding that

$$-S_{ac} \frac{\delta^2\mathcal{W}}{\delta\bar{\eta}_c\delta\eta_b}|_{\eta=\bar{\eta}=0} = \delta_{ab}. \quad (3.145)$$

Then by multiplying the expansion by  $S_{a'a}$ , we get

$$\bar{\eta}_a = \bar{\phi}_{a'} S_{a'a} + \frac{1}{2} S_{a'a} \eta_{b'} \bar{\eta}_{d'} \bar{\eta}_{c'} \frac{\delta^4\mathcal{W}}{\delta\bar{\eta}_{c'}\delta\bar{\eta}_{d'}\delta\eta_{b'}\delta\eta_{a'}}|_{\eta=\bar{\eta}=0} + \dots \quad (3.146)$$

A similar expansion for  $\phi_{a'}$  and multiplication by  $S_{aa'}$  gives

$$\eta_a = S_{aa'}\phi_{a'} - \frac{1}{2}S_{aa'}\bar{\eta}_{b'}\eta_{d'}\eta_{c'}\frac{\delta^4\mathcal{W}}{\delta\eta_{c'}\delta\eta_{d'}\delta\bar{\eta}_{b'}\delta\eta_{a'}}|_{\eta=\bar{\eta}=0} + \dots \quad (3.147)$$

Inserting the first order expressions  $\eta = S\phi$  and  $\bar{\eta} = \bar{\phi}^T S$  into the third-order term in (3.146), we get

$$\bar{\eta}_a = \bar{\phi}_{a'}S_{a'a} + \frac{1}{2}\phi_b\bar{\phi}_d\bar{\phi}_cS_{a'a}S_{b'b}S_{dd'}S_{cc'}\frac{\delta^4\mathcal{W}}{\delta\bar{\eta}_{c'}\delta\bar{\eta}_{d'}\delta\eta_{b'}\delta\eta_{a'}}|_{\eta=\bar{\eta}=0} + \dots \quad (3.148)$$

In contrast, a direct expansion of  $\bar{\eta}$  around  $(\phi, \bar{\phi}) = (0, 0)$  gives<sup>3</sup>

$$\bar{\eta}_a = \frac{\delta\Gamma}{\delta\phi_a} \quad (3.149)$$

$$= \bar{\phi}_{a'}\frac{\delta^2\Gamma}{\delta\bar{\phi}_{a'}\delta\phi_a}|_{\phi=\bar{\phi}=0} + \frac{1}{2}\phi_b\bar{\phi}_d\bar{\phi}_c\frac{\delta^4\Gamma}{\delta\bar{\phi}_c\delta\bar{\phi}_d\delta\phi_b\delta\phi_a}|_{\phi=\bar{\phi}=0} + \dots \quad (3.150)$$

Comparing the first order terms in the two expansions (3.148) and (3.150), we get the important relation

$$\frac{\delta^2\Gamma}{\delta\bar{\phi}_{a'}\delta\phi_a}|_{\phi=\bar{\phi}=0} = S_{a'a} \equiv (\mathcal{G}_c^{-1})_{a'a}, \quad (3.151)$$

i.e. the second functional derivative of the effective action equals the inverse of the full connected one-particle propagator. Since we know from the Dyson equation that

$$(\mathcal{G}_c^{-1})_{a'a} = (\mathcal{G}_0^{-1})_{a'a} - \Sigma_{a'a}, \quad (3.152)$$

where  $\mathcal{G}_0$  is the free propagator and  $\Sigma$  the irreducible self-energy, the second derivative of  $\Gamma$  essentially delivers the self-energy.

Comparing terms with coefficients  $\phi_b\bar{\phi}_d\bar{\phi}_c$ , we get

$$\frac{\delta^4\Gamma}{\delta\bar{\phi}_c\delta\bar{\phi}_d\delta\phi_b\delta\phi_a}|_{\phi=\bar{\phi}=0} = S_{a'a}S_{b'b}S_{dd'}S_{cc'}\frac{\delta^4\mathcal{W}}{\delta\bar{\eta}_{c'}\delta\bar{\eta}_{d'}\delta\eta_{b'}\delta\eta_{a'}}|_{\eta=\bar{\eta}=0}, \quad (3.153)$$

or in terms of the connected one-particle and two-particle Green's functions,

$$\frac{\delta^4\Gamma}{\delta\bar{\phi}_c\delta\bar{\phi}_d\delta\phi_b\delta\phi_a}|_{\phi=\bar{\phi}=0} = -(\mathcal{G}_c^{-1})_{a'a}(\mathcal{G}_c^{-1})_{b'b}(\mathcal{G}_c^{-1})_{dd'}(\mathcal{G}_c^{-1})_{cc'}\mathcal{G}_c^{(2)}(c', d'; a', b'). \quad (3.154)$$

Thus the fourth functional derivative of  $\Gamma$  gives the proper interaction vertex, i.e. the connected two-particle Green's function from which the external propagators have been amputated. We therefore define the anti-symmetrized, proper interaction vertex

$$\Gamma_2(c, d; a, b) := \frac{\delta^4\Gamma}{\delta\phi_c\delta\phi_d\delta\phi_b\delta\phi_a}|_{\phi=\bar{\phi}=0}. \quad (3.155)$$

---

<sup>3</sup>Here we should include also derivative terms that do not contain an equal number of  $\phi$ 's and  $\bar{\phi}$ 's, but they can be shown to vanish due to charge invariance.



Since the one-particle and two-particle proper vertices are obtained from the full connected Green's functions simply by amputating the external propagators, all symmetry properties derived in Sect. 3.2 apply to vertices as well. Using Eqs. (3.33) and (3.79), the self-energy  $\Sigma$  can be parametrized by

$$\Sigma(\omega_1, i_1, \alpha_1; \omega_2, i_2, \alpha_2) = \Sigma(\omega_1) \beta \delta_{\omega_1, \omega_2} \delta_{i_1 i_2} \delta_{\alpha_1 \alpha_2}, \quad (3.156)$$

where  $\Sigma(\omega_1)$  is odd and purely imaginary due to Eq. (3.81). Using Eq. (3.41), the proper vertex  $\Gamma_2$  can be parametrized by

$$\begin{aligned} & \Gamma_2((\omega_1, i_1, \alpha_1), (\omega_2, i_2, \alpha_2); (\omega_3, i_3, \alpha_3), (\omega_4, i_4, \alpha_4)) \\ &= [\Gamma_{si_1 i_2}(s, t, u) \sigma_{\alpha_1 \alpha_3}^k \sigma_{\alpha_2 \alpha_4}^k + \Gamma_{di_1 i_2}(s, t, u) \delta_{\alpha_1 \alpha_3} \delta_{\alpha_2 \alpha_4}] \\ & \quad \times \delta_{i_1 i_3} \delta_{i_2 i_4} \beta \delta_{\omega_1 + \omega_2, \omega_3 + \omega_4} - (1 \leftrightarrow 2), \end{aligned} \quad (3.157)$$

where the Mandelstam variables  $s, t$  and  $u$  were defined in Eq. (3.82) and  $\Gamma_{si_1 i_2}(s, t, u)$  and  $\Gamma_{di_1 i_2}(s, t, u)$  are even functions in each variable separately due to Eqs. (3.83), (3.84) and (3.85).

Continuing the expansion, one can derive expressions for the higher-order derivatives. Diagrammatically, one can then convince oneself of the fact that all the diagrams generated by  $\Gamma[\bar{\phi}, \phi]$  are one-particle irreducible, i.e. they are obtained from the full connected Green's function by amputating the external propagators and subtracting any one-particle reducible parts. One can also prove this property algebraically by modifying the propagator such that any internal lines are essentially cut and by then showing that the contribution to  $\Gamma[\bar{\phi}, \phi]$  from these new terms is still represented by a connected diagram, which proves the one-particle irreducibility of all diagrams contributing to  $\Gamma$ [55]. Since we will later only work with one-particle and two-particle interaction vertices, whose relations (3.151) and (3.154) to connected Green's functions we have already found, we skip these proofs and move on to deriving the general fermionic functional renormalization group equations for  $\Gamma$ .

# Chapter 4

## Functional renormalization group

*In this chapter, we introduce the full machinery of functional renormalization group (FRG). Section 4.1 is devoted to an introduction to renormalization. The aim is to bridge the gap between what is commonly considered renormalization and the modern FRG. In Section 4.2, we derive the exact functional differential equation for the effective action and then apply the flow equations to the one-particle irreducible vertex functions in Section 4.3. At this point, the similarity of the flow equations to perturbation theory becomes clear and we represent the flow equations diagrammatically. The truncations and the choice of the cut-off function are discussed in Sections 4.4 and 4.5. In Section 4.6 we apply the symmetries found in Section 3.2 to finally derive the flow equations for the spin system. Diagrammatic representation is stressed throughout due to its simplicity and intuitivity.*

### 4.1 Introduction

Historically, renormalization group was born to handle divergent expressions in quantum field theory. The problem arises in perturbation theory from loop integrations over virtual states with arbitrarily large energies and momenta, which makes the perturbation expansion diverge. The problem is the locality of quantum field theories, which stipulates that the theory should work all the way to the smallest length scales and largest energies, which cannot be true if one runs into ultraviolet divergent expressions.

The first step in the renormalization process is always regularization: one adds to the theory a new dimensionful parameter that makes all integrals finite and algebraic manipulations possible. In quantum field theory, the most popular regularization method is the dimensional regularization, in which the dimension of the space-time  $d = 4$  is replaced by  $d = 4 - \epsilon$ , where  $\epsilon > 0$  is a small parameter. To make sure that integrals  $\int d^d k$  over momenta  $k$  are still of mass dimension 4, one must also introduce a dimensionful parameter  $\mu$  such that  $\mu^\epsilon \int d^d k$  is of mass dimension 4. In principle, the value of  $\mu$  is arbitrary, but it turns out that perturbative corrections are small only if one chooses this energy scale to be of the same order of magnitude as the energies of the incoming particles in the scattering experiment. The next step is renormalization: for each parameter of the theory, one needs to introduce

a counter-term in the free Lagrangian to remove the  $1/\epsilon^n$  infinities. The value of each counter-term is fixed by given experimental constraints, and different choices lead to different renormalization schemes that have different advantages. But the main point is that since the theory now depends on  $\mu$  (since it appears in the loop integrals of the perturbative expansion), all physical parameters such as the measurable electron mass or the effective coupling constant depend on  $\mu$ : they *flow* with the energy scale. This is the essence of perturbative renormalization group that "sweeps infinities under the rug"[6]. The basic idea is simply to separate the energy scales at which the theory is valid from scales at which it is not.

This view on renormalization as a mathematical trick was strongly modified by Kenneth G. Wilson in the 1970's[56]. Inspired by Kadanoff's block-spin real-space renormalization techniques[57], he noticed that the problem of taking continuum limit in the field theory is common to both high-energy physics and statistical physics and understood how renormalization group was the correct tool to take the limit[8]. Renormalization group also gave birth to the all-important idea of universality: even though two systems may look completely different at small length scales, renormalization group flow may take them to a common fixed point at large length scales, making e.g. all critical exponents coincide.

In the Wilson's formulation of renormalization group, the idea was to sharply separate the modes into "slow" modes and "fast" modes. By integrating out the fast modes in the functional integral, one gets an "effective" action  $S_\Lambda$  (not to be confused with the effective action  $\Gamma$ ) for the low-energy behaviour[58]. This procedure of partial functional integration is, however, quite cumbersome in practice. Polchinski introduced in the free action an arbitrary regulator function  $R^\Lambda$  that suppresses some of the modes and then derived an exact differential equation for the generating functional of Green's functions[9]. This marks the birth of functional renormalization group. In 1993, Wetterich[10] then derived a functional differential equation for the effective action  $\Gamma_\Lambda$  and noticed that his equation contained many practical advantages over Polchinski's formulation, such as the one-loop structure, which admits new approximative flows.

Applications of renormalization group to condensed matter physics began in the solution for the long-standing problem in impurity physics, the Kondo problem. In 1970, Anderson[59] was able to calculate scalings laws for the Kondo model with his "poor man's scaling" method and a few years later, Wilson was able to solve the problem more accurately with his numerical RG[8]. The theory of renormalization group for interacting electron gases was developed relatively late, in the beginning of the 1990's[58]. One of the main reasons for the delay was probably the success of perturbation theory. Even though the second-order perturbation theory for interacting electron gas includes divergent loop integrals, this problem is easily tackled by summing the loop integrals to an infinite order. The necessity to include diagrams of infinite order is one manifestation of the fact that the reference state of free fermions is not suitable for a straight-forward perturbation expansion: one needs to include a non-perturbative collective effect (screening) to describe weakly interacting quasi-particles. As long as the renormalized interaction remains weak and one is close to the Fermi liquid fixed point, there is basically no reason for renormalization. How-

ever, for correlated electrons in reduced dimensions, Fermi liquid theory may break down, and renormalization group is the method of choice for handling competing instabilities in an unbiased manner.

Fermionic functional renormalization group equations were first derived by Salmhofer for Wick-ordered Green's functions[60, 61], which was then applied to the two-dimensional Hubbard model on a square lattice by Halboth and Metzner[62]. The two-dimensional Hubbard model is believed to describe the electronic degrees of freedom in cuprate superconductors and is tailor-made for RG approaches due to the difficulty of handling the competing instabilities related to Fermi surface nesting and van Hove singularities. Zanchi and Schulz[63] calculated the flow of amputated Green's functions and developed a patching algorithm that allowed to keep the momentum dependence in the numerical solution even in systems with non-regular Fermi surfaces. Using the patching scheme, Honerkamp *et al.*[64] applied the FRG to one-particle irreducible vertex functions and found a possible breakdown of the Fermi liquid behaviour due to Umklapp scattering. In recent ten years, FRG has then become one of the standard methods in studying correlated electron systems, and has been applied e.g. to Luttinger liquids with impurities[65, 66], single-impurity Anderson model[67, 68], ultra-cold fermions[69], charge transport[70], and recently to quantum spin systems[14], which will be the case of our interest.

Before diving into equations, let us briefly state the course of our progress. The free Hamiltonian typically contains a part quadratic in fermionic operators (free part) and a term quartic in fermionic operators (interaction). The main idea of FRG is to introduce an infra-red cutoff  $\Lambda$  in the free propagator such that only the high-energy modes are active in the perturbation expansion, which regularizes any possible infrared divergences. Of course, FRG can be used as a method to sum Feynman diagrams even in the absence of any such instabilities. Initially, one chooses  $\Lambda$  such that all quantum corrections are shut down and the theory is trivial to solve. The goal is then to approach the physical limit  $\Lambda \rightarrow 0^+$ . When  $\Lambda$  is decreased but is still large enough such that the ratio  $V/\Lambda$  is small, the perturbation expansion in interaction  $V$  is essentially an expansion in  $V/\Lambda$  and one can use diagrammatic expansion techniques even for strong bare interactions, with no resort to FRG. However, when  $\Lambda \sim V$ , the perturbation expansion breaks down and one must resort to the FRG flow equations to be derived below to sum up diagrams to an infinite order, in a more or less controlled manner. The idea of FRG is not to sum all diagrams to an infinite order, which is typically impossible, but to single out the most important ones by their scaling behaviour in the flow.

## 4.2 Exact flow equation for fermions

The goal of this chapter is to derive the flow equation for a general fermionic action that consists of a quadratic part  $S_0[\bar{\psi}, \psi]$  and a quartic part  $V[\bar{\psi}, \psi]$ . The derivation given here is based on Ref. [12], but since the derivation therein skips many non-trivial steps, we present a full derivation. In addition, we want to derive the flow equation for the grand canonical potential, which was omitted in Ref. [12]. For

convenience, some of our definitions will differ by a minus sign from Ref. [12]. The derivation is very general in the sense that we also allow symmetry-breaking terms such as  $\bar{\psi}_1\bar{\psi}_2$  in the action<sup>1</sup>. Thus, we assume the free part to be of the form

$$S_0[\bar{\psi}, \psi] = \frac{1}{2} (\bar{\psi}^T, \psi^T) \mathbf{Q} \begin{pmatrix} \bar{\psi} \\ \psi \end{pmatrix}, \quad (4.1)$$

where e.g.  $\psi = (\psi_1, \psi_2, \dots)^T$  contains all the fields. When charge symmetry is not broken, one can write  $\mathbf{Q}$  in the form

$$\mathbf{Q} = \begin{pmatrix} 0 & -\mathcal{G}_0^{-1} \\ \mathcal{G}_0^{-1T} & 0 \end{pmatrix}, \quad (4.2)$$

where  $\mathcal{G}_0$  is the free propagator in matrix form. In general, one can only conclude based on the anticommuting property of the fields that  $\mathbf{Q}$  is skew-symmetric,  $\mathbf{Q}^T = -\mathbf{Q}$ . In addition, we define

$$\Psi = \begin{pmatrix} \bar{\psi} \\ \psi \end{pmatrix} \quad (4.3)$$

so that we can simply write

$$S_0[\Psi] = \frac{1}{2} (\Psi, \mathbf{Q}\Psi). \quad (4.4)$$

To clean up the notation, we define the Gaussian measure (cf. Eq. (3.91))<sup>2</sup>

$$d\mu_{\mathbf{C}}(\Psi) = \frac{\mathcal{D}\Psi e^{-S_0[\Psi]}}{\int \mathcal{D}\Psi e^{-S_0[\Psi]}}. \quad (4.5)$$

where  $\mathbf{C} = \mathbf{Q}^{-1}$  is the covariance. For the charge-symmetric case, one has

$$\mathbf{C} = \begin{pmatrix} 0 & \mathcal{G}_0^T \\ -\mathcal{G}_0 & 0 \end{pmatrix}. \quad (4.6)$$

Using this notation, we write the generating functional  $Z[\bar{\eta}, \eta]$  in the compact form<sup>3</sup>

$$Z[\bar{\eta}, \eta] \equiv \frac{\mathcal{Z}}{\mathcal{Z}_0} \left\langle e^{(\bar{\psi}, \eta) + (\bar{\eta}, \psi)} \right\rangle \quad (4.7)$$

$$= \int d\mu_{\mathbf{C}}(\Psi) e^{-V[\Psi] + (H, \Psi)}, \quad (4.8)$$

---

<sup>1</sup>For a more transparent derivation for the symmetry-conserving case, see Ref. [71]. Note that most of the definitions therein differ by a minus sign from our notation.

<sup>2</sup>Any problems related to the fact that the measure in functional integral is of the form  $d\bar{\psi}_1 d\psi_1 d\bar{\psi}_2 d\psi_2 \dots$  and not  $d\bar{\psi}_1 d\bar{\psi}_2 \dots d\psi_1 d\psi_2 \dots$  as in Eq. (3.91), we sweep under the rug by noting that all objects of interest are ratios of two functional integrals and therefore minus signs common to all integrals do not play a role.

<sup>3</sup>In contrast to Eq. (3.132), we now normalize  $Z[\bar{\eta}, \eta]$  such that  $Z[0, 0] = \mathcal{Z}/\mathcal{Z}_0$ , for future convenience.

where  $H = (-\eta, \bar{\eta})^T$ . The generator of connected Green's functions is

$$\mathcal{W}[H] = -\log Z[H] \quad (4.9)$$

and the effective action defined in Eq. (3.138) becomes

$$\Gamma[\Phi] = \mathcal{W}[\tilde{H}(\Phi)] - (\tilde{H}(\Phi), \Phi), \quad (4.10)$$

where the field  $\Phi = (\bar{\phi}, \phi)^T$  satisfies (compare with according Eqs. (3.139), (3.140), (3.141) and (3.142))

$$\frac{\delta \mathcal{W}[H]}{\delta H} = \tilde{\Phi}(H) \quad (4.11)$$

and

$$\frac{\delta \Gamma[\Phi]}{\delta \Phi} = \tilde{H}(\Phi). \quad (4.12)$$

Above,  $\tilde{H}(\Phi)$  is the function that returns the source field  $H$  when given an average field  $\Phi$  and vice versa for  $\tilde{\Phi}(H)$ . Basically, one could write simply  $H$  instead of  $\tilde{H}(\Phi)$ , but this notation makes it clearer that in this case,  $\Phi$  is the free variable.

In FRG, the free propagator is modified such that covariance  $\mathbf{C}$  depends on a parameter  $\Lambda$ . Our goal is to calculate the derivative  $d\Gamma_\Lambda[\Phi]/d\Lambda$ . Since  $\mathbf{C} = \mathbf{C}_\Lambda$ , also  $\mathcal{W}$  depends on  $\Lambda$  and so does the relation between  $H$  and  $\Phi$ . The derivative of  $\mathcal{W}_\Lambda[\tilde{H}_\Lambda(\Phi)]$  is by chain rule

$$\frac{d}{d\Lambda} \mathcal{W}_\Lambda[\tilde{H}_\Lambda(\Phi)] = \dot{\mathcal{W}}_\Lambda[\tilde{H}_\Lambda(\Phi)] + \left( \dot{\tilde{H}}_\Lambda(\Phi), \underbrace{\frac{\delta \mathcal{W}_\Lambda[\tilde{H}_\Lambda(\Phi)]}{\delta H}}_{\Phi} \right). \quad (4.13)$$

Therefore, from (4.10) we get

$$\dot{\Gamma}_\Lambda[\Phi] = \dot{\mathcal{W}}_\Lambda[\tilde{H}_\Lambda(\Phi)]. \quad (4.14)$$

To calculate the partial derivative of  $\mathcal{W}_\Lambda[H]$ , we note that in the expression for  $\mathcal{W}_\Lambda$ ,

$$\mathcal{W}_\Lambda[H] \equiv -\log Z[H] = -\log \int d\mu_{\mathbf{C}_\Lambda}(\Psi) e^{-V[\Psi] + (H, \Psi)}, \quad (4.15)$$

only the measure

$$d\mu_{\mathbf{C}_\Lambda}(\Psi) = \frac{\mathcal{D}\Psi e^{-\frac{1}{2}(\Psi, \mathbf{Q}_\Lambda \Psi)}}{\int \mathcal{D}\Psi e^{-\frac{1}{2}(\Psi, \mathbf{Q}_\Lambda \Psi)}}$$

depends on  $\Lambda$ . The explicit expression for the normalization factor is by Eq. (3.90) the determinant:

$$\int \mathcal{D}\Psi e^{-\frac{1}{2}(\Psi, \mathbf{Q}_\Lambda \Psi)} = \sqrt{\det \mathbf{Q}_\Lambda}. \quad (4.16)$$

Using the identity

$$\frac{d}{d\alpha} \det \mathbf{A}(\alpha) = -\det \mathbf{A}(\alpha) \text{tr} \left( \mathbf{A}(\alpha) \frac{d}{d\alpha} \mathbf{A}^{-1}(\alpha) \right), \quad (4.17)$$

where  $\mathbf{A}(\alpha)$  is an invertible matrix smoothly dependent on a parameter  $\alpha$ , we get ( $\mathbf{C}_\Lambda = \mathbf{Q}_\Lambda^{-1}$ )

$$\frac{d}{d\Lambda} d\mu_{\mathbf{C}_\Lambda}(\Psi) \equiv \mathcal{D}\Psi \frac{d}{d\Lambda} \left( \sqrt{\det \mathbf{Q}_\Lambda^{-1}} e^{-\frac{1}{2}(\Psi, \mathbf{Q}_\Lambda \Psi)} \right) \quad (4.18)$$

$$= -\frac{1}{2} \mathcal{D}\Psi \sqrt{\det \mathbf{Q}_\Lambda^{-1}} \text{tr} \left( \mathbf{C}_\Lambda \dot{\mathbf{Q}}_\Lambda \right) e^{-\frac{1}{2}(\Psi, \mathbf{Q}_\Lambda \Psi)} \\ - \frac{1}{2} \mathcal{D}\Psi \sqrt{\det \mathbf{Q}_\Lambda^{-1}} (\Psi, \dot{\mathbf{Q}}_\Lambda \Psi) e^{-\frac{1}{2}(\Psi, \mathbf{Q}_\Lambda \Psi)} \quad (4.19)$$

$$= -\frac{1}{2} \left( \text{tr} \left( \mathbf{C}_\Lambda \dot{\mathbf{Q}}_\Lambda \right) + (\Psi, \dot{\mathbf{Q}}_\Lambda \Psi) \right) d\mu_{\mathbf{C}_\Lambda}(\Psi). \quad (4.20)$$

Therefore,

$$\dot{\mathcal{W}}_\Lambda[H] = \frac{1}{2} \text{tr} \left( \mathbf{C}_\Lambda \dot{\mathbf{Q}}_\Lambda \right) + \frac{1}{2} \frac{1}{Z_\Lambda[H]} \int d\mu_{\mathbf{C}_\Lambda}(\Psi) (\Psi, \dot{\mathbf{Q}}_\Lambda \Psi) e^{-V[\Psi] + (H, \Psi)} \quad (4.21)$$

$$= \frac{1}{2} \text{tr} \left( \mathbf{C}_\Lambda \dot{\mathbf{Q}}_\Lambda \right) + \frac{1}{2} \frac{1}{Z_\Lambda[H]} \left( \frac{\delta}{\delta H}, \dot{\mathbf{Q}}_\Lambda \frac{\delta}{\delta H} \right) Z_\Lambda[H]. \quad (4.22)$$

More explicitly,

$$\left( \frac{\delta}{\delta H}, \dot{\mathbf{Q}}_\Lambda \frac{\delta}{\delta H} \right) Z[H] = \int dX dY \left[ \frac{\delta}{\delta H(X)} \dot{\mathbf{Q}}_\Lambda(X, Y) \frac{\delta}{\delta H(Y)} \right] e^{-\mathcal{W}[H]} \quad (4.23)$$

$$= \int dX dY \frac{\delta}{\delta H(X)} \dot{\mathbf{Q}}_\Lambda(X, Y) \left( -\frac{\delta \mathcal{W}}{\delta H(Y)} \right) e^{-\mathcal{W}[H]} \quad (4.24)$$

$$= \int dX dY \frac{\delta \mathcal{W}}{\delta H(X)} \dot{\mathbf{Q}}_\Lambda(X, Y) \frac{\delta \mathcal{W}}{\delta H(Y)} e^{-\mathcal{W}[H]} \\ - \int dX dY \dot{\mathbf{Q}}_\Lambda(X, Y) \frac{\delta^2 \mathcal{W}}{\delta H(X) \delta H(Y)} e^{-\mathcal{W}[H]} \quad (4.25)$$

$$= \left[ \left( \frac{\delta \mathcal{W}}{\delta H}, \dot{\mathbf{Q}}_\Lambda \frac{\delta \mathcal{W}}{\delta H} \right) + \text{tr} \left( \dot{\mathbf{Q}}_\Lambda \frac{\delta^2 \mathcal{W}}{\delta H^2} \right) \right] e^{-\mathcal{W}[H]}. \quad (4.26)$$

All in all, we get

$$\dot{\mathcal{W}}_\Lambda[H] = \frac{1}{2} \text{tr} \left( \mathbf{C}_\Lambda \dot{\mathbf{Q}}_\Lambda \right) + \frac{1}{2} \left( \frac{\delta \mathcal{W}}{\delta H}, \dot{\mathbf{Q}}_\Lambda \frac{\delta \mathcal{W}}{\delta H} \right) + \frac{1}{2} \text{tr} \left( \dot{\mathbf{Q}}_\Lambda \frac{\delta^2 \mathcal{W}}{\delta H^2} \right). \quad (4.27)$$

Using Eqs. (4.14), (4.11) and the fact that

$$\frac{\delta^2 \mathcal{W}}{\delta H^2}[\tilde{H}(\Phi)] = \left[ \frac{\delta^2 \Gamma[\Phi]}{\delta \Phi^2} \right]^{-1}, \quad (4.28)$$

which can be derived from Eq. (4.11) by differentiation with respect to  $\Phi$  and using the chain rule, we finally arrive at the exact flow equation for the effective action:

$$\dot{\Gamma}_\Lambda[\Phi] = \frac{1}{2} \text{tr} \left( \mathbf{C}_\Lambda \dot{\mathbf{Q}}_\Lambda \right) + \frac{1}{2} \left( \Phi, \dot{\mathbf{Q}}_\Lambda \Phi \right) + \frac{1}{2} \text{tr} \left( \dot{\mathbf{Q}}_\Lambda \left[ \frac{\delta^2 \Gamma[\Phi]}{\delta \Phi^2} \right]^{-1} \right). \quad (4.29)$$

### 4.3 Flow equations for the 1PI vertex functions

The exact flow equation (4.29) is a non-linear functional integro-differential equation that cannot be solved directly. To approach the solution, one must parametrize the dependence on the field  $\Phi$  somehow. Whereas for statistical field theories there are many kinds of parametrizations such as the local potential approximation or derivative expansions[11], for fermionic fields the only viable option is to expand  $\Gamma[\Phi]$  in powers of fields. Remembering that  $\Gamma[\Phi]$  is the generating functional of one-particle irreducible vertex functions, the expansion coefficients will be precisely these functions. The flow equations for the one-particle irreducible vertex functions were first derived by Morris for bosonic fields[72].

We expand the effective action in powers of fields:

$$\Gamma_\Lambda[\Phi] = \sum_{m=0,2,\dots} \frac{1}{m!} \int d^m \mathbf{X} \gamma_m^\Lambda(X_1, \dots, X_m) \Phi(X_1) \dots \Phi(X_m). \quad (4.30)$$

Due to the assumed parity symmetry of the Hamiltonian ( $\psi \rightarrow -\psi$ ,  $\bar{\psi} \rightarrow -\bar{\psi}$ ), we only include terms with an even number of fields  $\Phi(X)$ . Since the fields  $\Phi(X_j)$  anticommute, we can assume the vertex functions  $\gamma_m^\Lambda$  to be fully antisymmetric in  $(X_1, \dots, X_m)$ . The partial derivatives of  $\Gamma_\Lambda[\Phi]$  with respect to fields are

$$\frac{\delta}{\delta \Phi(X_1)} \dots \frac{\delta}{\delta \Phi(X_m)} \Gamma_\Lambda[\Phi = 0] = \gamma_m^\Lambda(X_m, \dots, X_1), \quad (4.31)$$

where the inverse ordering of  $(X_1, \dots, X_m)$  on the right-hand side is necessary due to the fact that we defined the Grassmann derivative as a left derivative. Often this problem is circumvented by defining Grassmann derivatives such that they act from the right, which is customary especially in particle physics.

To compare the powers of  $\Phi$  on the left and right-hand side of (4.29), one must expand the term

$$\text{tr} \left( \dot{\mathbf{Q}}_\Lambda \left[ \frac{\delta^2 \Gamma_\Lambda[\Phi]}{\delta \Phi^2} \right]^{-1} \right)$$

in powers of  $\Phi$ . The second derivative of  $\Gamma_\Lambda[\Phi]$  can be written as

$$\begin{aligned} \frac{\delta}{\delta \Phi(X_2)} \frac{\delta}{\delta \Phi(X_1)} \Gamma_\Lambda[\Phi] &= \gamma_2^\Lambda(X_1, X_2) \\ &+ \sum_{m=2,4,\dots} \frac{1}{m!} \int d^m \mathbf{X}' \gamma_{m+2}^\Lambda(X_1, X_2, X'_1, \dots, X'_m) \Phi(X'_1) \dots \Phi(X'_m). \end{aligned} \quad (4.32)$$

Defining the term on the second row to be  $\tilde{\Gamma}_\Lambda(X_1, X_2; \Phi)$ , we can write

$$\frac{\delta}{\delta \Phi(X_2)} \frac{\delta}{\delta \Phi(X_1)} \Gamma_\Lambda[\Phi] = - \left[ \gamma_2^\Lambda \left( 1 - \mathbf{G}_\Lambda \tilde{\Gamma}_\Lambda(\cdot, \cdot; \Phi) \right) \right] (X_2, X_1), \quad (4.33)$$

where  $\mathbf{G}_\Lambda = -(\gamma_2^\Lambda)^{-1}$  and we used the skew-symmetry of all matrices to replace  $(X_1, X_2)$  by  $(X_2, X_1)$ . The minus sign in the definition of  $\mathbf{G}_\Lambda$  differs from Ref. [12]



but is convenient. Now we can expand the inverse:

$$\left[ \frac{\delta^2 \Gamma_\Lambda[\Phi]}{\delta \Phi^2} \right]^{-1} = \left[ 1 - \mathbf{G}_\Lambda \tilde{\Gamma}_\Lambda(\cdot, \cdot; \Phi) \right]^{-1} \mathbf{G}_\Lambda \quad (4.34)$$

$$= \sum_{p=0}^{\infty} (\mathbf{G}_\Lambda \tilde{\Gamma}_\Lambda(\cdot, \cdot; \Phi))^p \mathbf{G}_\Lambda. \quad (4.35)$$

The flow equation becomes

$$\begin{aligned} \dot{\Gamma}_\Lambda[\Phi] &= \frac{1}{2} \text{tr} \left( \mathbf{C}_\Lambda \dot{\mathbf{Q}}_\Lambda \right) + \frac{1}{2} \left( \Phi, \dot{\mathbf{Q}}_\Lambda \Phi \right) + \frac{1}{2} \text{tr} \left( \mathbf{G}_\Lambda \dot{\mathbf{Q}}_\Lambda \right) \\ &\quad + \frac{1}{2} \text{tr} \left( \mathbf{G}_\Lambda \dot{\mathbf{Q}}_\Lambda \sum_{p=1}^{\infty} \left( \mathbf{G}_\Lambda \tilde{\Gamma}_\Lambda(\cdot, \cdot; \Phi) \right)^p \right). \end{aligned} \quad (4.36)$$

Defining the so-called single-scale propagator

$$\mathbf{S}_\Lambda = -\mathbf{G}_\Lambda \dot{\mathbf{Q}}_\Lambda \mathbf{G}_\Lambda, \quad (4.37)$$

the lowest-order flow equations are easy to read off by comparing coefficients:

$$\dot{\gamma}_0^\Lambda = \frac{1}{2} \text{tr} \left[ \dot{\mathbf{Q}}_\Lambda (\mathbf{C}_\Lambda + \mathbf{G}_\Lambda) \right], \quad (4.38)$$

$$\dot{\gamma}_2^\Lambda(X_1, X_2) = \dot{\mathbf{Q}}_\Lambda(X_1, X_2) - \frac{1}{2} \text{tr} \left( \mathbf{S}_\Lambda \gamma_4^\Lambda(\cdot, \cdot, X_1, X_2) \right). \quad (4.39)$$

In the fourth order of fields  $\Phi$ , one gets the equation

$$\begin{aligned} &\frac{1}{4!} \int d\mathbf{X} \dot{\gamma}_4^\Lambda(X_1, X_2, X_3, X_4) \Phi(X_1) \Phi(X_2) \Phi(X_3) \Phi(X_4) \\ &= -\frac{1}{2 \times 4!} \int d\mathbf{X} \text{tr} \left( \mathbf{S}_\Lambda \gamma_6^\Lambda(\cdot, \cdot, X_1, X_2, X_3, X_4) \right) \Phi(X_1) \Phi(X_2) \Phi(X_3) \Phi(X_4) \\ &\quad - \frac{1}{2^3} \int d\mathbf{X} \text{tr} \left( \mathbf{S}_\Lambda \gamma_4^\Lambda(\cdot, \cdot, X_1, X_2) \mathbf{G}_\Lambda \gamma_4^\Lambda(\cdot, \cdot, X_3, X_4) \right) \\ &\quad \times \Phi(X_1) \Phi(X_2) \Phi(X_3) \Phi(X_4). \end{aligned} \quad (4.40)$$

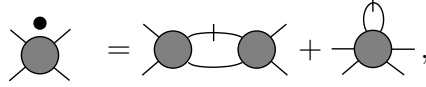
Whereas the coefficients on the left-hand side and in the first term on the right-hand side are fully antisymmetric, the coefficient of the last term must be antisymmetrized if one wants to compare the coefficients. Antisymmetrization delivers the flow equation

$$\begin{aligned} \dot{\gamma}_4^\Lambda(X_1, X_2, X_3, X_4) &= -\frac{1}{2} \text{tr} \left( \mathbf{S}_\Lambda \gamma_6^\Lambda(\cdot, \cdot, X_1, X_2, X_3, X_4) \right) \\ &\quad - \frac{1}{2} \left\{ \text{tr} \left[ \mathbf{S}_\Lambda \gamma_4^\Lambda(\cdot, \cdot, X_1, X_2) \mathbf{G}_\Lambda \gamma_4^\Lambda(\cdot, \cdot, X_3, X_4) + (\mathbf{S}_\Lambda \leftrightarrow \mathbf{G}_\Lambda) \right] \right. \\ &\quad \left. - \text{tr} \left[ \mathbf{S}_\Lambda \gamma_4^\Lambda(\cdot, \cdot, X_1, X_3) \mathbf{G}_\Lambda \gamma_4^\Lambda(\cdot, \cdot, X_2, X_4) + (\mathbf{S}_\Lambda \leftrightarrow \mathbf{G}_\Lambda) \right] \right. \\ &\quad \left. + \text{tr} \left[ \mathbf{S}_\Lambda \gamma_4^\Lambda(\cdot, \cdot, X_1, X_4) \mathbf{G}_\Lambda \gamma_4^\Lambda(\cdot, \cdot, X_2, X_3) + (\mathbf{S}_\Lambda \leftrightarrow \mathbf{G}_\Lambda) \right] \right\}. \end{aligned} \quad (4.41)$$

Equations (4.39) and (4.41) can be represented diagrammatically as



$$\text{---}\bullet\text{---} = \text{---}\text{loop}\text{---} \quad (4.42)$$



$$\text{---}\bullet\text{---} = \text{---}\text{loop}\text{---} + \text{---}\text{loop}\text{---}, \quad (4.43)$$

where the dot denotes scale-derivative  $d/d\Lambda$ , the slashed propagator is the single-scale propagator  $\mathbf{S}_\Lambda$  and the propagator with no slash is the full interacting propagator  $\mathbf{G}_\Lambda$ . The connection to perturbation theory becomes clearly visible in the diagrammatic representation. The flow of self-energy is given by the first-order perturbation theory diagram, with the bare interaction replaced by the full scale-dependent two-particle vertex function. The flow of the two-particle vertex function is given by the second-order perturbative diagram and the one-loop coupling to the three-particle vertex. One can note that since the exact flow equation (4.29) contains a trace, the diagrammatic representation of the flow equations always contains exactly one loop, which turns out to be advantageous in the practical solution of the equations. For this reason, FRG for one-particle irreducible vertex functions is often called one-loop FRG.

Continuing in this way, one can derive the flow equations for all vertex functions  $\gamma_m^\Lambda$ . It should be clear how the flow equations form an infinite hierarchy: the flow of  $\gamma_m^\Lambda$  is coupled to  $\gamma_{m+2}^\Lambda$ , the flow of which is then coupled to  $\gamma_{m+4}^\Lambda$ , and so on. The solution of this infinite hierarchy of equations would deliver the exact solution, but since it is not possible in general, one must resort to approximations and truncate the hierarchy somehow. Before discussing the truncations, let us assume charge symmetry to make the flow equations more transparent.

We write  $\bar{\psi} = \psi_+$  and  $\psi = \psi_-$ , which means that  $\Psi = (\psi_+, \psi_-)^T$ . Due to charge symmetry, all propagator matrices are of the form

$$\mathbf{A} = \begin{pmatrix} 0 & A \\ -A^T & 0 \end{pmatrix}. \quad (4.44)$$

Matrix  $\mathbf{Q}_\Lambda$  can be written as (Eq. (4.2))

$$\mathbf{Q}_\Lambda = \begin{pmatrix} 0 & -Q_\Lambda \\ Q_\Lambda^T & 0 \end{pmatrix}, \quad (4.45)$$

where  $Q_\Lambda = \mathcal{G}_{0\Lambda}^{-1}$  is the inverse propagator. On the other hand, matrix  $\mathbf{G}_\Lambda = \delta^2 \mathcal{W}_\Lambda[H=0]/\delta H^2$  is of the form

$$\mathbf{G}_\Lambda = \begin{pmatrix} 0 & -\mathcal{G}_\Lambda^T \\ \mathcal{G}_\Lambda & 0 \end{pmatrix}, \quad (4.46)$$

which follows from the fact that

$$\mathcal{G}_\Lambda = -\frac{\delta^2 \mathcal{W}_\Lambda}{\delta \bar{\eta} \delta \eta} = \frac{\delta^2 \mathcal{W}_\Lambda}{\delta H_- \delta H_+}, \quad (4.47)$$

where  $H = (H_+, H_-)^T \equiv (-\eta, \bar{\eta})^T$ . The single-scale propagator becomes

$$\mathbf{S}_\Lambda \equiv -\mathbf{G}_\Lambda \dot{\mathbf{Q}}_\Lambda \mathbf{G}_\Lambda = \begin{pmatrix} 0 & -S_\Lambda^T \\ S_\Lambda & 0 \end{pmatrix}, \quad (4.48)$$

where

$$S_\Lambda = \mathcal{G}_\Lambda \dot{Q}_\Lambda \mathcal{G}_\Lambda. \quad (4.49)$$

Note that the definitions of  $\mathbf{S}_\Lambda$  and  $S_\Lambda$  are analogous, but differ by a minus sign.

Since  $\gamma_2^\Lambda = -\mathbf{G}_\Lambda^{-1}$ , Eq. (4.46) implies that

$$\gamma_2^\Lambda = \begin{pmatrix} 0 & -\mathcal{G}_\Lambda^{-1} \\ \mathcal{G}_\Lambda^{-1T} & 0 \end{pmatrix}. \quad (4.50)$$

Due to charge symmetry,  $\gamma_2(X_1, X_2)$  and  $\gamma_4(X_1, X_2, X_3, X_4)$  are fully determined by the quantities

$$\mathcal{G}_\Lambda^{-1}(\xi_1, \xi_2) = -\gamma_2^\Lambda(\xi_1+, \xi_2-) \quad (4.51)$$

and

$$\Gamma_2^\Lambda(\xi_1, \xi_2; \xi_3, \xi_4) = \gamma_4^\Lambda(\xi_1+, \xi_2+, \xi_4-, \xi_3-), \quad (4.52)$$

where  $X = (\xi, c)$  contains the single-particle quantum number and Matsubara index  $\xi$  and the charge index  $c = \pm$ . This definition of  $\Gamma_2$  is consistent with the definition in Eq. (3.155), where  $\Gamma_2$  was defined as the proper interaction vertex. To derive the flow equations for  $\gamma_0^\Lambda$ ,  $\mathcal{G}_\Lambda^{-1}$  and  $\Gamma_2^\Lambda$ , one uses the general flow equations (4.38), (4.39) and (4.41). This delivers for  $\gamma_0^\Lambda$  and  $\mathcal{G}_\Lambda^{-1}$

$$\dot{\gamma}_0^\Lambda = \text{tr} \left[ \dot{Q}_\Lambda (\mathcal{G}_{0\Lambda} - \mathcal{G}_\Lambda) \right], \quad (4.53)$$

$$\dot{\mathcal{G}}_\Lambda^{-1}(\xi_1, \xi_2) = \dot{Q}_\Lambda(\xi_1, \xi_2) + \text{tr} \left[ S_\Lambda \Gamma_2^\Lambda(\cdot, \xi_1; \cdot, \xi_2) \right], \quad (4.54)$$

where the traces now only extend over the single-particle quantum numbers and Matsubara frequencies. Noting that  $\gamma_0^\Lambda = \beta \Omega_{int}^\Lambda$  is the interaction part of the grand canonical potential and that the full Green's function  $\mathcal{G}_\Lambda$  and the irreducible self-energy  $\Sigma^\Lambda$  are connected by the Dyson equation  $\mathcal{G}_\Lambda^{-1} = Q_\Lambda - \Sigma^\Lambda$ , we finally get

$$\dot{\Omega}_{int}^\Lambda = \frac{1}{\beta} \text{tr} \left[ \dot{Q}_\Lambda (\mathcal{G}_{0\Lambda} - \mathcal{G}_\Lambda) \right], \quad (4.55)$$

$$\dot{\Sigma}^\Lambda(\xi_1, \xi_2) = -\text{tr} \left[ S_\Lambda \Gamma^\Lambda(\cdot, \xi_1; \cdot, \xi_2) \right]. \quad (4.56)$$

The flow equation for the proper interaction vertex becomes

$$\begin{aligned} \dot{\Gamma}_2^\Lambda(\xi_1, \xi_2, \cdot; \xi_3, \xi_4) &= \sum_{\eta_1, \eta_2} S_\Lambda(\eta_1, \eta_2) \Gamma_3^\Lambda(\eta_2, \xi_1, \xi_2; \eta_1, \xi_3, \xi_4) \\ &+ \frac{1}{2} \sum_{\substack{\eta_1, \eta_2 \\ \eta_3, \eta_4}} P_\Lambda(\eta_2, \eta_1; \eta_3, \eta_4) \Gamma_2^\Lambda(\xi_1, \xi_2; \eta_3, \eta_2) \Gamma_2^\Lambda(\eta_4, \eta_1; \xi_3, \xi_4) \\ &- \sum_{\substack{\eta_1, \eta_2 \\ \eta_3, \eta_4}} P_\Lambda(\eta_2, \eta_1; \eta_4, \eta_3) \Gamma_2^\Lambda(\eta_3, \xi_2; \eta_2, \xi_4) \Gamma_2^\Lambda(\eta_1, \xi_1; \eta_4, \xi_3) \\ &+ \sum_{\substack{\eta_1, \eta_2 \\ \eta_3, \eta_4}} P_\Lambda(\eta_2, \eta_1; \eta_4, \eta_3) \Gamma_2^\Lambda(\eta_3, \xi_1; \eta_2, \xi_4) \Gamma_2^\Lambda(\eta_1, \xi_2; \eta_4, \xi_3), \end{aligned} \quad (4.57)$$

where

$$P_\Lambda(\eta_1, \eta_2; \eta_3, \eta_4) = S_\Lambda(\eta_1, \eta_2) \mathcal{G}_\Lambda(\eta_3, \eta_4) + \mathcal{G}_\Lambda(\eta_1, \eta_2) S_\Lambda(\eta_3, \eta_4) \quad (4.58)$$

contains the loop propagators and

$$\Gamma_3^\Lambda(1', 2', 3'; 1, 2, 3) \equiv \frac{\delta^6 \Gamma_\Lambda[\Phi = 0]}{\delta \bar{\phi}_1 \delta \bar{\phi}_{2'} \delta \bar{\phi}_{3'} \delta \phi_3 \delta \phi_2 \delta \phi_1} \quad (4.59)$$

$$= -\gamma_6^\Lambda(1'+, 2'+, 3'+, 3-, 2-, 1-) \quad (4.60)$$

is the proper three-particle vertex. Equations (4.56) and (4.57) can be presented diagrammatically as

$$\text{Diagram with a dot on a circle} = \text{Diagram with a loop on a circle} \quad (4.61)$$

$$\begin{aligned} \text{Diagram with a dot on a circle} &= \text{Diagram with two circles and a slash} + \text{Diagram with two circles and a slash} + \text{Diagram with two circles and a slash} \\ &+ \text{Diagram with a loop on a circle} \end{aligned} \quad (4.62)$$

Here the slashed propagator  $\rightarrow\!-\!\rightarrow$  is the single-scale propagator  $S_\Lambda$  and the internal propagator  $\rightarrow\!\rightarrow$  with no slash is the full interacting propagator. All terms with multiple internal propagators must be interpreted such that any one of them may be the slashed one (Eq. (4.58)). Therefore, each of the diagrams on the first row of Eq. (4.62) actually contains two terms. Note that if the full two-particle vertex in the flow equation (4.61) is replaced by the bare interaction, the value of the scale derivative is the negative of the first-order perturbative result. In perturbation theory, each interaction vertex comes with a minus sign, which is not present in (4.56), since the minus sign in the equation has to be related to the fermionic loop. Similarly, the flow equation for the amputated two-particle Green's function ( $-\Gamma_2^\Lambda$ ) is minus the second-order perturbative result (plus the three-particle vertex term). The minus signs arise from our sign definition for  $S_\Lambda$ , which has been chosen to conform to existing literature. With this exception of an additional minus sign, all signs and factors of 1/2 can be deduced from these equations by using standard diagrammatic rules[50] for Hugenholtz diagrams.

The three diagrams in the flow equation for  $\Gamma_2^\Lambda$  are referred to as

$$\begin{aligned} \text{Diagram 1: } s\text{-channel, "BCS"} \\ \text{Diagram 2: } t\text{-channel, "zero-sound"} \\ \text{Diagram 3: } u\text{-channel, "exchange zero-sound"} \end{aligned}$$

The names "BCS" and "zero-sound" are customary in the theory of Fermi liquids. The names  $s$ -,  $t$ - and  $u$ -channel refer to the fact that at the bare level, the dependence of each diagram on the external momenta only depends on the corresponding Mandelstam variable  $s$ ,  $t$  or  $u$ .

This concludes the derivation of flow equations. In the following, we discuss the truncations used in the approximate solution of Eqs. (4.55), (4.56) and (4.57) and present different choices for the cut-off function.

## 4.4 Truncations

To extract physical information out of the infinite hierarchy of flow equations, one must truncate the hierarchy somehow. In some special cases, the flow equations can be solved exactly[73, 74], but these models can be solved in other means as well. The close resemblance of the flow equations to perturbation theory makes it, however, easy to devise practical truncations. For example, if one is only interested in one-particle properties, the simplest available approximation is to set the effective interaction  $\Gamma_2^\Lambda$  equal to the bare interaction  $V$  for all  $\Lambda$  and set  $\Gamma_{n \geq 3}^\Lambda = 0$ . The flow equation for the self-energy then resembles the self-consistent Hartree-Fock approximation, but can deliver physically better results than the iterative solution of the self-consistent equations[65].

In the early studies on the two-dimensional Hubbard model, the flows of both the self-energy and  $\Gamma_{n \geq 3}^\Lambda$  were neglected[62, 63, 64]. The flow equation for the three-particle vertex is of third order in the renormalized interaction strength and can therefore be neglected for weak coupling. Typically the flows lead, however, to strong coupling and the approximation breaks down, but FRG seemed to reproduce good results anyway. This can be understood by arguments showing that for fermions with curved Fermi surfaces,  $\Gamma_{n \geq 3}^\Lambda$  remain small in the course of the flow[12].

However, the simple truncation  $\Gamma_{n \geq 3}^\Lambda = 0$  turns out to be insufficient to obtain e.g. the correct BCS gap[75]. Katanin studied the fulfillment of Ward identities related to charge symmetry and was able to show that the fulfillment can be improved by including some terms from the three-particle vertex[76]. The modification can be included in the closed flow equation for the two-particle vertex by simply modifying the single-scale propagator  $S_\Lambda$ . The Katanin modification can be derived heuristically as follows.

The flow equation for the antisymmetrized three particle vertex contains only a single term that is of the third order in the two-particle vertex  $\gamma_4^\Lambda$ :

$$\text{Diagram with a shaded circle and a dot on top} = \text{Diagram with two shaded circles connected by a horizontal line} + \mathcal{O}((\gamma_4^\Lambda)^4) \quad (4.63)$$

$$= -\frac{d}{d\Lambda} \text{Diagram with two shaded circles connected by a horizontal line and a shaded circle above} + \mathcal{O}((\gamma_4^\Lambda)^4), \quad (4.64)$$

where the second line holds since the scale derivatives of each two-particle vertex lead to terms of the order  $\mathcal{O}((\gamma_4^\Lambda)^2)$  and the single-scale propagator is  $\mathbf{S}_\Lambda = -d\mathbf{G}_\Lambda/d\Lambda + \mathcal{O}(\gamma_4^\Lambda)$ . Therefore by integration,

$$\text{Diagram 1} = -\text{Diagram 2} + \mathcal{O}((\gamma_4^\Lambda)^4). \quad (4.65)$$

Substituting the three-particle vertex in the flow equation for the antisymmetrized two-particle vertex,

$$\text{Diagram 3} = \text{Diagram 4} + \text{Diagram 5},$$

one gets

$$\text{Diagram 3} = \text{Diagram 4} - \text{Diagram 6} - \text{Diagram 7} + \dots \quad (4.66)$$

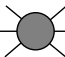
The upper propagators in the first and the second diagram can be combined to give

$$-\mathbf{G}_\Lambda \left[ \dot{\mathbf{Q}}_\Lambda - \frac{1}{2} \text{tr} (\mathbf{S}_\Lambda \gamma_\Lambda^4) \right] \mathbf{G}_\Lambda \stackrel{\text{Eq. (4.39)}}{=} -\mathbf{G}_\Lambda \left[ -\frac{d}{d\Lambda} \mathbf{G}_\Lambda^{-1} \right] \mathbf{G}_\Lambda = -\frac{d}{d\Lambda} \mathbf{G}_\Lambda. \quad (4.67)$$

Therefore, the second diagram can be absorbed into the truncated flow equation

$$\text{Diagram 3} = \text{Diagram 4}$$

simply by using the replacement  $\mathbf{S}_\Lambda \rightarrow \tilde{\mathbf{S}}_\Lambda = -\frac{d}{d\Lambda} \mathbf{G}_\Lambda$ . The third diagram in Eq. (4.66) is a diagram with a so-called "overlapping loop" and is often discarded[12]. Note also how the feedback of the three-particle vertex in the flow equation for the two-particle vertex produces two-loop diagrams.

Since its introduction, Katanin modification has become the standard method for the truncation of flow equations and it has delivered surprisingly good results even for moderately strong interactions[67, 68]. In addition, the modification solves the BCS gap problem and even allows one to derive the Eliashberg equations from FRG flow equations[75, 74]. In later sections, we show how the FRG flow for the spin system runs into the antiferromagnetic instability and diverges at a finite scale, if one uses the simple truncation  $\Gamma_3^\Lambda = 0$ . Later we will refer to the Katanin modified FRG as "Katanin FRG" or, unless otherwise noted, simply "FRG". In Sect. 5.4, where we study the importance of the Katanin truncation, we refer to the truncation with no Katanin modification as "FRG,  = 0" or "naive FRG".

Even after the truncation of the flow equations, the remaining flow equation for the two-particle vertex can still be too complicated to solve, since the vertex

typically depends on three momenta and three Matsubara frequencies. Therefore, one is often also forced to neglect some of the dependence on these quantities. For example, in the two-dimensional Brillouin zone, the direction perpendicular to the Fermi surface is irrelevant in the RG sense and can therefore be neglected in the low-energy regime[58]. Similarly, the dependence on the Matsubara frequency can be neglected in some cases, leading to so-called "static FRG"[66].

For the special case of localized electrons, for which the propagator is diagonal in site indices, it turns out that the spatial dependence can be parametrized by a single parameter, i.e. the distance between sites. Since the scaling of the problem as a function of the system size is only linear, one can also include the full frequency dependence of both the self-energy and the two-particle vertex without encountering huge computational difficulties. In addition, it was shown earlier for quantum spin models that if the frequency-dependence of the two-particle interaction vertex is neglected, the electron self-energy remains zero in the flow[14]. As a consequence, the flow always runs into the unphysical antiferromagnetic instability caused by the absence of damping. Therefore, we retain the full frequency-dependence of the vertices and the only approximation that we make in the solution of the flow equations is the Katanin truncation. The price to pay for the locality is that there is no Fermi surface and the truncation of the flow equations by setting  $\Gamma_{n \geq 3}^\Lambda = 0$  (in the Katanin sense) cannot be justified. This is one of the main motivating factors for this work: to see whether the truncated flow equations can describe the physics of spin systems accurately.

## 4.5 Choice of the cut-off function

The final point to discuss in the FRG flow equations is the choice of the cut-off function. In principle, the function can be chosen freely, as long as the theory is easy to solve for some value of the parameter  $\Lambda$  and any infrared singularities are regularized by the parameter. The most typical choice for kinetic electrons on a translationally invariant lattice is the momentum-space cut-off:

$$\mathcal{G}_{0\Lambda}(\mathbf{k}, \omega_n, \sigma) = \Theta(|\xi_{\mathbf{k}}| - \Lambda) \mathcal{G}_0(\mathbf{k}, \omega_n, \sigma), \quad (4.68)$$

which shuts down modes close to the Fermi surface. Here  $\xi_k = \epsilon_k - \mu$  is the kinetic energy relative to the Fermi surface. This choice is closest in spirit to Wilson's momentum-space RG known from statistical physics, with the exception that whereas in statistical physics one renormalizes towards the point  $k = 0$ , in fermionic systems one renormalizes towards a surface.

In absence of translational invariance or for other reasons, one can introduce a cut-off in the Matsubara frequency space<sup>4</sup>:

$$\mathcal{G}_{0\Lambda}(i, j; \omega_n, \sigma) = \Theta(|\omega_n| - \Lambda) \mathcal{G}_0(i, j; \omega_n, \sigma). \quad (4.69)$$

---

<sup>4</sup>For  $T > 0$ , when Matsubara frequencies are constrained to discrete values  $\omega_n = (2n + 1)\pi T$ , it may be more convenient to use a smoothened step function as a cut-off.

Since our free propagator

$$\mathcal{G}_0(\omega) = \frac{1}{i\omega}$$

will only depend on frequency, we choose to use cut-off in frequency, as earlier[14]. The scale-dependent interacting propagator is then

$$\mathcal{G}_\Lambda \equiv \frac{1}{\mathcal{G}_{0\Lambda}^{-1} - \Sigma^\Lambda(\omega)} = \frac{\Theta(|\omega| - \Lambda)}{i\omega - \Theta(|\omega| - \Lambda)\Sigma^\Lambda(\omega)}. \quad (4.70)$$

The single-scale propagator (4.49) becomes

$$S_\Lambda(\omega) = \mathcal{G}_\Lambda^2 \frac{d}{d\Lambda} \frac{i\omega}{\Theta(|\omega| - \Lambda)} \quad (4.71)$$

$$= \frac{\Theta(|\omega| - \Lambda)^2}{[i\omega - \Theta(|\omega| - \Lambda)\Sigma^\Lambda(\omega)]^2} \frac{i\omega\delta(|\omega| - \Lambda)}{\Theta(|\omega| - \Lambda)^2} \quad (4.72)$$

$$= \frac{i\omega\delta(|\omega| - \Lambda)}{[i\omega - \Theta(|\omega| - \Lambda)\Sigma^\Lambda(\omega)]^2}. \quad (4.73)$$

Using Morris' Lemma[72],

$$\delta(a)F(\Theta(a); a) = \delta(a) \int_0^1 d\Theta F(\Theta; a), \quad (4.74)$$

one can write

$$S_\Lambda(\omega) = i\omega\delta(|\omega| - \Lambda) \int_0^1 dt \frac{1}{[i\omega - t\Sigma^\Lambda(\omega)]^2} \quad (4.75)$$

$$= \frac{\delta(|\omega| - \Lambda)}{i\omega - \Sigma^\Lambda(\omega)}. \quad (4.76)$$

Thus the single-scale propagator is equal to the full propagator with the additional property that the frequency is constrained at the cut-off scale. Therefore, the loop integration over frequency on the right-hand side of flow equations is eliminated by the delta function, which makes the numerical solution of the truncated flow equations easy. In the Wick-ordered version[61] of FRG, the flow equations contain one-particle reducible terms that do not contain a loop integration, meaning that the delta function remains and one has to take special care in the numerical solution. This is one of the major assets of using the one-particle irreducible version of FRG. We also note that unlike in Eq. (4.76), the single-scale propagator in the Wick-ordered version does not contain the self-energy feedback.

In the Katanin modified scheme, the single-scale propagator is

$$\tilde{S}_\Lambda(\omega) = -\frac{d\mathcal{G}_\Lambda(\omega)}{d\Lambda} \quad (4.77)$$

$$= \delta(|\omega| - \Lambda)\mathcal{G}_\Lambda(\omega) - \mathcal{G}_\Lambda(\omega)^2\dot{\Sigma}^\Lambda(\omega). \quad (4.78)$$



Since the second term does not contain a delta function, each loop integration has to be carried out and the numerical solution becomes notably slower, but remains manageable.

In addition to cut-offs in momentum or energy space, one can also use e.g. temperature[77], strength of the interaction[78] or even an imaginary chemical potential of reservoirs[79] as the flow parameter. Since the analytical properties of Green's functions are altered by the cut-off functions, one may violate e.g. fluctuation-dissipation theorem or causality. The influence of various cut-off functions on equilibrium and non-equilibrium analyticity theorems are discussed in Ref. [80].

## 4.6 Flow equations for the spin system

Let us now derive the flow equations for the spin system. Writing  $\xi = (\omega, i, \alpha)$ , where the indices are the Matsubara frequency  $\omega$ , site index  $i$  and the spin index  $\alpha$ , the parametrization (3.157)

$$\Gamma_2^\Lambda(\xi_1, \xi_2; \xi_3, \xi_4) = [\Gamma_{si_1i_2}^\Lambda(s, t, u) \sigma_{\alpha_1\alpha_3}^k \sigma_{\alpha_2\alpha_4}^k + \Gamma_{di_1i_2}^\Lambda(s, t, u) \delta_{\alpha_1\alpha_3} \delta_{\alpha_2\alpha_4}] \times \delta_{i_1i_3} \delta_{i_2i_4} \beta \delta_{\omega_1+\omega_2, \omega_3+\omega_4} - [1 \leftrightarrow 2] \quad (4.79)$$

can be presented diagrammatically as

$$\begin{aligned} & \begin{array}{c} (\omega_3, i_3, \alpha_3) \quad (\omega_1, i_1, \alpha_1) \\ \swarrow \quad \searrow \\ \text{---} \text{---} \text{---} \text{---} \\ \nwarrow \quad \nearrow \\ (\omega_4, i_4, \alpha_4) \quad (\omega_2, i_2, \alpha_2) \end{array} = \begin{array}{c} \xrightarrow{\omega_3} \quad \xrightarrow{\omega_1} \\ \text{---} \text{---} \text{---} \text{---} \\ \text{---} \text{---} \text{---} \text{---} \\ \xrightarrow{\omega_4} \quad \xrightarrow{\omega_2} \end{array} \sigma_{\alpha_1\alpha_3}^k \sigma_{\alpha_2\alpha_4}^k \delta_{i_1i_3} \delta_{i_2i_4} \beta \delta_{\omega_1+\omega_2, \omega_3+\omega_4} \\ & + \begin{array}{c} \xrightarrow{\omega_3} \quad \xrightarrow{\omega_1} \\ \text{---} \text{---} \text{---} \text{---} \\ \text{---} \text{---} \text{---} \text{---} \\ \xrightarrow{\omega_4} \quad \xrightarrow{\omega_2} \end{array} \delta_{\alpha_1\alpha_3} \delta_{\alpha_2\alpha_4} \delta_{i_1i_3} \delta_{i_2i_4} \beta \delta_{\omega_1+\omega_2, \omega_3+\omega_4} \\ & + \text{exchange } (1 \leftrightarrow 2). \end{aligned} \quad (4.80)$$

Here the red and blue dashed lines represent the spin-spin interaction

$$\Gamma_{si_1i_2}^\Lambda(s, t, u) = \begin{array}{c} \xrightarrow{\omega_3} \quad \xrightarrow{\omega_1} \\ \text{---} \text{---} \text{---} \text{---} \\ \text{---} \text{---} \text{---} \text{---} \\ \xrightarrow{\omega_4} \quad \xrightarrow{\omega_2} \end{array}$$

and the density-density interaction

$$\Gamma_{di_1i_2}^\Lambda(s, t, u) = \begin{array}{c} \xrightarrow{\omega_3} \quad \xrightarrow{\omega_1} \\ \text{---} \text{---} \text{---} \text{---} \\ \text{---} \text{---} \text{---} \text{---} \\ \xrightarrow{\omega_4} \quad \xrightarrow{\omega_2} \end{array},$$

respectively. Substituting the parametrization in the truncated flow equation

$$\text{Diagram 1} = \text{Diagram 2} + \text{Diagram 3} + \text{Diagram 4},$$

carrying out the spin sums and comparing terms with coinciding spin and site structure gives the flow equations

$$\begin{aligned} \text{Diagram 1} &= -2 \text{Diagram 2} + \text{Diagram 3} + \text{Diagram 4} \\ &+ 2 \text{Diagram 5} - \text{Diagram 6} + \text{Diagram 7} \\ &- \text{Diagram 8} + \text{Diagram 9} \\ &+ 2 \text{Diagram 10} + \text{Diagram 11} + \text{Diagram 12} \end{aligned} \quad (4.81)$$

and

$$\begin{aligned} \text{Diagram 1} &= \text{Diagram 2} + 3 \text{Diagram 3} \\ &+ 2 \text{Diagram 4} + 3 \text{Diagram 5} + \text{Diagram 6} \\ &+ 3 \text{Diagram 7} + \text{Diagram 8} \\ &+ 3 \text{Diagram 9} + \text{Diagram 10} \end{aligned} \quad (4.82)$$

In these flow equations, the spin structure has been eliminated by using the rotational symmetry, but the site and frequency structures remain. For example, the RPA diagrams with internal loops contain a summation over all sites. The explicit

presentation of the flow equations is given in App. A and in Ref. [14], App. A. Note that our definition of  $P_\Lambda$  differs from  $P^\Lambda$  of Ref. [14] by a minus sign and a symmetry term.

The flow equation

for the self-energy becomes

where we have parametrized the scale-dependent self-energy by (cf. Eq. (3.156))

$$\Sigma^\Lambda(\omega_1, i_1, \alpha_1; \omega_2, i_2, \alpha_2) = \Sigma^\Lambda(\omega_1) \beta \delta_{\omega_1, \omega_2} \delta_{i_1 i_2} \delta_{\alpha_1 \alpha_2}. \quad (4.84)$$

What are the initial conditions if the flow is started at  $\Lambda = \infty$ ? The correct initial conditions can be derived rigorously from the formalism[71], but for our purposes, it suffices to remember that e.g.  $\Sigma^\Lambda$  is just the interacting self-energy for a system in which the free propagator contains an infrared cut-off  $\Lambda$ . Therefore, the value can be calculated perturbatively in  $J/\Lambda$ , and only the first-order terms  $\mathcal{O}(J)$  survive in the limit  $\Lambda \rightarrow \infty$ . Comparing parametrizations (4.79) and (4.84) with the bare action (3.127), we see that the initial conditions are  $\Gamma_{sij}^{\Lambda=\infty}(s, t, u) = J_{ij}/4$ ,  $\Gamma_{dij}^{\Lambda=\infty}(s, t, u) = 0$  and  $\Sigma^{\Lambda=\infty}(\omega) = 0^5$ .

The flow equation (4.55) for the interacting part of the grand canonical potential is

$$\dot{\Omega}_{int}^\Lambda \equiv \frac{1}{\beta} \text{tr} \left\{ \dot{Q}_\Lambda [\mathcal{G}_{0\Lambda} - \mathcal{G}_\Lambda] \right\} \quad (4.85)$$

$$= 2N \int \frac{d\omega}{2\pi} \frac{i\omega \delta(|\omega| - \Lambda)}{\Theta(|\omega| - \Lambda)^2} \left[ \frac{\Theta(|\omega| - \Lambda)}{i\omega} - \frac{\Theta(|\omega| - \Lambda)}{i\omega - \Theta(|\omega| - \Lambda) \Sigma^\Lambda(\omega)} \right] \quad (4.86)$$

$$= -2N \int \frac{d\omega}{2\pi} \Sigma^\Lambda(\omega) \delta(|\omega| - \Lambda) \frac{1}{i\omega - \Theta(|\omega| - \Lambda) \Sigma^\Lambda(\omega)} \quad (4.87)$$

$$\stackrel{\text{Eq. (4.74)}}{=} -2N \int \frac{d\omega}{2\pi} \Sigma^\Lambda(\omega) \delta(|\omega| - \Lambda) \int_0^1 \frac{dt}{i\omega - t \Sigma^\Lambda(\omega)} \quad (4.88)$$

$$= 2N \int \frac{d\omega}{2\pi} \log \left( 1 - \frac{\Sigma^\Lambda(\omega)}{i\omega} \right) \delta(|\omega| - \Lambda) \quad (4.89)$$

$$= \frac{2N}{\pi} \log \left( 1 + \frac{\gamma^\Lambda(\Lambda)}{\Lambda} \right), \quad (4.90)$$

where, in the last line, we defined  $\gamma^\Lambda(\omega) = i\Sigma^\Lambda(\omega)$ .  $N$  is the number of sites in our translationally invariant system. Since we work at  $T = 0$  and  $\mu = 0$  and the ground

---

<sup>5</sup>The zero value of the self-energy is not trivial, but both Hartree and Fock terms are zero because of the absence of local spin and density interactions.

state energy of the free system is  $E_0 = 0$ ,  $\Omega_{int}$  is equal to the interacting ground state energy  $E$ . The initial condition is  $\Omega_{int}^{\Lambda=\infty} = 0$ .

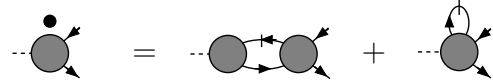
In addition to the flow equations for ground state energy, one-particle self-energy and the two-particle proper vertex, we need flow equations for the main observables of interest, spin and density susceptibilities. The relevant flow equations for any one-particle operator  $A(\xi)$  can be straightforwardly derived by adding to the action the coupling term  $\sum_{\xi} a(\xi)A(\xi)$  and calculating the flows of the response vertex function

$$V_A^{\Lambda}(\xi; \xi_1, \xi_2) = \frac{\delta^3 \Gamma_{\Lambda}[\Phi = 0]}{\delta a(\xi) \delta \bar{\phi}(\xi_1) \delta \phi(\xi_2)} \quad (4.91)$$

and the connected susceptibility

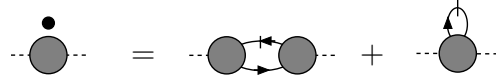
$$X_A^{\Lambda}(\xi, \xi') = \frac{\delta^2 \Gamma_{\Lambda}[\Phi = 0]}{\delta a(\xi) \delta a(\xi')} \quad (4.92)$$

and taking the limit  $a \rightarrow 0$  [62, 12]. The form of the resulting flow equations should be easy to guess based on the diagrammatic representation: the flow equation for the vertex  $V^{\Lambda}$  is (with the additional minus sign, see the discussion after Eqs. (4.61) and (4.62))



$$\text{---} \bullet \text{---} = \text{---} \text{---} + \text{---} \text{---} \quad (4.93)$$

and for the susceptibility



$$\text{---} \bullet \text{---} = \text{---} \text{---} + \text{---} \text{---} \quad (4.94)$$

The initial condition of the vertex determines for which observable the flows are calculated. For the fluctuation density operator

$$\tilde{n}_i = \sum_{\alpha} \left( c_{i\alpha}^{\dagger} c_{i\alpha} - \langle c_{i\alpha}^{\dagger} c_{i\alpha} \rangle \right),$$

the vertex function

$$V_d((\tau, i); (\tau_1, i_1, \alpha_1), (\tau_2, i_2, \alpha_2)) = \left\langle T_{\tau} \tilde{n}_i(\tau) c_{i_1 \alpha_1}(\tau_1) c_{i_2 \alpha_2}^{\dagger}(\tau_2) \right\rangle_{amp} \quad (4.95)$$

can be parametrized in frequency space by

$$V_d^{\Lambda}(\omega, i; (\omega_1, i_1, \alpha_1), (\omega_2, i_2, \alpha_2)) = v_{dii_1}^{\Lambda}(\omega, s) \beta \delta_{\omega, \omega_1 - \omega_2} \delta_{i_1 i_2} \delta_{\alpha_1 \alpha_2}, \quad (4.96)$$

and the initial condition is given by the bare value  $v_{dii_1}^{\Lambda=\infty}(\omega, s) = \delta_{ii_1}$ . Here we have used conservation of frequency to conclude that  $\omega + \omega_2 = \omega_1$  and used  $s = \omega_1 + \omega_2$  as the second relevant bosonic frequency variable. It is then straightforward to show using the methods of Chap. 3.2 that time-reversal invariance implies that

$$v_{dij}^{\Lambda}(\omega, s) = v_{dij}^{\Lambda}(-\omega, s) \quad (4.97)$$

and the particle-hole transformation gives

$$v_{di}^\Lambda(\omega, s) = v_{di}^\Lambda(\omega, -s). \quad (4.98)$$

In addition, we have used the local particle number conservation to conclude that  $i_1 = i_2$  for a non-vanishing contribution.

Similarly for the spin operator

$$S_i^z = \frac{1}{2} \sum_{\alpha\beta} \sigma_{\alpha\beta}^z c_{i\alpha}^\dagger c_{i\beta},$$

we use for the vertex

$$V_s((\tau, i); (\tau_1, i_1, \alpha_1), (\tau_2, i_2, \alpha_2)) = \left\langle T_\tau S_i^z(\tau) c_{i_1\alpha_1}(\tau_1) c_{i_2\alpha_2}^\dagger(\tau_2) \right\rangle_{amp} \quad (4.99)$$

the parametrization

$$V_s^\Lambda(\omega, i; (\omega_1, i_1, \alpha_1), (\omega_2, i_2, \alpha_2)) = v_{sii_1}^\Lambda(\omega, s) \beta \delta_{\omega, \omega_1 - \omega_2} \delta_{i_1 i_2} \sigma_{\alpha_1 \alpha_2}^z \quad (4.100)$$

with the initial condition  $v_{sii_1}^{\Lambda=\infty}(\omega, s) = \delta_{ii_1}/2$ . The symmetry properties (4.97) and (4.98) also hold for the spin vertex. Diagrammatically, we write

$$\begin{array}{c} (\omega, i) \text{---} \bullet \\ \swarrow \quad \searrow \\ (\omega_2, i_2, \alpha_2) \quad (\omega_1, i_1, \alpha_1) \end{array} = \begin{array}{c} \omega_2 \\ \swarrow \quad \searrow \\ \text{---} \frac{\omega}{i} \text{---} \bullet_{i_1} \\ \swarrow \quad \searrow \\ \omega_1 \end{array} \beta \delta_{\omega, \omega_1 - \omega_2} \delta_{i_1 i_2} \delta_{\alpha_1 \alpha_2} \quad (4.101)$$

for the density vertex and

$$\begin{array}{c} (\omega, i) \text{---} \bullet \\ \swarrow \quad \searrow \\ (\omega_2, i_2, \alpha_2) \quad (\omega_1, i_1, \alpha_1) \end{array} = \begin{array}{c} \omega_2 \\ \swarrow \quad \searrow \\ \text{---} \frac{\omega}{i} \text{---} \bullet_{i_1} \\ \swarrow \quad \searrow \\ \omega_1 \end{array} \beta \delta_{\omega, \omega_1 - \omega_2} \delta_{i_1 i_2} \sigma_{\alpha_1 \alpha_2}^z \quad (4.102)$$

for the spin vertex.

Substituting the parametrizations in the truncated flow equation

$$\begin{array}{c} \bullet \\ \swarrow \quad \searrow \\ \text{---} \bullet \end{array} = \begin{array}{c} \bullet \\ \swarrow \quad \searrow \\ \text{---} \bullet \end{array} \begin{array}{c} \bullet \\ \swarrow \quad \searrow \\ \text{---} \bullet \end{array} \begin{array}{c} \bullet \\ \swarrow \quad \searrow \\ \text{---} \bullet \end{array} \quad (4.103)$$

and using also parametrization (4.80), we arrive at

$$\begin{array}{c} \bullet \\ \swarrow \quad \searrow \\ \text{---} \bullet \end{array} = \begin{array}{c} \bullet \\ \swarrow \quad \searrow \\ \text{---} \bullet \end{array} \begin{array}{c} \bullet \\ \swarrow \quad \searrow \\ \text{---} \bullet \end{array} \begin{array}{c} \bullet \\ \swarrow \quad \searrow \\ \text{---} \bullet \end{array} + 3 \begin{array}{c} \bullet \\ \swarrow \quad \searrow \\ \text{---} \bullet \end{array} \begin{array}{c} \bullet \\ \swarrow \quad \searrow \\ \text{---} \bullet \end{array} \begin{array}{c} \bullet \\ \swarrow \quad \searrow \\ \text{---} \bullet \end{array} + 2 \begin{array}{c} \bullet \\ \swarrow \quad \searrow \\ \text{---} \bullet \end{array} \begin{array}{c} \bullet \\ \swarrow \quad \searrow \\ \text{---} \bullet \end{array} \begin{array}{c} \bullet \\ \swarrow \quad \searrow \\ \text{---} \bullet \end{array} \quad (4.104)$$

for the density vertex and

$$= - \text{diagram} + \text{diagram} + 2 \text{diagram} \quad (4.105)$$

for the spin vertex. Explicitly, the flow equations are

$$\begin{aligned} \dot{v}_{dij}^{\Lambda}(\omega, s) &= \int \frac{d\nu}{2\pi} P_{\Lambda}(\nu, \nu + \omega) \\ &\times [v_{dij}^{\Lambda}(\omega, 2\nu + \omega) \Gamma_{dii}^{\Lambda}(\omega_1 + \nu, \omega_2 - \nu, \omega) \\ &+ 3v_{dij}^{\Lambda}(\omega, 2\nu + \omega) \Gamma_{sii}^{\Lambda}(\omega_1 + \nu, \omega_2 - \nu, \omega) \\ &- 2 \sum_k v_{dik}^{\Lambda}(\omega, 2\nu + \omega) \Gamma_{dkj}^{\Lambda}(\omega_1 + \nu, \omega, \omega_2 - \nu)] \end{aligned} \quad (4.106)$$

and

$$\begin{aligned} \dot{v}_{sij}^{\Lambda}(\omega, s) &= \int \frac{d\nu}{2\pi} P_{\Lambda}(\nu, \nu + \omega) \\ &\times [-v_{sij}^{\Lambda}(\omega, 2\nu + \omega) \Gamma_{sii}^{\Lambda}(\omega_1 + \nu, \omega_2 - \nu, \omega) \\ &+ v_{sij}^{\Lambda}(\omega, 2\nu + \omega) \Gamma_{dii}^{\Lambda}(\omega_1 + \nu, \omega_2 - \nu, \omega) \\ &- 2 \sum_k v_{sik}^{\Lambda}(\omega, 2\nu + \omega) \Gamma_{skj}^{\Lambda}(\omega_1 + \nu, \omega, \omega_2 - \nu)] . \end{aligned} \quad (4.107)$$

Here  $\omega_1 = (\omega + s)/2$  and  $\omega_2 = (-\omega + s)/2$  are the outgoing and incoming fermion frequencies, respectively.

The truncated flow equation

$$= \text{diagram} \quad (4.108)$$

delivers for the density susceptibility

$$D_{ij}(\omega) = \int_0^{\infty} d\tau e^{i\omega\tau} \langle T_{\tau} \tilde{n}_i(\tau) \tilde{n}_j \rangle_{conn} \quad (4.109)$$

the flow equation

$$\dot{D}_{ij}^{\Lambda}(\omega) = 2 \sum_k \int \frac{d\nu}{2\pi} v_{dik}^{\Lambda}(\omega, 2\nu + \omega) v_{dkj}^{\Lambda}(-\omega, 2\nu + \omega) P_{\Lambda}(\nu, \nu + \omega). \quad (4.110)$$

The flow equation for the spin susceptibility

$$\chi_{ij}(\omega) = \int_0^{\infty} d\tau e^{i\omega\tau} \langle T_{\tau} S_i^z(\tau) S_j^z \rangle_{conn} \quad (4.111)$$

becomes

$$\dot{\chi}_{ij}^{\Lambda}(\omega) = 2 \sum_k \int \frac{d\nu}{2\pi} v_{sik}^{\Lambda}(\omega, 2\nu + \omega) v_{skj}^{\Lambda}(-\omega, 2\nu + \omega) P_{\Lambda}(\nu, \nu + \omega). \quad (4.112)$$

In the Katanin-modified flow scheme, one encounters the question whether one should use the modified single-scale propagator  $\tilde{S}_{\Lambda} = -dG_{\Lambda}/d\Lambda$  in the flow equations for the susceptibility vertices and the susceptibilities as well, in order to partially include the neglected terms appearing in Eqs. (4.93) and (4.94). If no Katanin truncation is applied in either equation, it turns out that the susceptibilities diverge even though the interaction vertices do not. If Katanin truncation is applied in both equations, the correction becomes too strong and e.g. the local spin correlations  $\chi_{ii}$  turn out to be negative, which is a non-sensible result. Therefore, we choose to apply the Katanin-modified single-scale propagator  $\tilde{S}_{\Lambda} = -dG_{\Lambda}/d\Lambda$  only in the flow equations for the susceptibility vertices (and for interaction vertices, of course). Diagrammatic considerations seem to suggest, however, that the modification should be done in the flow equation for the susceptibility as well, but since this leads to completely unsatisfactory results, we choose not to.

# Chapter 5

## Results

*In this Chapter, we present the application of functional renormalization group (FRG) method to spin systems in reduced dimensions. In Section 5.1, we discuss the numerical implementation and define various related parameters. Section 5.2 is devoted to briefly discussing the numerical complexity of the problem and showing how a simple parallelization results in a notable speed-up. The reliability of our numerical solution is demonstrated in Section 5.3.1. To benchmark the validity of FRG, we do the calculations for the simple two-site Heisenberg model, for which exact results are easy to derive. The physical interpretation of FRG results is postponed to Section 5.3.2. In Section 5.4, we apply FRG to an antiferromagnetic Heisenberg chain and discuss the importance of Katanin truncation in regularizing the antiferromagnetic instability. In addition, we see whether FRG is able to reproduce the algebraically decaying correlations known from the exact solution.*

### 5.1 Discussion of numerics

**Discretization:** In this section, we study systematically the numerical solution of the flow equations presented in Sect. 4.6 and App. A. The flow equations are coupled non-linear integro-differential equations and the number of variables is continuously infinite due to the continuity of the frequency variables at  $T = 0$ . Thus, the first task in the numerical solution is to discretize the frequency axis and reduce the number of variables to a finite value that can be handled numerically. As shown in Sect. 3.2, we only have to consider the positive frequency axis, since the self-energy and vertex functions are odd and even functions in frequency variables, respectively. We have chosen to use a geometric mesh, where the smallest frequency is 0 and the non-zero frequencies are at

$$\omega_n = \omega_0 \frac{a^n - 1}{a - 1}, \quad n = 1, 2, \dots, N_f. \quad (5.1)$$

$\omega_0$  determines the smallest non-zero frequency and  $a$  is a scaling variable such that

$$\omega_{n+1} - \omega_n = a^n \omega_0, \quad (5.2)$$



i.e. the distance between neighboring frequencies increases exponentially. Considering the computational complexity of the problem, the most crucial variable in the numerical implementation is the number of frequencies,  $N_f$ , since one then has to solve the differential equations for  $N_f^3$  vertex functions, which determines the size scaling of the problem. By default, we set the smallest non-zero frequency to  $\omega_0 = 10^{-4}$  and the largest frequency to  $\omega_{max} = 250J$ , which fixes the scaling parameter to be  $a \approx 1.48$  for  $N_f = 37$ .

**Differential equation solver:** To solve the set of non-linear differential equations, we implement an explicit fourth-order Runge-Kutta method (RK45) in Fortran90 language. In earlier implementations, the authors used an explicit Euler method with a fixed step-size[17]. The validity of such a crude integration is very questionable, since it will turn out that e.g. for a given Mandelstam variable  $s$ ,  $\Gamma_{sij}(s, s, s)$  always has a kink at  $\Lambda = s/2$  such that the derivative is discontinuous at this point. Therefore, one has to integrate carefully with a small step-size to not overshoot over these kinks. Therefore, we include an adaptive step-size algorithm to slow down the integration at these points. In addition, adaptive step-size makes sure that the integration of the flow equations is fast for  $\Lambda \gg J$ , i.e. at large scales where the interaction is weak and the flow is smooth. We use the differential equation solver package of Ref. [81], Chap. 16.

Even though RK45 may not be the optimal solver available for our problem, since it requires five derivative evaluations per step and these evaluations may cost a lot of time for a large number of discrete frequencies, we decided that RK45 was the best compromise between simplicity and reliability. In the integration, we set the relative error tolerance to  $10^{-2}$  and the absolute error tolerance to  $10^{-3}$ . We have checked carefully that the results change neither qualitatively nor quantitatively when higher accuracy is required, but the computational time is dramatically increased. We choose the actual flow parameter to be  $s$  defined such that  $\Lambda(s) = \Lambda_0 e^{-s}$  (not to be confused with the Mandelstam variable  $s$ ), which forces the integration to first advance rapidly and then to slow down in the critical region  $\Lambda \rightarrow 0^+$ . We set the maximum step size to  $\Delta s = 0.1$  in order to get smooth flow curves. In case there is no divergence of the flow at a non-zero scale  $\Lambda_{cr}$ , we stop the flow at  $\Lambda = \omega_0/2$ . All physical observables of interest should have converged well at this point, since physically, there should be nothing happening far below the energy scale  $J$  of the problem.

**Interpolation:** As the next important point, one has to notice that when calculating the flow derivative of an interaction vertex at some given discrete frequencies, the right-hand side of the flow equations will contain vertices evaluated at frequency points that do not, in general, coincide with the discretization. Therefore, one needs to devise an interpolation scheme. The simplest interpolation scheme would be the nearest-neighbor interpolation, but this leads to discontinuities in the frequency space and may turn out to be non-ideal especially for the numerical integration required by the Katanin truncation. Therefore, we choose to interpolate linearly. For a large number of frequencies, the two interpolation schemes should, of course, lead to identical results. This has been explicitly checked e.g. in Ref. [68], where the authors applied FRG to the single impurity Anderson model. For the evaluation of the

self-energy, linear interpolation reduces to a simple one-dimensional linear interpolation. The interaction vertices, on the other hand, have three frequency variables, so it may seem that one has to implement a trilinear interpolation scheme. This is not the case, however, since on the right-hand side of the flow equations one of the three frequency variables is always equal to a given  $s$ ,  $t$  or  $u$ , and therefore bilinear interpolation in two dimensions is enough.

**Initial values:** In the numerical implementation, we are forced to start the FRG flow at some finite value of  $\Lambda_0$  instead of  $\Lambda_0 = \infty$ . This raises the question of correct initial values: for  $\Lambda_0 = \infty$ , the correct initial values would be simply the bare values as explained in Sect. 4.6. For finite  $\Lambda_0$ , one can calculate the initial values using perturbation theory: since all propagators have an infra-red cut-off at  $\Lambda_0$ , a perturbation theory in  $J/\Lambda_0$  emerges, and one can simply calculate the lowest-order perturbation theory diagrams to obtain corrections of the order  $\mathcal{O}(J/\Lambda_0)$  to the initial values. This is, however, not necessary, since one can easily increase  $\Lambda_0$  with basically no extra computational cost to such a large value that the corrections are negligible. Typically we choose  $\Lambda_0 = 10^4 J$ .

**Numerical frequency integration:** In Katanin's flow scheme, the additional part in the single-scale propagator does not contain a delta function in frequency (Eq. (4.78)), which means that one has to integrate over the frequency axis in the flow equations for interaction vertices. The step-functions constrain, however, the integration region. For example in the  $s$ -channel, the step functions in

$$\begin{aligned} \tilde{P}_\Lambda(\nu, \nu + s) = P_\Lambda(\nu, \nu + s) - \frac{\Theta(|\nu| - \Lambda)}{\nu + \gamma^\Lambda(\nu)} \frac{\Theta(|\nu + s| - \Lambda)}{\nu + s + \gamma^\Lambda(\nu + s)} \\ \times \left[ \frac{\dot{\gamma}^\Lambda(\nu)}{\nu + \gamma^\Lambda(\nu)} + \frac{\dot{\gamma}^\Lambda(\nu + s)}{\nu + s + \gamma^\Lambda(\nu + s)} \right] \end{aligned} \quad (5.3)$$

restrict the integration to the three regions ( $s \geq 0$ )

$$\begin{cases} -\infty & < \nu \leq -\Lambda - s, \\ \Lambda & \leq \nu < \infty, \\ \Lambda - s & \leq \nu \leq -\Lambda, \text{ if } s > 2\Lambda. \end{cases} \quad (5.4)$$

As the integration routine, we choose the Romberg integration algorithm of Ref. [81]. The propagators on the right-hand side of flow equations (A.7) and (A.8) decay as  $1/\nu^2$  for large frequencies, which means that one can do the integrations even over semi-infinite regions very accurately. In addition, we use a routine that evaluates the function at points that are evenly spaced in  $1/\nu$ , which is especially suited for integrating decaying functions up to infinity. In the integration algorithm, the order of integration is iteratively increased until the desired accuracy is achieved. The relative and absolute error tolerances in the integration are set to  $10^{-2}$  and  $10^{-3}$ , respectively.

The default values of chosen numerical parameters are summarized in Table 5.1. Unless otherwise noted, these parameters were used in all calculations.

Parameter	default value
Number of non-zero frequencies in the geometric mesh, $N_f$	36
Smallest non-zero frequency $\omega_0$	$10^{-4}J$
Largest frequency $\omega_{N_f}$	$250J$
Initial cut-off $\Lambda_0$	$10^4J$
Interpolation method	linear/bilinear
Relative error tolerance in RK45	$10^{-2}$
Absolute error tolerance in RK45	$10^{-3}$
Relative error tolerance in Romberg integration	$10^{-2}$
Absolute error tolerance in Romberg integration	$10^{-3}$

Table 5.1: The default values of numerical parameters used in this work.

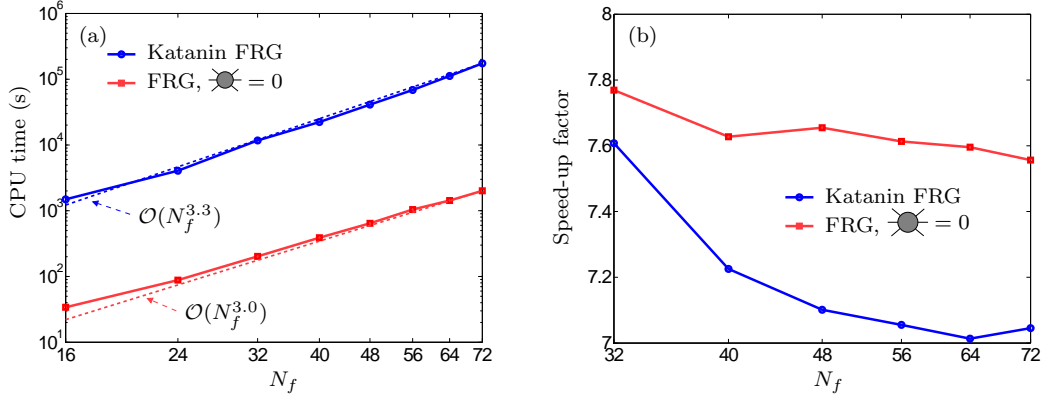


Figure 5.1: (a) CPU times in the Katanin FRG and naive FRG as a function of the number of frequencies in the discretization. (b) Parallelization speed-up factor for  $P = 8$  processors.

## 5.2 Computational complexity

In the numerical solution, the evaluation of the derivatives  $\dot{\Gamma}_{sij}^\Lambda(s, t, u)$  and  $\dot{\Gamma}_{dij}(s, t, u)$  for each combination of  $s$ ,  $t$  and  $u$  results in a  $\mathcal{O}(N_f^3)$  scaling of the computational time, which is the most important bottleneck restricting the quick solution of the flow equations. The evaluations of the derivatives are, however, completely independent and therefore easily parallelizable. To parallelize the frequency loops, we use the OpenMP application programming interface[82]. OpenMP is especially suited for "single instruction, multiple data" type tasks and very easy to use, since the user does not have to deal with message passing between CPUs. Of course, one has to be very careful in declaring shared variables to make sure that the common data used by all CPUs are not altered in the parallel portions of the program.

Let us first study the time scaling without using any parallelization. In Fig. 5.1(a), we plot the required CPU time in seconds as a function of the number of frequencies  $N_f$  with and without the Katanin modification. All calculations have been done on the high performance computing cluster of RWTH Aachen University[83]. Since one cannot control which cores are used for the computing, we have additionally checked that the computational time varies only by a few percent if the computation is started at another time. Of course, more regular curves could be obtained if the running times were averaged over multiple runs. Without the Katanin modification, the CPU time scales as  $\mathcal{O}(N_f^3)$ . In the Katanin-modified flow scheme, where the evaluation of each derivative requires numerical integration over frequency axis, the scaling becomes  $\mathcal{O}(N_f^{3.3})$  for a dense mesh. The most important observation is, however, that the scaling with Katanin modification in our case is not  $\mathcal{O}(N_f^4)$ , as was stated in Ref. [14].

Figure 5.1(b) shows the speed-up factor  $S$ , defined as the ratio of the computational CPU time and the computational real time as the loop over frequency derivatives  $\dot{\Gamma}_{s/d,i_1i_2}(s_i, t_j, u_k)$ ,  $i, j, k = 1, 2, \dots, N_f$  is parallelized using  $P = 8$  threads.

We only parallelize in the frequency space, not in spatial indices since the scaling in system size is only linear. In addition, we only parallelize the computations of  $\dot{\Gamma}_{s/d,i_1i_2}(s, t, u)$  and not e.g. the frequency loops in vertex functions  $v_{s/d,i_1i_2}(\omega_i, s_j)$ ,  $i, j = 1, 2, \dots, N_f$ , since the time scaling in frequencies is only quadratic. From the figure, we can approximate the speed-up factor with the Katanin modification to be  $S \approx 7.0$  for  $P = 8$ . Then, Gustafson's law[84] states that a portion of

$$\alpha = 1 - \frac{P}{S(P-1)} \approx 0.84 \quad (5.5)$$

has been parallelized in the program. This value of  $\alpha$  can then be used to estimate the speed-up  $S$  as the number of processors  $P$  is varied, which we have not checked explicitly.

## 5.3 Two-site Heisenberg model

### 5.3.1 Numerics

In the next two sections, we present the FRG results for the two-site Heisenberg model:

$$H = J\mathbf{S}_1 \cdot \mathbf{S}_2 = \frac{J}{4}\sigma_{\alpha\beta}^k\sigma_{\gamma\delta}^k c_{1\alpha}^\dagger c_{2\gamma}^\dagger c_{2\delta} c_{1\beta}. \quad (5.6)$$

The goal of this section is to show that the numerical solution is reliable and free of any numerical artifacts. This is essential if we wish to attach physical interpretation for the FRG results. The discussion of physical properties is postponed to the next section. In order to be sure that the flow equations have been implemented correctly, we have compared the results with two independently written programs[17, 85]. As a control variable, we choose the damping  $\gamma(\omega) = i\Sigma(\omega)$ . If the self-energies at the end of the flow ( $\Lambda = \omega_0/2$ ) agree, we infer that the flows coincide. In addition, we show results for the instant spin-spin correlations

$$\chi_{ij}(t=0) = \int \frac{d\omega}{2\pi} \chi_{ij}(\omega), \quad (5.7)$$

which requires the numerical integration of  $\chi_{ij}(\omega)$  (as calculated by FRG) and is therefore a sensitive probe for numerical errors. We use the Katanin truncation in all calculations to avoid unphysical divergences (see Section 5.4).

Figure 5.2(a) shows the self-energy  $\gamma(\omega)$  at the end of the flow as the number of frequencies in the discretization is either decreased ( $N_f = 28$ , blue solid) or increased ( $N_f = 44$ , green dotted-dashed) from the default value  $N_f = 36$  (red, dashed). Whereas the result for  $N_f = 28$  disagrees slightly with the result for  $N_f = 36$ , the self-energies for  $N_f = 36$  and  $N_f = 44$  agree very well, which shows that the results are reliable when the discretization  $N_f = 36$  is chosen.

In Fig. 5.2(b), we plot the self-energy as a function of the flow parameter  $\Lambda$ . As one can see, the self-energy has converged and one can try to interpret the result physically. It can also be seen how the self-energy only starts to flow visibly at

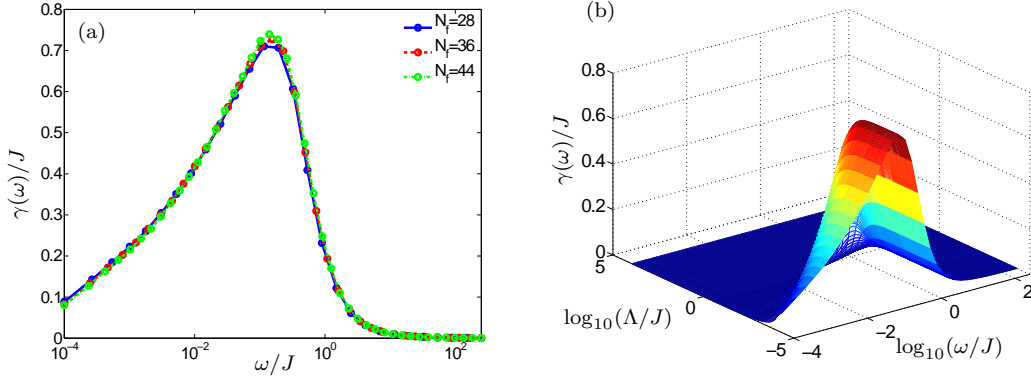


Figure 5.2: (a) The self-energy  $\gamma(\omega)$  for the two-site Heisenberg model at  $\Lambda = \omega_0/2$  as the number of frequencies  $N_f$  in the discretization is varied. The results for  $N_f = 36$  and  $N_f = 44$  agree very well, so we can choose  $N_f = 36$  in subsequent calculations. (b) The flow of self-energy  $\gamma^\Lambda(\omega)$  for  $N_f = 36$ . The visible flow starts at  $\Lambda \sim J$ , where the interaction  $J/\Lambda$  starts to become strong. The peak is at  $\omega \approx 0.15J$  at the end of the flow.

$\Lambda \sim J$ , where the cut-off scale  $\Lambda$  is of the same order as the bare interaction  $J$  and perturbation theory breaks down. As  $\Lambda$  decreases, the peak in the self-energy moves to smaller frequencies and converges to a value of  $\omega \approx 0.15J$ .

Figures 5.3(a) and 5.3(b) shows the flows of instant and nearest-neighbor spin-spin correlation functions, respectively. The dependence of the flows on the number of frequencies is very weak, even though even small discrepancies in the numerical values of  $\chi(\omega)$  would be enhanced in the numerical integration over  $\omega$ . The  $\omega$ -dependence of the correlation functions is discussed in the next section. The oscillations in  $\chi_{11}(t=0)$  at  $\Lambda \sim J$  arise from the discretization and become visibly smaller as the mesh becomes denser, as expected. Note that the local spin-spin correlation starts to flow towards the free value  $1/8$  (see discussion in the next section) even without interactions, which explains the qualitative differences in the flows of  $\chi_{11}$  and  $\chi_{12}$ . For  $\Lambda \sim J$ , the spin-spin interactions start to dominate the flow and both correlation functions start to grow.

As another example of how we made sure that the numerical solution is reliable, let us study the effect of changing the smallest non-zero frequency  $\omega_0$  in the mesh to see if there are any numerical artifacts arising from the discretization in the low-energy sector. With the largest frequency in the mesh fixed at  $\omega_{max} = 250J$  and the number of non-zero frequencies set to  $N_f = 36$ , we vary the smallest frequency from  $\omega_0 = 10^{-4}J$  (corresponding to scaling parameter  $a \approx 1.48$ ) to  $\omega_0 = 10^{-3}J$  ( $a \approx 1.37$ ) and  $\omega_0 = 10^{-5}J$  ( $a \approx 1.58$ ). As always, we stop the flows  $\Lambda = \omega_0/2$ , which means that we now also get to probe the effect of stopping the flow before the physical point  $\Lambda = 0$ .

Figure 5.4(a) shows the self-energies at the end of the flow. One can clearly see that the large-frequency properties for  $\omega \gtrsim 0.01J$  are independent of  $\omega_0$ , whereas for

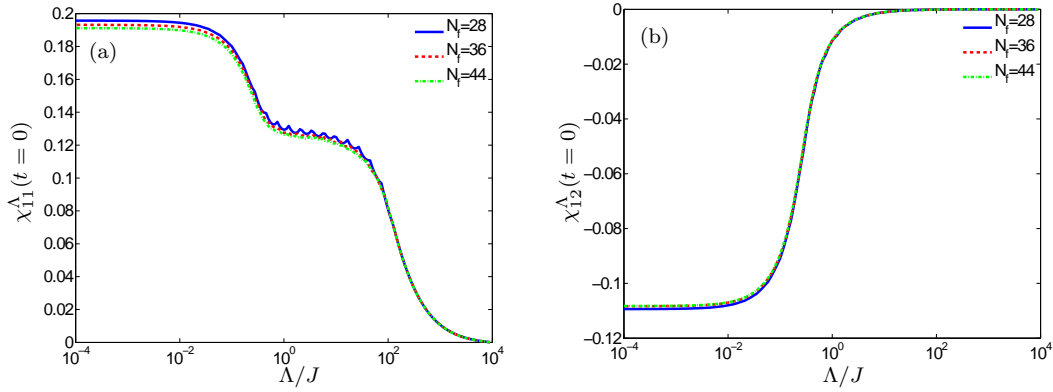


Figure 5.3: The flow of the (a) local and (b) nearest-neighbor instant spin-spin correlation functions for the two-site Heisenberg model. As the instant correlation functions are calculated by numerical integration over dynamic correlation functions, any discrepancies arising from the numerical discretization should be visible. For  $N_f = 28$ , one can see oscillations in  $\chi_{11}^\Lambda(t=0)$  at  $\Lambda \sim J$ , but since these oscillations are washed away by increasing  $N_f$ , we can again be confident that the choice  $N_f = 36$  leads to reliable results.

$\omega \lesssim 0.01J$ , there are some differences that arise from the numerical discretization and the related stopping of the flow at  $\Lambda = \omega_0/2$ . However, these differences in very low frequencies do not play any role in the physical observables and are not even visible when the self-energy is plotted on a linear frequency scale (not shown). To demonstrate the irrelevance of these differences, we have plotted the flows of ground state energies  $E^\Lambda$  in Fig. 5.4(b). Note that the flow of energy is only dependent on the self-energy  $\gamma^\Lambda(\Lambda)$  (Eq. (4.90)). Even though the exact values start to differ slightly for  $\Lambda < 0.01J$ , the accuracy of agreement is more than enough for our purposes.

In a similar manner, we have shown that the choice of the largest frequency  $\omega_{max}$  in the discretization is not important, as long as one uses  $\omega_{max} \gg J$ . However, since e.g. each of the dynamic susceptibilities  $\chi^\Lambda(\omega_i)$  starts to flow approximately at  $\Lambda \sim \omega_i$ , the numerically calculated integrals  $\int d\omega \chi^\Lambda(\omega)$  do depend on the discretization. Therefore, one cannot attach a physical significance to the flow values of instant susceptibilities  $\chi^\Lambda(t=0)$  (even if  $\Lambda$  were a physical parameter). This numerical artifact is demonstrated for the local susceptibility in Fig. 5.5(a). For  $\Lambda \ll J$ , however, only the small frequencies contribute significantly to the integral and the final values at  $\Lambda \rightarrow 0^+$  are independent of the large-frequency discretization. Figure 5.5(b) shows that since  $\chi_{12}^\Lambda(t=0)$  only starts to flow at  $\Lambda \sim J$ , where the discretization is dense in all cases, similar differences in the flows cannot be observed.

In conclusion, we have shown that our numerical solution of the flow equation is free of any numerical artifacts and we can start to interpret the results physically, which is the goal of the next section.

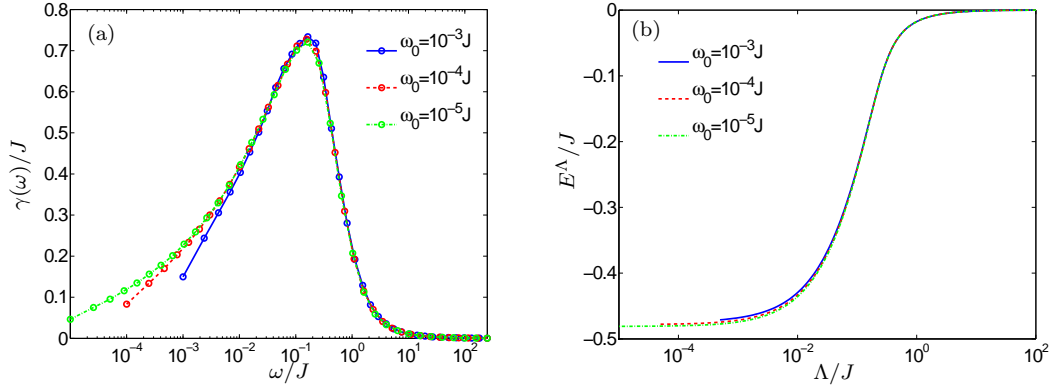


Figure 5.4: (a) The dependence of the self-energy  $\gamma(\omega)$  for the two-site Heisenberg model on the smallest non-zero frequency  $\omega_0$  in the frequency mesh. (b) The corresponding flows of ground state energies.

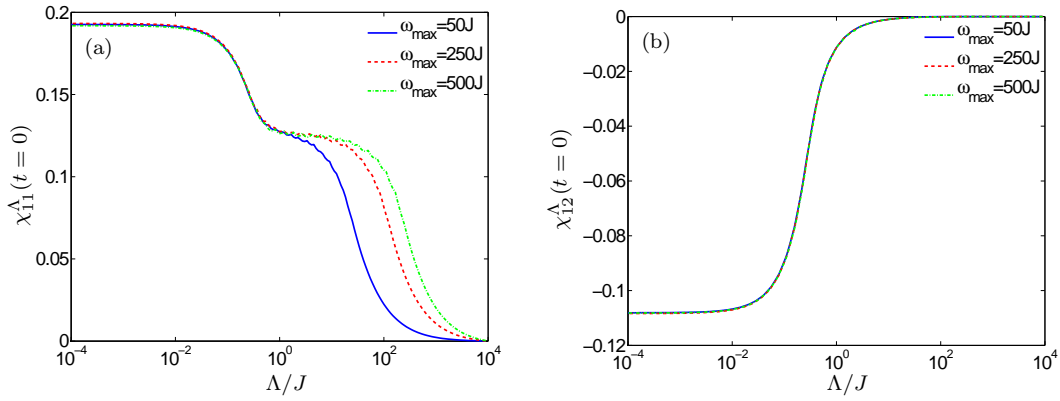


Figure 5.5: (a) Local and (b) nearest-neighbor spin-spin correlation functions for the two-site Heisenberg model. As the largest frequency  $\omega_{\max}$  in the discretization is increased, the local correlations start to flow for larger  $\Lambda$ , but the value converges to the same value at the end of the flow.

### 5.3.2 Physical observables

As discussed in Section 2.2, the two-site model (5.6) can be easily solved exactly. Eigenstates are the singlet state ( $S = 0$ )

$$|s\rangle = \frac{1}{\sqrt{2}} (|\uparrow\downarrow\rangle - |\downarrow\uparrow\rangle) \quad (5.8)$$

with energy  $E_s = -3J/4$  and the triplet states ( $S = 1$ )

$$\begin{cases} |t_0\rangle &= \frac{1}{\sqrt{2}} (|\uparrow\downarrow\rangle + |\downarrow\uparrow\rangle), \\ |t_+\rangle &= |\uparrow\uparrow\rangle, \\ |t_-\rangle &= |\downarrow\downarrow\rangle, \end{cases} \quad (5.9)$$



which are degenerate with the energy  $E_t = J/4$ . Since we study antiferromagnetic interactions ( $J > 0$ ), singlet state is the ground state. The exact spin-spin correlation functions are easily calculated in the Lehmann representation at  $T = 0$ :

$$\chi_{ij}(\omega) = \sum_n \frac{\langle n | S_i^z | s \rangle \langle s | S_j^z | n \rangle}{i\omega - (E_n - E_s)} + c.c. \quad (5.10)$$

The unphysical states, which are eigenstates with energy  $E = 0$ , have vanishing matrix elements with the singlet state. A simple calculation shows that only the state  $|t_0\rangle$  can couple to the singlet state by the single spin operators, and therefore the exact dynamic correlation function is

$$\chi_{ij}(\omega) = (-1)^{(i-j)} \frac{J}{2\omega^2 + J^2}, \quad (5.11)$$

a Lorentzian with broadening  $J$ . The broadening arises from the singlet-triplet excitation gap. Analytic continuation to the real axis ( $i\omega \rightarrow \omega + i\eta$ ) delivers the retarded correlation function

$$\chi_{ij}^R(\omega) = -\frac{J}{2} \mathcal{P} \left( \frac{1}{\omega^2 - J^2} \right) + i\frac{\pi}{4} [\delta(\omega - J) + \delta(\omega + J)]. \quad (5.12)$$

The instant spin-spin correlations are obtained by integration of  $\chi_{ij}(\omega)$  over  $\omega$ , which delivers

$$\int \frac{d\omega}{2\pi} \chi_{ij}(\omega) = (-1)^{(i-j)} \frac{1}{4}, \quad (5.13)$$

i.e. perfect (anti-)correlation, as expected for the singlet state. Of course, this last result could have been derived directly by calculating the expectation value of  $S_i^z S_j^z$  in the singlet ground state.

Figure 5.6(a) shows the dynamic FRG spin-spin correlation functions at the end of the flow, compared with the exact result. Clearly, the disagreement is large even on a qualitative level. FRG susceptibilities behave as  $\log(\omega^{-1})$  for small frequencies, even though the exact result states that there should be no frequency dependence for  $\omega \ll J$ . If the flow was stopped at  $\Lambda \gtrsim J$ , the  $\omega$ -dependence would resemble a Lorentzian (not shown), but of course, such a stopping of the flow before the physical limit  $\Lambda \rightarrow 0$  cannot be justified.

In Fig. 5.6(b) we plot the instant susceptibilities obtained by integration over frequencies. The flows have been presented already in Fig. 5.3, but are reproduced here for convenience. Before the interaction scale  $\Lambda \sim J$ , the local susceptibility converges to a value  $\chi_{11}(t=0) = 1/8$ . This is expected for the free system, where the density matrix is a linear combination of the states  $|0\rangle$ ,  $|\uparrow\rangle$ ,  $|\downarrow\rangle$  and  $|\uparrow\downarrow\rangle$ . In the region of strong interactions,  $\Lambda \lesssim J$ , the tendency towards a singlet state starts to build up and both the local and non-local susceptibilities grow almost evenly, naturally with opposite signs. Therefore, we see how FRG is successful in the sense that instant susceptibilities are able to deliver physically sensible information for the two-site problem. FRG is not, however, able to reproduce the quantitative property of the singlet state that the local and nearest-neighbor correlations agree (apart from sign).

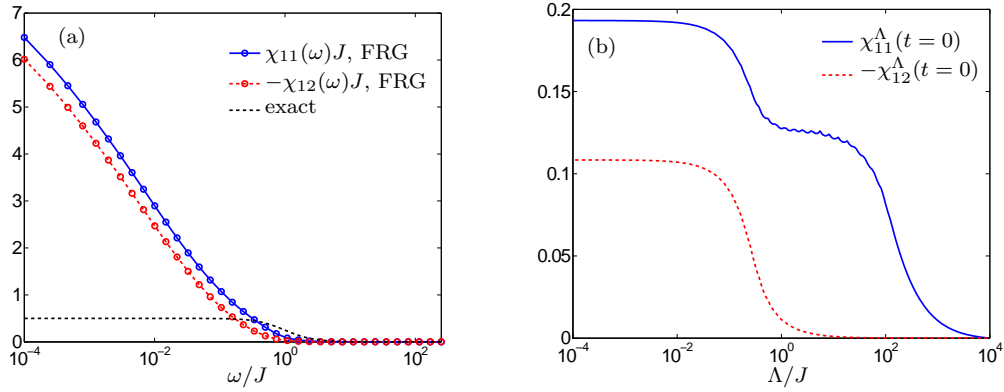


Figure 5.6: (a) The dynamic spin-spin correlation functions compared to the exact result. FRG correlations diverge logarithmically for  $\omega \rightarrow 0$ , whereas the exact result is practically a constant for small  $\omega$ . (b) The flows of instant correlation functions. In the weakly-interacting region  $\Lambda \gtrsim J$ , the local spin correlations converge to a value  $1/8$  as expected (see text). Spin-spin interactions increase the value to  $\chi_{11}(t=0) \approx 0.19$ . Instant spin-spin correlation between the sites is  $\chi_{12}(t=0) \approx -0.11$  at the end of the flow.

To discuss fluctuations in the particle number, we show the FRG result for the the density-density correlation function  $D_{ij}^\Lambda(\omega)$  in Fig. 5.7(a). Since all exact energy eigenstates are eigenstates of the particle number operator, there should be no fluctuations. However, just as the spin-spin correlations, also the dynamic density-density correlations diverge logarithmically for small frequencies, meaning that the fluctuations are very strong.

Figure 5.7(b) shows how the instant local density-density correlation functions. Once again, the local correlation function converges to the free value of  $1/2$  before the interaction parameter  $J/\Lambda$  starts to become strong. The interactions suppress the fluctuations to a value of  $D_{11}(t=0) \approx 0.42$ . This corresponds to a RMS fluctuation value of  $\Delta n_{rms} = \sqrt{\langle n^2 \rangle - \langle n \rangle^2} \approx 0.65$ . The correlation between the sites is  $D_{12}(t=0) \approx -7.9 \times 10^{-3}$  at the end of the flow. Whereas the non-local density correlations are negligible, the local density fluctuations are definitely not small and the spin-spin interactions do not seem to suppress fluctuations in the particle number adequately. Therefore, the failure of FRG in the study of gapped spin systems seems to be the evident conclusion. The dynamic correlation functions diverge logarithmically, and whereas the instant spin-spin correlations resemble a singlet state, there are still strong unphysical fluctuations in the particle number.

For the fermionic Hamiltonian in the grand canonical ensemble, one can also calculate the single-particle Green's function. The Green's function is a sensible object only when particle number fluctuations are allowed, so the comparison of the FRG self-energy and the exact self-energy delivers direct information about the justifiability of the Katanin truncation. The truncation is, after all, the only approximation in our method to solve the many-body Hamiltonian (5.6).

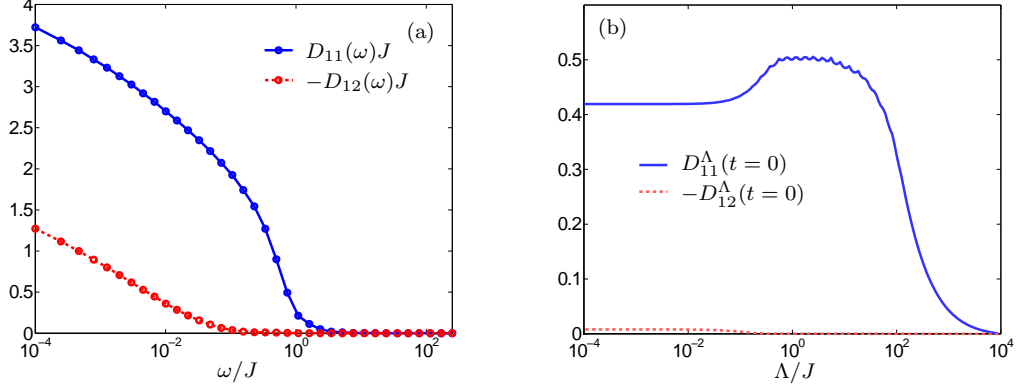


Figure 5.7: (a) The dynamic density-density correlation functions at the end of the flow as calculated by FRG. Even though density fluctuations should be small in the spin model, the fluctuations seem to diverge as  $\log(\omega^{-1})$  for small frequencies. (b) The flow of instant density-density correlation functions. In the weakly-interacting region  $\Lambda \gtrsim J$ , the local density fluctuations converge to a value of  $1/2$ . Spin-spin interactions suppress the fluctuations to  $D_{11}(t=0) \approx 0.42$ .

A straightforward calculation in the Lehmann representation delivers the one-particle Green's function on the imaginary axis

$$\mathcal{G}(\omega) = \frac{-i\omega}{\omega^2 + (3J/4)^2}, \quad (5.14)$$

giving the self-energy

$$\Sigma(\omega) = -i \frac{(3J/4)^2}{\omega}. \quad (5.15)$$

The spectral function describing the interacting density of states is

$$\rho(\omega) = -2\text{Im } \mathcal{G}(i\omega \rightarrow \omega + i0^+) = \pi \left[ \delta\left(\omega - \frac{3J}{4}\right) + \delta\left(\omega + \frac{3J}{4}\right) \right], \quad (5.16)$$

meaning that one can excite a particle at energy  $\omega = 3J/4$  or a hole with energy  $\omega = -3J/4$ .

In Fig. 5.8 we plot the FRG self-energy  $\gamma(\omega) = i\Sigma(\omega)$  at the end of the flow and compare with the exact result given above. Unlike the exact self-energy, the FRG self-energy vanishes as  $\omega \rightarrow 0$ , meaning that there are undamped excitations in the low-energy sector. Due to this fundamental disagreement, it is plausible that physical properties such as spin-spin correlation functions come out wrong. The value of the FRG ground state energy is  $E \approx -0.48J$  (Fig. 5.4(b)), which disagrees with the exact result  $E_s = -3J/4$  by 36 % due to too small self-energy. For  $\omega \gg J$ , the FRG self-energy decays as  $\sim \omega^{-1.09}$  (Fig. 5.8, inset), which is quite close to the exact decay  $\sim \omega^{-1}$ .

Analytical continuation of the self-energy and other dynamic correlation functions to the real frequency axis would allow us to calculate the spectral function

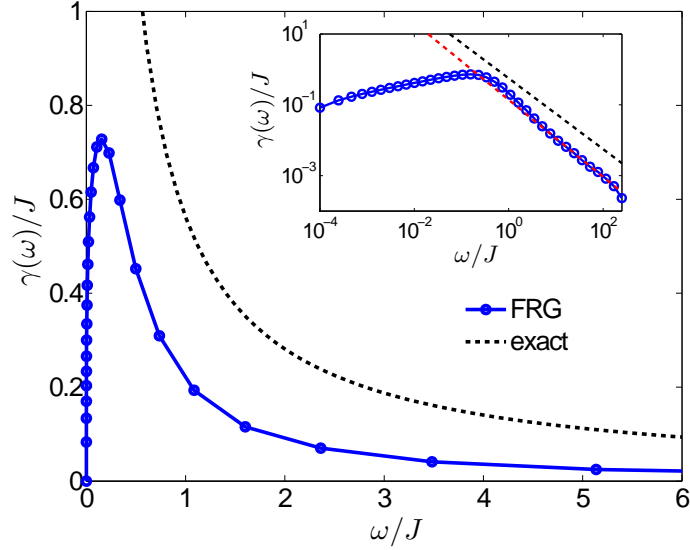


Figure 5.8: FRG self-energy  $\gamma(\omega)$  for the two-site model compared to the exact result. The FRG self-energy vanishes for  $\omega \rightarrow 0$ , whereas the exact result diverges, the latter signaling a gapped state. Inset: Self-energies in the log-log scale and a power-law fit  $\gamma(\omega) \sim \omega^{-1.09}$  to the FRG result (red, dashed).

and gain more precise information about the state described by FRG and how the excitations are damped, for example. Unfortunately, we have not been able to do the analytical continuation in a reliable way. Even though simple Padé approximant methods[86] have been successful in the past (see e.g. Ref. [68]), our results were not numerically robust. A typical symptom of this is that the spectral function depends on whether the Green's function or the self-energy is analytically continued, which should be irrelevant. In addition, the spectral function may even turn out to be negative, which is absurd for fermions. In the next section, we apply FRG to a quantum spin chain to see if spatial correlation functions give more information about the performance of FRG.

## 5.4 Quantum Heisenberg spin chain

In this section, we move on to study a Heisenberg chain with periodic boundary conditions. The values of numerical parameters are again those given in Table 5.1. Although we have already shown in previous section how FRG cannot produce correct physical results for the two-site model, we are interested in learning how FRG performs in real one-dimensional systems where the finite-size gap of excitations is notably smaller. Especially, we are interested in seeing whether FRG can reproduce algebraically decaying correlations (2.8) known from the exact solution.

Let us first back up a little by discussing the truncation. In the previous sections, we employed the Katanin-modified flow scheme, the importance of which we now

justify. On a classical level, the ground state would be antiferromagnetically long-range ordered, which shows up as a divergence in the staggered susceptibility  $\chi(q = \pi)$ . In the quantum model, long-range order is destroyed by quantum fluctuations and we call the antiferromagnetic instability is unphysical. Let us now show how this instability arises from the diagrammatic random phase approximation (RPA) for the spin interaction[87]. The comparison with RPA gives us a better understanding of the physics contained in the FRG truncation.

In RPA theory, one sets the effective interaction  $W = \text{---} \text{---} \text{---}$  equal to an infinite series of loop diagrams:

$$\text{---} \text{---} \text{---} = \text{---} \text{---} \text{---} + \text{---} \text{---} \text{---} \text{---} + \text{---} \text{---} \text{---} \text{---} \text{---} + \dots \quad (5.17)$$

where  $J = \text{---} \text{---} \text{---}$  is the bare interaction. In Fermi liquids, the importance of loop terms is related to the fact that they contain a free momentum integration over the Fermi surface and they are therefore dominant in the high-density limit. In our case of non-mobile electrons, it is apparent that only the loop terms contain a summation over all sites and therefore, they are responsible for long-range phenomena. We include cut-off  $\Theta(|\omega| - \Lambda)$  in the free propagator  $\mathcal{G}_0(\omega) = 1/i\omega$  to regularize the infrared divergence of the particle-hole bubble. In real space, the effective interaction satisfies the Dyson-like equation

$$W_{ij}^\Lambda(\omega) = J_{ij} + 2 \sum_k J_{ik} \Pi^\Lambda(\omega) W_{kj}^\Lambda(\omega) \quad (5.18)$$

where for our case, the bare interaction is  $J_{ij} = J/4$  for  $j = i \pm 1$  and zero otherwise. The factor of 2 comes from the spin sum and the scale-dependent pair bubble is defined

$$\Pi^\Lambda(\omega) = \int \frac{d\nu}{2\pi} \mathcal{G}_{0\Lambda}(\nu) \mathcal{G}_{0\Lambda}(\nu + \omega), \quad (5.19)$$

which reduces for  $\omega = 0$  to

$$\Pi^\Lambda(\omega = 0) = -\frac{1}{\pi\Lambda}. \quad (5.20)$$

In Fourier space, the static effective interaction is then given by

$$W^\Lambda(q, \omega = 0) = \frac{J(q)}{1 + 2J(q)/\pi\Lambda}, \quad (5.21)$$

where  $J(q) = (J/2) \cos(q)$  is the Fourier-transformed bare interaction. The spin-spin correlation function is given in RPA by

$$\chi_{ij}(\omega) = \text{---} \text{---} \text{---} \text{---} \text{---} + \text{---} \text{---} \text{---} \text{---} \text{---}, \quad (5.22)$$

where the vertex is

$$\begin{matrix} (i_2, \alpha_2, \omega_2) \\ \text{---} \text{---} \text{---} \\ (i_1, \alpha_1, \omega_1) \end{matrix} = \frac{1}{2} \beta \delta_{\omega, \omega_1 - \omega_2} \delta_{i_1 i_2} \delta_{i_1 j} \sigma_{\alpha_1 \alpha_2}^z. \quad (5.23)$$

Translating Eq. (5.22), we get

$$\chi^\Lambda(q, \omega) = -\frac{1}{2}\Pi^\Lambda(q, \omega) [1 + 2W(q, \omega)\Pi^\Lambda(\omega)]. \quad (5.24)$$

Focusing on the static, staggered correlations, one gets the analytical result

$$\chi^\Lambda(q = \pi, \omega = 0) = \frac{1}{2\pi\Lambda} \left[ 1 + \frac{J}{\pi\Lambda(1 - J/\pi\Lambda)} \right]. \quad (5.25)$$

The susceptibility diverges at the critical scale  $\Lambda_{cr}^{RPA} = 1/\pi$ , which is the antiferromagnetic instability leading to long-range order. On a cubic lattice in  $d$  spatial dimensions, one gets similarly  $\Lambda_{cr}^{RPA} = d/\pi$ . It is straightforward to show that RPA can be reproduced exactly in FRG by using the flow equations

$$\Sigma^\Lambda(\omega) = 0, \quad (5.26)$$

$$\begin{array}{c} \text{---} \bullet \text{---} \\ \text{---} \bullet \text{---} \end{array} = 2 \begin{array}{c} \text{---} \bullet \text{---} \\ \text{---} \bullet \text{---} \end{array} \quad , \quad (5.27)$$

$$\begin{array}{c} \text{---} \bullet \text{---} \\ \text{---} \bullet \text{---} \end{array} = 2 \begin{array}{c} \text{---} \bullet \text{---} \\ \text{---} \bullet \text{---} \end{array} \quad (5.28)$$

and Eq. (4.112) for the susceptibility, which shows that the full infinite-order RPA is included even in the truncated flow equations.

Let us now study a 16-site Heisenberg ring. Figure 5.9 shows the staggered susceptibilities  $\chi(q = \pi, \omega = 0)$  as calculated in RPA and compared to FRG results with and without the Katanin modification. Whereas the RPA susceptibility diverges at  $\Lambda = J/\pi \approx 0.318J$ , the second-order FRG diverges already at  $\Lambda \approx 0.346J$ . Even though self-energy corrections included in FRG are expected to regularize the instability due to damping of quasiparticles, the inclusion of all diagrams in Eqs. (4.81) and (4.82) drives the instability to an even larger  $\Lambda$ . Most importantly, however, the Katanin modification regularizes the flow, as already shown in Ref. [14] for the  $J_1$ - $J_2$ -model in two dimensions. Even though there is still a logarithmic divergence in the susceptibility for  $\Lambda \rightarrow 0^+$  (not shown), the finite-scale antiferromagnetic instability is taken care of.

What is the physics contained in the FRG without the Katanin truncation? The static correlation function  $\chi_{ij}(\omega = 0)$  is shown in Fig. 5.10(a) for various values of the flow parameter  $\Lambda$ . The signs of correlations alternate as expected for an antiferromagnetic system, so we only plot the absolute values to see the decay. Clearly, the decay of correlations is exponential:  $\chi_{ij} \sim \exp(-|i - j|/\xi)$ , where  $\xi$  is the correlation length. As natural, the correlation length diverges as  $\Lambda$  approaches the critical value  $\Lambda_{cr} = 0.346J$ . The flow of the inverse correlation length is shown in Fig. 5.10(b). For  $\Lambda \gg \Lambda_{cr}$ , the inverse correlation length scales as

$$\frac{1}{\xi\Lambda} \sim \log \left( \frac{\Lambda}{\Lambda_c} \right), \quad (5.29)$$

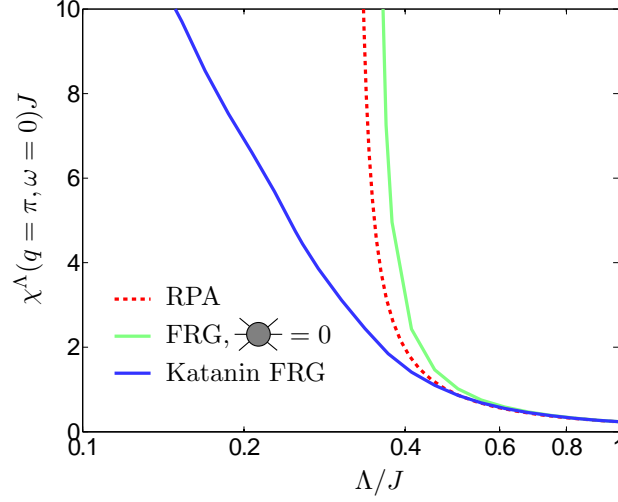


Figure 5.9: The flow of static staggered susceptibilities for the 16-site Heisenberg model in RPA and two FRG truncations. The RPA susceptibility diverges at  $\Lambda_{cr} = J/\pi \approx 0.318J$  and the naive FRG at  $\Lambda_{cr} \approx 0.346J$ . Katanin-modified FRG regularizes the antiferromagnetic instability.

which corresponds to a flow equation

$$\frac{d\xi^\Lambda}{d\log(\Lambda)} \sim -(\xi^\Lambda)^2. \quad (5.30)$$

In the critical region  $\Lambda \gtrsim \Lambda_{cr}$ , the RPA correlation length would diverge as  $\xi^\Lambda \sim (\Lambda - \Lambda_{cr})^{-1/2}$ , which is the typical mean-field result. For FRG the critical scaling is  $\xi^\Lambda \sim (\Lambda - \Lambda_{cr})^{-\nu}$  with  $\nu \approx 0.52$ , so the critical exponent is slightly modified. The critical scaling is shown in the inset of Fig. 5.10(b).

For the Katanin truncation, the instant susceptibilities converge for  $\Lambda \rightarrow 0^+$  (Figs. 5.6(b)) and one can compare the obtained results with the exact result. For 16 sites, the exact result can be calculated by forming the full Hamiltonian matrix as the tensor product of  $\sigma$ -matrices, meaning that the  $2^{16}$ -dimensional Hamiltonian matrix is written in the Ising basis. Whereas the calculation of dynamic correlations would require the determination of all low-energy eigenstates and subsequent use of Lehmann representation, only the ground state is required to calculate instant correlations. Therefore, one can restrict the diagonalization to the subspace  $S_{tot}^z = 0$ , making the restricted Hamiltonian  $\binom{16}{8} = 65536$ -dimensional. Figure 5.11(a) shows the exact and FRG correlations as function of distance. In the exact result, the slow algebraic decay of correlations is clear. In contrast, the correlations decay exponentially in FRG even with Katanin modification. Instead of a critical state, the FRG leads to a quantum-disordered ground state, as would be expected for a finite temperature. So even though the modified FRG is successful in the sense that it does not generate physically false long-range order, one cannot achieve the critical behaviour.

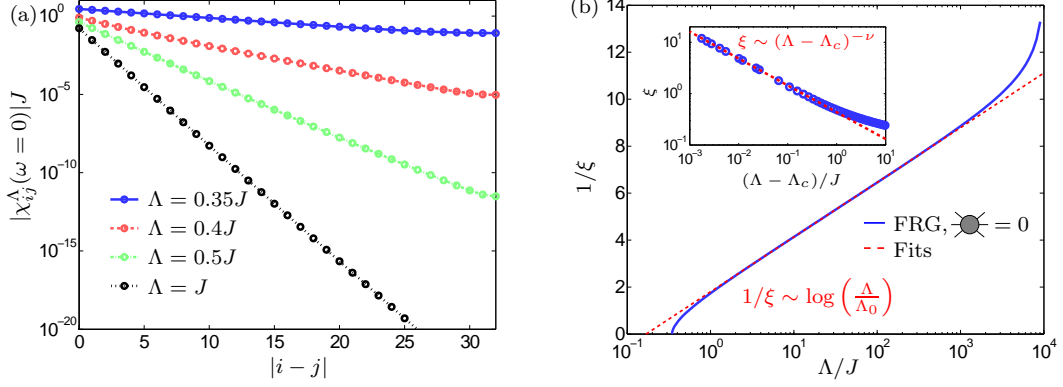


Figure 5.10: (a) The absolute values of the static correlation function  $\chi_{ij}^\Lambda(\omega = 0)$  for various values of  $\Lambda$  in the naive FRG. The number of sites is set to  $N = 64$  and the number of non-zero frequencies to  $N_f = 28$ . The staggered correlations decay exponentially. Similar decays are obtained by using pure RPA. (b) The flow of correlation length in naive FRG. For  $\Lambda \gtrsim J$ , correlation length grows as  $\xi \sim 1/\log(\Lambda/\Lambda_0)$ , where  $\Lambda_0 \approx 0.17J$ . *Inset*: For  $\Lambda \lesssim J$ , correlation length diverges as  $\xi \sim (\Lambda - \Lambda_c)^{-\nu}$ , where  $\nu \approx 0.52$ .

To see how the correlation length scales in Katanin FRG, we must first decide whether to calculate the correlation length from the static or instant correlatoins. In Fig. 5.10, we calculated the correlation length from the decay of the static correlation function  $\chi_{ij}(\omega = 0)$ , but Fig. 5.11(a) shows that also the instant correlations decay exponentially. Interestingly, it turns out that the values of correlation lengths calculated from  $\chi_{ij}(\omega = 0)$  and  $\chi_{ij}(t = 0)$  disagree.

We define two correlation lengths  $\xi_{stat}^\Lambda$  and  $\xi_{inst}^\Lambda$  such that  $\xi_{stat}^\Lambda$  is determined from the decay of  $\chi_{ij}^\Lambda(\omega = 0)$  and  $\xi_{inst}^\Lambda$  from the decay of  $\chi_{ij}^\Lambda(t = 0)$ . The flows of correlation lengths are plotted in Fig. 5.11(b). The values agree for  $\Lambda \gtrsim J$ , but visibly differ below the interaction scale  $\Lambda \lesssim J$ . The most notable difference is that whereas  $\xi_{stat}^\Lambda$  diverges logarithmically for  $\Lambda \rightarrow 0^+$ ,  $\xi_{inst}^\Lambda$  converges to a value  $\xi_{inst} \approx 1.49$ . Therefore, static correlation functions determined from FRG are very pathological in the sense that not only do the values diverge logarithmically, but also the corresponding correlation length diverges. We conclude that even though the values for instant correlation functions disagree with the exact result, they contain more physically interesting information than the dynamic correlations that are plagued by divergencies.

This ends our study of the Heisenberg chain. Since the correlations are short-ranged in FRG, the dependence on system size is very weak and therefore results are qualitatively identical with the two-site model. FRG self-energy is universally of the form shown in Fig. 5.8. The dependence of the ground state energy per spin on system size is weak and does not coincide with the scaling known from the exact result. Some of these results are reported elsewhere[88, 18].



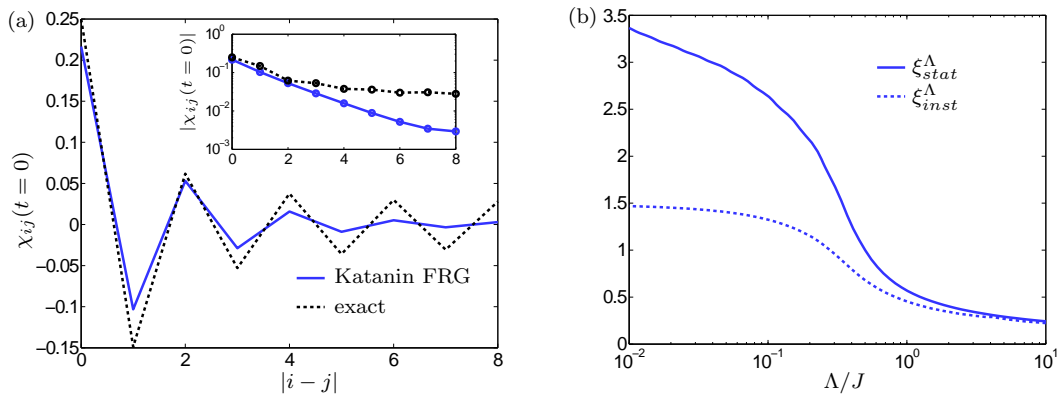


Figure 5.11: (a) The instant spin-spin correlation function  $\chi_{ij}(t=0)$  for the 16-site Heisenberg model in Katanin FRG compared with the exact result. *Inset:* Correlations on a logarithmic scale. In FRG correlations decay exponentially, corresponding to a "quantum disordered" ground state with a finite correlation length  $\xi \approx 1.49$ . In the exact result, correlations decay very slowly. (b) The comparison of the static correlation length  $\xi_{stat}^\Lambda$  and the instant correlation length  $\xi_{inst}^\Lambda$  for the 16-site chain. Whereas  $\xi_{stat}^\Lambda$  diverges logarithmically for  $\Lambda \rightarrow 0^+$ ,  $\xi_{inst}^\Lambda$  converges to the value  $\xi_{inst} \approx 1.49$ .

# Chapter 6

## Conclusions

In this work, we have studied the applicability of the fermionic functional renormalization group (FRG) method to quantum spin chain problems. Since the method has been introduced and also applied to various systems earlier[14, 15, 16], it is important to recapitulate our contribution. First of all, we have rigorously studied the symmetries of the model. In addition to showing how rotational spin invariance and local particle number conservation lead to parametrizations discussed in Sect. 3.2, we presented how one can use time-reversal and particle-hole symmetry to simplify the numerics. In earlier work, related symmetries were derived *a posteriori* from flow equations[14]. The asset of our derivation is that when the model is modified, it is immediately clear which of the symmetries are broken. For example, inclusion of a finite magnetic field would break the spin rotational symmetry and time-reversal invariance. When deriving the flow equations, we presented a fully diagrammatic representation that offers an intuitive understanding for each term appearing in the equations. In addition, we derived flow equations for the ground state energy and for spin and density susceptibilities.

In the numerical part, we demonstrated that the numerical solution of the flow equations is completely free of any numerical artifacts, which is the basis for all conclusions made based on the results. For the two-site Heisenberg model, we showed how (i) the spin susceptibilities only weakly correspond to the singlet ground state, (ii) Matsubara self-energy does not diverge for small  $\omega$  as expected based on the exact solution, and (iii) ground state energy differs from the exact result by over 30 percent. Therefore, the only possible conclusion is that FRG is neither qualitatively nor quantitatively a useful tool to tackle quantum spin systems in low dimensions.

On a positive side, it was shown how Katanin's modification of the truncated flow equations regularizes the unphysical antiferromagnetic instability in one spatial dimension at  $T = 0$ . Unfortunately, the spatial correlations turned out to correspond to a quantum-disordered ground state and no critical algebraic decay was generated. Such a critical behaviour would require a very precise fine-tuning between disorder and long-range order, which seems to be a herculean task for truncated FRG flow equations that are, after all, rigorously only valid in the weak-coupling limit.

Considering the failure of the method, it is interesting to ask how one could improve the results. Starting from the quantum spin system, we have made two

approximations: (1) the constraint  $n_i = 1$  of singly-occupied sites was relaxed to thermal average  $\langle n_i \rangle = 1$  by moving to the grand canonical ensemble, and (2) the flow equations were truncated either naively or by using Katanin's modification. Approximation (2) is definitely invalid, as the failure to reproduce the correct self-energy for the two-site model shows. This is perhaps expected, since due to the absence of a kinetic term, the pure spin Hamiltonian is the ultimate strongly interacting model and a good agreement between our "RG-enhanced perturbation theory" and exact results could be described as a lucky surprise.

As for approximation (1), we saw that local fluctuations in the particle number are  $\Delta n_{rms} \approx 0.62$ . Therefore, it was shown quantitatively that the relaxation of the particle number constraint cannot be justified even *a posteriori*. But what role do the density fluctuations play in the failure to reproduce e.g. correct spin-spin correlations? The question could be answered by studying a model for which the FRG truncation becomes exact, since this would isolate approximation (1). One candidate for such a model is the toy model of spatially constant spin interaction,

$$H = J \sum_{\substack{i,j=1 \\ i \neq j}}^N \mathbf{S}_i \cdot \mathbf{S}_j. \quad (6.1)$$

Since the interaction is ultimately long-ranged, one could expect mean-field terms (loop diagrams) to dominate and Katanin truncation to become exact in the limit  $N \rightarrow \infty$ . However, preliminary studies seem to suggest that the FRG ground-state energies are not correct, meaning that either mean-field is not exact or that the unphysical states somehow affect even ground-state quantities. Another way to study the influence of unphysical fluctuations could perhaps be to introduce auxiliary density interactions in the model, which would penalize empty and doubly-occupied sites. Further developments on this problem are left for future studies.

What is, then, the future of fermionic FRG for quantum spin systems? Even though the results presented in this work may be considered discouraging, it has been shown earlier that FRG can reproduce some known phase transition points for more complicated models in two and three dimensions[14, 15, 16]. This is perhaps not that surprising, since the true strength of renormalization group methods is, after all, in tackling subtle interplay between various competing instabilities. Therefore, the usefulness of FRG e.g. in the study of e.g. frustrated spin systems cannot be assessed based on the results presented here. If the dominant instabilities can be reliably detected by FRG, the method possesses several advantages as compared to other methods: (1) the method is very flexible and various different systems can be studied simply by modifying the initial conditions, (2) increase in system size only leads to a linear scaling in the computational complexity of the problem (at least when correlations are short-ranged), and (3) solving differential equations is easy. Considering these advantages, further studies on the applications of FRG on quantum spin systems may well be worth the effort.

# Bibliography

- [1] E. Ising, Z. Phys. **31**, 253 (1925).
- [2] L. Onsager, Phys. Rev. **65**, 117 (1944).
- [3] P. W. Anderson, Science **235**, 1196 (1987).
- [4] P. A. Lee, N. Nagaosa, and X.-G. Wen, Rev. Mod. Phys. **78**, 17 (2006).
- [5] E. Manousakis, Rev. Mod. Phys. **63**, 1 (1991).
- [6] S. S. Schweber, *Q.E.D. and the Men Who Made It* (Princeton University Press, 1994).
- [7] H. A. Bethe, Phys. Rev. **72**, 339 (1947).
- [8] K. G. Wilson, Rev. Mod. Phys. **47**, 773 (1975).
- [9] J. Polchinski, Nucl. Phys. B **231**, 269 (1984).
- [10] C. Wetterich, Phys. Lett. B **301**, 90 (1993).
- [11] J. Berges, N. Tetradis, and C. Wetterich, Phys. Rep. **363**, 223 (2002).
- [12] M. Salmhofer and C. Honerkamp, Prog. Theor. Phys. **105**, 1 (2001).
- [13] W. Metzner, Prog. Theor. Phys. Suppl. **160**, 58 (2005).
- [14] J. Reuther and P. Wölfle, Phys. Rev. B **81**, 144410 (2010).
- [15] J. Reuther and R. Thomale, Phys. Rev. B **83**, 024402 (2011).
- [16] J. Reuther, P. Wölfle, R. Darradi, W. Brenig, M. Arlego, and J. Richter, Phys. Rev. B **83**, 064416 (2011).
- [17] J. Reuther, private communication.
- [18] S. Göttel, Master's thesis, RWTH Aachen University, to be published.
- [19] W. Heisenberg, Z. Phys. **49**, 619 (1928).
- [20] H. Bethe, Z. Phys. **71**, 205 (1931).

- [21] M. Takahashi, *Thermodynamics of One-Dimensional Solvable Models* (Cambridge University Press, 1999).
- [22] T. Giamarchi, *Quantum Physics in One Dimension* (Oxford University Press, USA, 2004).
- [23] M. Karbach and G. Müller, Comput. Phys. **11**, 36 (1997).
- [24] W. Marshall, Proc. R. Soc. A London **232**, 48 (1955).
- [25] L. Hulthén, Ark. Mat. Astron. Fys. **26A**.
- [26] J. des Cloizeaux and J. J. Pearson, Phys. Rev. **128**, 2131 (1962).
- [27] P. W. Anderson, Phys. Rev. **86**, 694 (1952).
- [28] L. D. Faddeev and L. A. Takhtajan, Phys. Lett. A **85**, 375 (1981).
- [29] Y. Endoh, G. Shirane, R. J. Birgeneau, P. M. Richards, and S. L. Holt, Phys. Rev. Lett. **32**, 170 (1974).
- [30] I. Affleck, D. Gepner, H. Schulz, and T. Ziman, J. Phys. A **22**, 511 (1989).
- [31] R. R. P. Singh, M. E. Fisher, and R. Shankar, Phys. Rev. B **39**, 2562 (1989).
- [32] T. Giamarchi and H. J. Schulz, Phys. Rev. B **39**, 4620 (1989).
- [33] N. D. Mermin and H. Wagner, Phys. Rev. Lett. **17**, 1133 (1966).
- [34] P. Jordan and E. Wigner, Z. Phys. **47**, 631 (1928).
- [35] A. Altland and B. Simons, *Condensed Matter Field Theory*, Second ed. (Cambridge University Press, 2010).
- [36] A. Luther and I. Peschel, Phys. Rev. B **12**, 3908 (1975).
- [37] F. D. M. Haldane, Phys. Rev. Lett. **45**, 1358 (1980).
- [38] F. D. M. Haldane, Phys. Lett. A **93**, 464 (1983).
- [39] F. D. M. Haldane, Phys. Rev. Lett. **50**, 1153 (1983).
- [40] S. R. White, Phys. Rev. Lett. **69**, 2863 (1992).
- [41] U. Schollwöck, Rev. Mod. Phys. **77**, 259 (2005).
- [42] L. E. Ballentine, *Quantum Mechanics: A Modern Development* (World Scientific Publishing Company, 1998).
- [43] E. Fradkin, *Field Theories of Condensed Matter Systems* (Perseus Books, 1991).
- [44] A. Auerbach, *Interacting Electrons and Quantum Magnetism* (Springer, 1994).

- [45] H. Schoeller, Lecture notes for the course "Quantentheorie der kondensierten Materie I", RWTH Aachen University, Fall 2009.
- [46] P. W. Anderson, Phys. Rev. **115**, 2 (1959).
- [47] V. Popov and S. Fedotov, Sov. Phys. JETP **67** (1988).
- [48] A. A. Abrikosov, L. P. Gorkov, and I. E. Dzyaloshinski, *Methods of Quantum Field Theory in Statistical Physics* (Dover Publications, 1975).
- [49] A. L. Fetter and J. D. Walecka, *Quantum Theory of Many-Particle Systems* (Dover Publications, 2003).
- [50] J. W. Negele and H. Orland, *Quantum Many-Particle Systems* (Addison-Wesley, 1988).
- [51] H. Bruus and K. Flensberg, *Many-Body Quantum Theory in Condensed Matter Physics: An Introduction* (Oxford University Press, USA, 2004).
- [52] R. Kubo, J. Phys. Soc. Japan **12**, 570 (1957).
- [53] A. Messiah, *Quantum Mechanics* (Dover Publications, 1999).
- [54] H. Knorrer, E. Trubowitz, and J. S. Feldman, *Fermionic Functional Integrals and the Renormalization Group* (American Mathematical Society, 2002).
- [55] J. Zinn-Justin, *Quantum Field Theory and Critical Phenomena*, 4th ed. (Clarendon Press, 2002).
- [56] K. G. Wilson, Phys. Rev. B **4**, 3174 (1971).
- [57] L. P. Kadanoff, Physics **2**, 263 (1966).
- [58] R. Shankar, Rev. Mod. Phys. **66**, 129 (1994).
- [59] P. W. Anderson, J. Phys. C: Solid State Phys. **3**, 2436 (1970).
- [60] M. Salmhofer, Comm. Math. Phys. **194**, 249 (1998).
- [61] M. Salmhofer, *Renormalization: An Introduction* (Springer, 1998).
- [62] C. J. Halboth and W. Metzner, Phys. Rev. B **61**, 7364 (2000).
- [63] D. Zanchi and H. J. Schulz, Phys. Rev. B **61**, 13609 (2000).
- [64] C. Honerkamp, M. Salmhofer, N. Furukawa, and T. M. Rice, Phys. Rev. B **63**, 035109 (2001).
- [65] V. Meden, W. Metzner, U. Schollwöck, and K. Schönhammer, Phys. Rev. B **65**, 045318 (2002).

- [66] S. Andergassen, T. Enss, V. Meden, W. Metzner, U. Schollwöck, and K. Schönhammer, Phys. Rev. B **70**, 075102 (2004).
- [67] R. Hedden, V. Meden, T. Pruschke, and K. Schönhammer, J. Phys. Condens. Matter **16**, 5279 (2004).
- [68] C. Karrasch *et al.*, J. Phys. Condens. Matter **20**, 345205 (2008).
- [69] C. Honerkamp and W. Hofstetter, Phys. Rev. Lett. **92**, 170403 (2004).
- [70] S. Andergassen, V. Meden, H. Schoeller, J. Splettstoesser, and M. R. Wegewijs, Nanotechnology **21**, 272001 (2010).
- [71] V. Meden, Functional renormalization group, <http://web.physik.rwth-aachen.de/~meden/funRG/>.
- [72] T. R. Morris, Int. J. Mod. Phys. A **9**, 2411 (1994).
- [73] F. Schütz, L. Bartosch, and P. Kopietz, Phys. Rev. B **72**, 035107 (2005).
- [74] C. Honerkamp and M. Salmhofer, Prog. Theor. Phys. **113**, 1145 (2005).
- [75] M. Salmhofer, C. Honerkamp, W. Metzner, and O. Lauscher, Prog. Theor. Phys. **112**, 943 (2004).
- [76] A. A. Katanin, Phys. Rev. B **70**, 115109 (2004).
- [77] C. Honerkamp and M. Salmhofer, Phys. Rev. B **64**, 184516 (2001).
- [78] C. Honerkamp, D. Rohe, S. Andergassen, and T. Enss, Phys. Rev. B **70**, 235115 (2004).
- [79] S. G. Jakobs, V. Meden, and H. Schoeller, Phys. Rev. Lett. **99**, 150603 (2007).
- [80] S. G. Jakobs, M. Pletyukhov, and H. Schoeller, J. Phys. A: Math. Theor. **43**, 103001 (2010).
- [81] W. Press, S. Teukolsky, W. Vetterling, and B. Flannery, *Numerical recipes in Fortran 90* (Cambridge University Press, New York, USA, 1996).
- [82] OpenMP website, <http://openmp.org/wp/>.
- [83] Rechen- und Kommunikationszentrum, RWTH Aachen, <http://www.rz.rwth-aachen.de/aw/cms/rz/Themen/~mem/hochleistungsrechnen/>.
- [84] J. L. Gustafson, Commun. ACM **31**, 532 (1988).
- [85] S. Göttel, private communication.
- [86] H. J. Vidberg and J. W. Serene, J. Low Temp. Phys. **29**, 179 (1977).
- [87] J. Brinckmann and P. Wölfe, Phys. Rev. B **70**, 174445 (2004).

- [88] K. Säaskilahti, S. Göttel, D. Schuricht, S. Andergassen, and C. Honerkamp, "Functional RG for Spin Chains", Poster at DPG Frühjahrstagung 2011, March 13-18, Dresden, Germany.



# Appendix A

## Flow equations

In this appendix, we present the full flow equations in algebraic form. The single-scale propagator is defined

$$S_\Lambda(\omega) = \frac{\delta(|\omega| - \Lambda)}{i\omega - \Sigma^\Lambda(\omega)}. \quad (\text{A.1})$$

In the Katanin-modified flow scheme (Sect. 4.4), one uses the single-scale propagator

$$\tilde{S}_\Lambda(\omega) = \frac{\delta(|\omega| - \Lambda)}{i\omega - \Sigma^\Lambda(\omega)} - \frac{\Theta(|\omega| - \Lambda)}{[i\omega - \Sigma^\Lambda(\omega)]^2} \dot{\Sigma}^\Lambda(\omega). \quad (\text{A.2})$$

instead of  $S_\Lambda$  in the flow equations (A.7), (A.8), (A.10) and (A.11) to be presented below. The loop propagator is the symmetric sum of the single-scale propagator and the full interacting propagator:

$$P_\Lambda(\omega_1, \omega_2) = S_\Lambda(\omega_1)\mathcal{G}_\Lambda(\omega_2) + S_\Lambda(\omega_2)\mathcal{G}_\Lambda(\omega_1), \quad (\text{A.3})$$

where the interacting propagator is

$$\mathcal{G}_\Lambda(\omega) = \frac{\Theta(|\omega| - \Lambda)}{i\omega - \Sigma^\Lambda(\omega)}. \quad (\text{A.4})$$

Flow equation (4.83) for the self-energy is in an algebraic form

$$\begin{aligned} \dot{\Sigma}^\Lambda(\omega) = \int \frac{d\nu}{2\pi} S_\Lambda(\nu) & \left[ 2 \sum_k \Gamma_{dik}^\Lambda(\omega + \nu, 0, \omega - \nu) \right. \\ & \left. + 3\Gamma_{sii}^\Lambda(\omega + \nu, \omega - \nu, 0) + \Gamma_{dii}^\Lambda(\omega + \nu, \omega - \nu, 0) \right], \end{aligned} \quad (\text{A.5})$$

where the site index  $i$  is arbitrary due to translational invariance. Initial condition is  $\Sigma^{\Lambda=\infty} = 0$ . Since  $\Sigma^\Lambda(\omega)$  is purely imaginary, we use the flow equation for the

damping  $\gamma^\Lambda(\omega) = i\Sigma^\Lambda(\omega)$  instead:

$$\begin{aligned} \dot{\gamma}^\Lambda(\omega) = & \frac{1}{2\pi} \left\{ 2 \sum_k [\Gamma_{dik}^\Lambda(\omega + \Lambda, 0, \omega - \Lambda) - \Gamma_{dik}^\Lambda(\omega - \Lambda, 0, \omega + \Lambda)] \right. \\ & + 3 [\Gamma_{sii}^\Lambda(\omega + \Lambda, \omega - \Lambda, 0) - \Gamma_{sii}^\Lambda(\omega - \Lambda, \omega + \Lambda, 0)] \\ & \left. + \Gamma_{dii}^\Lambda(\omega + \Lambda, \omega - \Lambda, 0) - \Gamma_{dii}^\Lambda(\omega - \Lambda, \omega + \Lambda, 0) \right\} \frac{1}{\Lambda + \gamma^\Lambda(\Lambda)}. \end{aligned} \quad (\text{A.6})$$

Here we have also eliminated the delta functions.

The flow equation (4.81) for the spin-spin interaction is in an algebraic form

$$\begin{aligned} \dot{\Gamma}_{sij}^\Lambda(s, t, u) = & \int \frac{d\nu}{2\pi} P_\Lambda(-\nu, s + \nu) \\ & \times [-2\Gamma_{sij}^\Lambda(s, -\omega_1 - \nu, \omega_2 + \nu)\Gamma_{sij}^\Lambda(s, \omega_3 + \nu, \omega_4 + \nu) \\ & + \Gamma_{dij}^\Lambda(s, -\omega_1 - \nu, \omega_2 + \nu)\Gamma_{sij}^\Lambda(s, \omega_3 + \nu, \omega_4 + \nu) \\ & + \Gamma_{sij}^\Lambda(s, -\omega_1 - \nu, \omega_2 + \nu)\Gamma_{dij}^\Lambda(s, \omega_3 + \nu, \omega_4 + \nu)] \\ & + \int \frac{d\nu}{2\pi} P_\Lambda(\nu, t + \nu) \\ & \times \left[ -2 \sum_k \Gamma_{sik}^\Lambda(\omega_1 + \nu, t, \omega_3 - \nu)\Gamma_{skj}^\Lambda(\omega_4 + \nu, t, -\omega_2 + \nu) \right. \\ & - \Gamma_{sij}^\Lambda(\omega_1 + \nu, \omega_3 - \nu, t)\Gamma_{sij}^\Lambda(\omega_4 + \nu, t, -\omega_2 + \nu) \\ & + \Gamma_{dij}^\Lambda(\omega_1 + \nu, \omega_3 - \nu, t)\Gamma_{sij}^\Lambda(\omega_4 + \nu, t, -\omega_2 + \nu) \\ & - \Gamma_{sij}^\Lambda(\omega_1 + \nu, t, \omega_3 - \nu)\Gamma_{sij}^\Lambda(\omega_4 + \nu, -\omega_2 + \nu, t) \\ & \left. + \Gamma_{sij}^\Lambda(\omega_1 + \nu, t, \omega_3 - \nu)\Gamma_{dij}^\Lambda(\omega_4 + \nu, -\omega_2 + \nu, t) \right] \\ & + \int \frac{d\nu}{2\pi} P_\Lambda(\nu, u + \nu) \\ & \times [2\Gamma_{sij}^\Lambda(\omega_2 - \nu, -\omega_3 - \nu, u)\Gamma_{sij}^\Lambda(\omega_4 - \nu, \omega_1 + \nu, u) \\ & + \Gamma_{sij}^\Lambda(\omega_2 - \nu, -\omega_3 - \nu, u)\Gamma_{dij}^\Lambda(\omega_4 - \nu, \omega_1 + \nu, u) \\ & + \Gamma_{dij}^\Lambda(\omega_2 - \nu, -\omega_3 - \nu, u)\Gamma_{sij}^\Lambda(\omega_4 - \nu, \omega_1 + \nu, u)], \end{aligned} \quad (\text{A.7})$$

with the initial condition  $\Gamma_{sij}^{\Lambda=\infty} = J_{ij}/4$ , where  $J_{ij}$  is the Heisenberg coupling constant between sites  $i, j$ . The flow equation (4.82) for the density-density interaction

can be written

$$\begin{aligned}
\dot{\Gamma}_{dij}^{\Lambda}(s, t, u) = & \int \frac{d\nu}{2\pi} P_{\Lambda}(-\nu, s + \nu) \\
& \times [\Gamma_{dij}^{\Lambda}(s, -\omega_1 - \nu, \omega_2 + \nu) \Gamma_{dij}^{\Lambda}(s, \omega_3 + \nu, \omega_4 + \nu) \\
& + 3 \Gamma_{sij}^{\Lambda}(s, -\omega_1 - \nu, \omega_2 + \nu) \Gamma_{sij}^{\Lambda}(s, \omega_3 + \nu, \omega_4 + \nu)] \\
& + \int \frac{d\nu}{2\pi} P_{\Lambda}(\nu, t + \nu) \\
& \times \left[ -2 \sum_k \Gamma_{dik}^{\Lambda}(\omega_1 + \nu, t, \omega_3 - \nu) \Gamma_{dkj}^{\Lambda}(\omega_4 + \nu, t, -\omega_2 + \nu) \right. \\
& + 3 \Gamma_{sij}^{\Lambda}(\omega_1 + \nu, \omega_3 - \nu, t) \Gamma_{dij}^{\Lambda}(\omega_4 + \nu, t, -\omega_2 + \nu) \\
& + \Gamma_{dij}^{\Lambda}(\omega_1 + \nu, \omega_3 - \nu, t) \Gamma_{dij}^{\Lambda}(\omega_4 + \nu, t, -\omega_2 + \nu) \\
& + 3 \Gamma_{dij}^{\Lambda}(\omega_1 + \nu, t, \omega_3 - \nu) \Gamma_{sij}^{\Lambda}(\omega_4 + \nu, -\omega_2 + \nu, t) \\
& \left. + \Gamma_{dij}^{\Lambda}(\omega_1 + \nu, t, \omega_3 - \nu) \Gamma_{dij}^{\Lambda}(\omega_4 + \nu, -\omega_2 + \nu, t) \right] \\
& + \int \frac{d\nu}{2\pi} P_{\Lambda}(\nu, u + \nu) \\
& \times [3 \Gamma_{sij}^{\Lambda}(\omega_2 - \nu, -\omega_3 - \nu, u) \Gamma_{sij}^{\Lambda}(\omega_4 - \nu, \omega_1 + \nu, u) \\
& + \Gamma_{dij}^{\Lambda}(\omega_2 - \nu, -\omega_3 - \nu, u) \Gamma_{dij}^{\Lambda}(\omega_4 - \nu, \omega_1 + \nu, u)] , \tag{A.8}
\end{aligned}$$

the initial condition being  $\Gamma_{dij}^{\Lambda=\infty} = 0$ . Here the Mandelstam variables and the inverse transformations are

$$\begin{cases} s = \omega_1 + \omega_2 \\ t = \omega_1 - \omega_3 \\ u = \omega_1 - \omega_4 \end{cases} \Leftrightarrow \begin{cases} \omega_1 = (s + t + u)/2 \\ \omega_2 = (s - t - u)/2 \\ \omega_3 = (s - t + u)/2 \\ \omega_4 = (s + t - u)/2. \end{cases} \tag{A.9}$$

Flow equation for the density susceptibility vertex is

$$\begin{aligned}
\dot{v}_{dij}^{\Lambda}(\omega, s) = & \int \frac{d\nu}{2\pi} P_{\Lambda}(\nu, \nu + \omega) \\
& \times [v_{dij}^{\Lambda}(\omega, 2\nu + \omega) \Gamma_{dii}^{\Lambda}(\omega_1 + \nu, \omega_2 - \nu, \omega) \\
& + 3 v_{dij}^{\Lambda}(\omega, 2\nu + \omega) \Gamma_{sii}^{\Lambda}(\omega_1 + \nu, \omega_2 - \nu, \omega) \\
& - 2 \sum_k v_{dik}^{\Lambda}(\omega, 2\nu + \omega) \Gamma_{dkj}^{\Lambda}(\omega_1 + \nu, \omega, \omega_2 - \nu)] . \tag{A.10}
\end{aligned}$$

with the initial condition  $v_{dij}^{\Lambda=\infty}(\omega, s) = 1$  and for the spin susceptibility vertex

$$\begin{aligned} \dot{v}_{sij}^{\Lambda}(\omega, s) = & \int \frac{d\nu}{2\pi} P_{\Lambda}(\nu, \nu + \omega) \\ & \times [-v_{sij}^{\Lambda}(\omega, 2\nu + \omega) \Gamma_{sii}^{\Lambda}(\omega_1 + \nu, \omega_2 - \nu, \omega) \\ & + v_{sij}^{\Lambda}(\omega, 2\nu + \omega) \Gamma_{dii}^{\Lambda}(\omega_1 + \nu, \omega_2 - \nu, \omega) \\ & - 2 \sum_k v_{sik}^{\Lambda}(\omega, 2\nu + \omega) \Gamma_{skj}^{\Lambda}(\omega_1 + \nu, \omega, \omega_2 - \nu)] , \end{aligned} \quad (\text{A.11})$$

with the initial condition  $v_{sij}^{\Lambda=\infty}(\omega, s) = 1/2$ . Here  $\omega_1 = (\omega + s)/2$  and  $\omega_2 = (s - \omega)/2$  are the outgoing and incoming fermion frequencies, respectively. The flow equations for the susceptibilities

$$D_{ij}(\omega) = \int d\tau e^{i\omega\tau} \langle T_{\tau} \tilde{n}_i(\tau) \tilde{n}_j \rangle \quad (\text{A.12})$$

and

$$\chi_{ij}(\omega) = \int d\tau e^{i\omega\tau} \langle T_{\tau} S_i^z(\tau) S_j^z \rangle \quad (\text{A.13})$$

are

$$\dot{D}_{ij}^{\Lambda}(\omega) = 2 \sum_k \int \frac{d\nu}{2\pi} v_{dik}^{\Lambda}(\omega, 2\nu + \omega) v_{dkj}^{\Lambda}(-\omega, 2\nu + \omega) P_{\Lambda}(\nu, \nu + \omega) \quad (\text{A.14})$$

and

$$\dot{\chi}_{ij}^{\Lambda}(\omega) = 2 \sum_k \int \frac{d\nu}{2\pi} v_{sik}^{\Lambda}(\omega, 2\nu + \omega) v_{skj}^{\Lambda}(-\omega, 2\nu + \omega) P_{\Lambda}(\nu, \nu + \omega), \quad (\text{A.15})$$

respectively. The initial conditions are  $D_{ij}^{\Lambda=\infty}(\omega) = \chi_{ij}^{\Lambda=\infty}(\omega) = 0$ .

Ground state energy is given by the flow equation

$$\dot{E}^{\Lambda} = \frac{2N}{\pi} \log \left( 1 + \frac{\gamma^{\Lambda}(\Lambda)}{\Lambda} \right), \quad (\text{A.16})$$

with the initial condition  $E^{\Lambda=\infty} = 0$ . Here  $N$  is the number of spins in the chain.